

**An *Ex Vivo* Model For The
Assessment Of Drug Toxicity On
The Human Retina**

Phillip Wright

**THESIS PRESENTED FOR THE DEGREE OF DOCTOR
OF PHILOSOPHY**

UNIVERSITY OF EAST ANGLIA, NORWICH, UK

SCHOOL OF PHARMACY

APRIL 2016

This copy of the thesis has been supplied on condition that anyone who consults it is understood to recognise that its copyright rests with the author and that use of any information derived there from must be in accordance with current UK Copyright Law. In addition, any quotation or extract must include full attribution

Abstract

Purpose: Retinal toxicity is a common cause of drug development attrition. The aims of this research were therefore to develop the *ex vivo* human retina as a suitable model for the assessment of retinotoxicity, and to explore the methods in which this may be investigated.

Methods: Post mortem and living donor human eyes were obtained, and the retinas dissected within 24h post mortem or 1h enucleation respectively. The *ex vivo* human retina was characterised using immunohistochemistry and QRT-PCR. The effect of multiple retinotoxins was investigated on the human retinal cell lines MIO-M1 (Müller cells) and ARPE19 (RPE cells), and CHQ on the human organotypic retinal culture (HORC) using the LDH and MTS assays. TUNEL, Western blotting and QRT-PCR were also used to investigate the effect of CHQ on the HORC, and CDK expression investigated by QRT-PCR.

Results: Cell specific markers were investigated in the post mortem and living donor, both possessed similar immunohistochemical and mRNA properties. CHQ was the most potent retinotoxin investigated in the cell lines, and when applied to the HORC, measureable toxicity was found along with an increase in the expression of multiple cell specific mRNA's. The expression profile of multiple CDK's in the *ex vivo* retina was investigated in relation to a retinotoxic Pan-CDK inhibitor, where differential expression was found. When exposed to the retinotoxic pan-CDK inhibitor, the cell lines displayed differences in toxicity.

Conclusion: The *ex vivo* human retina is an ideal tissue to investigate retinotoxicity. It possesses similar properties as the *in vivo* human retina, and displayed measureable toxicity when exposed to CHQ. The *ex vivo* human retina also proved its usefulness in the investigation genes associated to a novel retinotoxin. The *ex vivo* human retina could act as a bridge between animal and human studies, providing vital information about a drug's potential retinotoxicity.

List of Contents

List of Figures	8
List of Tables.....	10
Acknowledgements	11
1.1 Anatomy and function of the eye	12
1.1.1 Overview of the eye.....	12
1.1.2 The Cornea and Sclera.....	13
1.1.3 The Anterior and Posterior Chamber	14
1.1.4 The Ciliary Body	14
1.1.5 The Iris	15
1.1.6 The Lens	16
1.1.7 The Vitreous Chamber	17
1.2 The Retina	17
1.2.1 Retinal Function and Anatomy.....	17
1.2.2 Retinal Pigment Epithelium	22
1.2.3 Photoreceptors	23
1.2.4 Bipolar Cells.....	26
1.2.5 Ganglion Cells	28
1.2.6 Amacrine Cells	28
1.2.7 Horizontal Cells.....	29
1.2.8 Interplexiform Neurons	29
1.2.9 Müller Cells.....	30
1.2.10 Retinal Astrocytes	30
1.2.11 Retinal Microglia.....	31
1.3 Retinal Toxicity.....	32
1.3.1 Introduction	32
1.3.2 Drug Development Process	33

1.3.2 Models and Methods Used to Assess Retinal Toxicity.....	34
1.3.4 Known Retinotoxins.....	35
1.3.4.1 Chloroquine.....	36
1.3.4.2 Hydroxychloroquine.....	42
1.3.4.3 Indomethacin.....	43
1.3.4.4 Tamoxifen.....	45
1.3.5 Aims of Research.....	48
2.0 Methods.....	50
2.1 Donor Human Eyes.....	50
2.2 Retinal Dissection.....	50
2.3 Cell Culture.....	51
2.3.1 ARPE-19.....	52
2.3.2 MIO-M1.....	52
2.4 PCR.....	53
2.4.1 Planar Sectioning.....	53
2.4.2 RNA Extraction.....	54
2.4.4 RNA Clean-up.....	55
2.4.5 cDNA.....	55
2.4.6 PCR.....	56
2.4.7 PCR Analysis.....	58
2.5 Immunohistochemistry.....	59
2.5.1 Cryosectioning.....	59
2.5.2 Fluorescence Immunohistochemistry.....	60
2.5.3 Colorimetric Immunohistochemistry.....	62
2.5.3.1 Ventana Discovery.....	62
2.5.3.2 TUNEL Assay.....	63
2.5.3.3 Colorimetric Imaging.....	63

2.6 Western Blot.....	64
2.6.1 Protein extraction.	64
2.6.2 BCA Assay	64
2.6.3 Sample Preparation.....	64
2.6.4 SDS-PAGE.....	65
2.6.5 Gel Electrophoresis	65
2.6.6 Protein Transfer	65
2.6.7 Immunoblotting	66
2.6.8 Development	66
2.7 LDH Assay.....	67
2.8 MTS Assay.....	68
Chapter 3	70
3.0 Characterisation of retinal cell markers in the human retina	70
3.1 Introduction	70
3.2 Results.....	73
3.2.1 Immunohistochemical analysis of retinal cell marker proteins in the human retina.....	73
3.2.1.1 Neuronal Specific Enolase	73
3.2.1.2 Recoverin.....	74
3.2.1.3 Calbindin	75
3.2.1.4 Protein Kinase C α	76
3.2.1.5 NeuN	77
3.2.1.6 THY1.....	78
3.2.1.7 β III Tubulin	79
3.2.1.8 Glutamine Synthetase.....	80
3.2.1.9 AHNAK2.....	81
3.2.1.10 Heat Shock Protein 70.....	82

3.2.2 mRNA Expression of Cell Specific Markers Within Whole Macula and Paramacula Samples	83
3.2.3 mRNA Profiling of Retinal Cell Markers in the Human Retina	87
3.2.3.1 mRNA Profiling of Retinal Cell Markers in the Post Mortem Macula.....	87
3.2.3.2 mRNA Profiling of Retinal Cell Markers in the Living Donor Macula	90
3.2.3.3 mRNA Profiling of Retinal Cell Markers in the Post Mortem Paramacula	93
3.2.3.4 mRNA Profiling of Retinal Cell Markers in the Living Donor Paramacula	96
3.3 Discussion	99
3.4 Conclusion	105
4.0 The Effect of Known Retinotoxins on Retinal Cell Lines	107
4.1 Introduction	107
4.2 Results	109
4.2.1 ARPE19 Cells Response to Retinotoxins.....	109
4.2.1.1 Hydrogen Peroxide	109
4.2.1.2 Indomethacin	110
4.2.1.3 Tamoxifen	111
4.2.1.4 Chloroquine	112
4.2.2 MIO-M1 Cells Response to Retinotoxins	115
4.2.2.1 Hydrogen Peroxide	115
4.2.2.2 Indomethacin	116
4.2.2.3 Tamoxifen	117
4.2.2.4 Chloroquine	118
4.2.3 ARPE19 Cells Response to 24, 48 and 72h Chloroquine and Hydroxychloroquine Exposure.....	120
4.2.4 MIO-M1 cells response to 24, 48 and 72h Chloroquine and Hydroxychloroquine exposure	126
4.3 Discussion	130

4.4 Conclusion.....	135
5.0 Effect of Chloroquine on Human Organotypic Retina Cultures.....	137
5.1 Introduction	137
5.2 Results	139
5.2.1 The Effect of Hydrogen Peroxide on Cell Death in the HORC	139
5.2.2 The Effect of Chloroquine on Cell Death / Cell Viability in the HORC	140
5.2.3 Investigation of Chloroquine Induced Cell Death in the HORC.....	141
5.2.4 Effect of Chloroquine on mRNA Expression of Retinal Cell Markers in HORCs	144
5.2.5 Western Blot Analysis of Chloroquine Treated Samples.....	147
5.3 Discussion	150
5.4 Conclusion.....	157
6.0 Cyclin Dependent Kinase Expression in the Adult Human Retina.....	159
6.1 Introduction	159
6.2 Results	162
6.2.1 CDK Selection.....	162
6.2.2 Whole Explant CDK analysis.....	164
6.2.2 mRNA Profiling of the Macula and Paramacula Explants.....	165
6.2.3 Effect of AG-012986 on ARPE19 and MIO-M1 Cells.....	168
6.3 Discussion	169
6.4 Conclusion.....	175
7.0 General Discussion.....	176
7.1 Thesis summary.....	176
7.2 Future work	180
7.3 Concluding remarks	182
Supplementary Data	183
Abbreviations	184

List of Figures

Fig 1.1	Schematic diagram of the human eye in horizontal plane	12
Fig 1.2	Topographical map of the retina	19
Fig 1.3	Light micrograph and diagram of the retinal layers	20
Fig 1.4	Photoreceptor structure	24
Fig 1.5	Bipolar cell function	26
Fig 1.6	Stages of drug development	33
Fig 1.7	Structure of CHQ and HCQ	36
Fig 1.8	Pentose phosphate pathway	39
Fig 1.9	Glutathione redox cycle	40
Fig 1.10	Indomethacin metabolism	44
Fig 1.11	Tamoxifen metabolism	47
Fig 2.1	Macula / paramacula explant extraction	51
Fig 2.2	Planar sectioning technique	54
Fig 3.1	Neuronal specific enolase immunohistochemistry	73
Fig 3.2	Recoverin immunohistochemistry	74
Fig 3.3	Calbindin immunohistochemistry	75
Fig 3.4	Protein kinase C α immunohistochemistry	76
Fig 3.5	Neuronal nuclei immunohistochemistry	77
Fig 3.6	THY1 immunohistochemistry	78
Fig 3.7	β III tubulin immunohistochemistry	79
Fig 3.8	Glutamine synthetase immunohistochemistry	80
Fig 3.9	AHNAK2 immunohistochemistry	81
Fig 3.10	Heat shock protein 70 immunohistochemistry	82
Fig 3.11	Cell specific mRNA in whole paramacula and macula explants	83
Fig 3.12	Cell specific mRNA in whole paramacula and macula explants	85
Fig 3.13	Cell specific mRNA in whole paramacula and macula explants	86
Fig 3.14	Cell specific mRNA in planar sectioned macula PM retina	88
Fig 3.15	Cell specific mRNA in planar sectioned macula live retina	91
Fig 3.16	Cell specific mRNA in planar sectioned paramacula PM retina	94

Fig 3.17	Cell specific mRNA in planar sectioned paramacula live retina	97
Fig 4.1	LDH and MTS of ARPE19 cells exposed to H ₂ O ₂	109
Fig 4.2	LDH and MTS of ARPE19 cells exposed to Indomethacin	110
Fig 4.3	LDH and MTS of ARPE19 cells exposed to Tamoxifen	111
Fig 4.4	LDH and MTS of ARPE19 cells exposed to CHQ	112
Fig 4.5	LDH and MTS of MIO-M1 cells exposed to H ₂ O ₂	115
Fig 4.6	LDH and MTS of MIO-M1 cells exposed to Indomethacin	116
Fig 4.7	LDH and MTS of MIO-M1 cells exposed to Tamoxifen	117
Fig 4.8	LDH and MTS of MIO-M1 cells exposed to CHQ	118
Fig 4.9	LDH and MTS of ARPE19 cells exposed to 24h CHQ and HCQ	121
Fig 4.10	LDH and MTS of ARPE19 cells exposed to 48h CHQ and HCQ	122
Fig 4.11	LDH and MTS of ARPE19 cells exposed to 72h CHQ and HCQ	123
Fig 4.12	LDH and MTS of MIO-M1 cells exposed to 24h CHQ and HCQ	126
Fig 4.13	LDH and MTS of MIO-M1 cells exposed to 48h CHQ and HCQ	127
Fig 4.14	LDH and MTS of MIO-M1 cells exposed to 72h CHQ and HCQ	128
Fig 5.1	HORC LDH release after exposure to H ₂ O ₂	139
Fig 5.2	HORC LDH and MTS after exposure to CHQ	140
Fig 5.3	HORC % TUNEL positive pixels after exposure to CHQ	141
Fig 5.4	HORC % active caspase 3 positive pixels after exposure to CHQ	142
Fig 5.5	HORC % NeuN positive pixel after exposure to CHQ	143
Fig 5.6	HORC cell specific mRNA expression after CHQ exposure	145
Fig 5.7	HORC PARP cleavage after exposure to H ₂ O ₂	148
Fig 5.8	HORC PARP cleavage after exposure to CHQ	149
Fig 6.1	CDK family tree	160
Fig 6.2	CDK inhibitor affinities	163
Fig 6.3	CDK mRNA expression in macula and paramacula explants	164
Fig 6.4	CDK mRNA expression in planar sectioned macula and paramacula explants	166
Fig 6.5	ARPE19 and MIO-M1 LDH and MTS in after exposure to pan-CDK inhibitor	168

List of Tables

Table 2.1	List of primers / probes used	57
Table 2.2	Primary antibodies used for immunohistochemistry	60
Table 2.3	Secondary antibodies used for immunohistochemistry	62
Table 2.4	Antibodies used for western blotting	67
Table 4.1	LD50 values and significant from values in ARPE19 cells exposed to multiple retinotoxins	113
Table 4.2	LD50 values and significant from values in MIO-M1 cells exposed to multiple retinotoxins	119
Table 4.3	LD50 values and significant from values in ARPE19 cells exposed to CHQ and HCQ for 24, 48 and 72h	124
Table 4.4	LD50 values and significant from values in MIO-M1 cells exposed to CHQ and HCQ for 24, 48 and 72h	129

Acknowledgements

The research conducted throughout this thesis has given me infinite opportunities to pursue my interests in science. For that I am grateful to everyone who helped make this a possibility for me.

I would firstly like to thank my supervisor Dr Julie Sanderson for the endless help and guidance she provided me with whilst conducting this research. I would also like to thank Dr Guy Healing and Dr Janet Kelsall for their support and supervision within the project, and the opportunity they provided me with, to conduct research and learn new techniques at AstraZeneca. Many thanks go to AstraZeneca for the funding and materials they provided which aided in this work. Importantly, I would also like to thank previous and current members of the Norwich Eye Research group who provided guidance, and taught me many of the techniques required to conduct this research, Dr Andrew Osborne, Dr Ning Ma, Dr Andrew Smith, Dr Julie Eldred, Dr Amal Aldarwesh, Dr Sarah Russell, Dr Jeremy Rhodes and Dr Michael Wormstone.

It goes without saying that the East Anglian Eye Bank played a major role in this work, providing me with the tissue necessary to conduct the research. For that I would like to thank Mary Tottman and Matt Hewett-Emmet of the East Anglian Eye Bank who worked very hard to provide donor human eyes.

I must also thank my girlfriend Natasha Reed for the love and care she gave me whilst studying. And my friends, near and far, all who made my time whilst studying an unforgettable experience.

Finally, but certainly not least, I would like to thank my family. My parents for their love, support and encouragement throughout my studies. My brother for always being there for me and my grandparents, aunties, uncles and cousins for their care and support.

Chapter 1

1.1 Anatomy and function of the eye

1.1.1 Overview of the eye

The eye (Figure 1.1) is a specialised organ the purpose of which is to receive light and convert this energy into a neural signal for the brain to process this information to create the sense that is “sight”. In order to receive light in an effective manner the eye has evolved so that light is first refracted by the cornea and lens and focussed onto the photosensitive cells of the retina which enable visual transduction. Within this chapter the main regions of the eye that enable visual transduction are described, starting with where light first enters the eye, the cornea, and ending where it is converted to a neural signal within the retina.

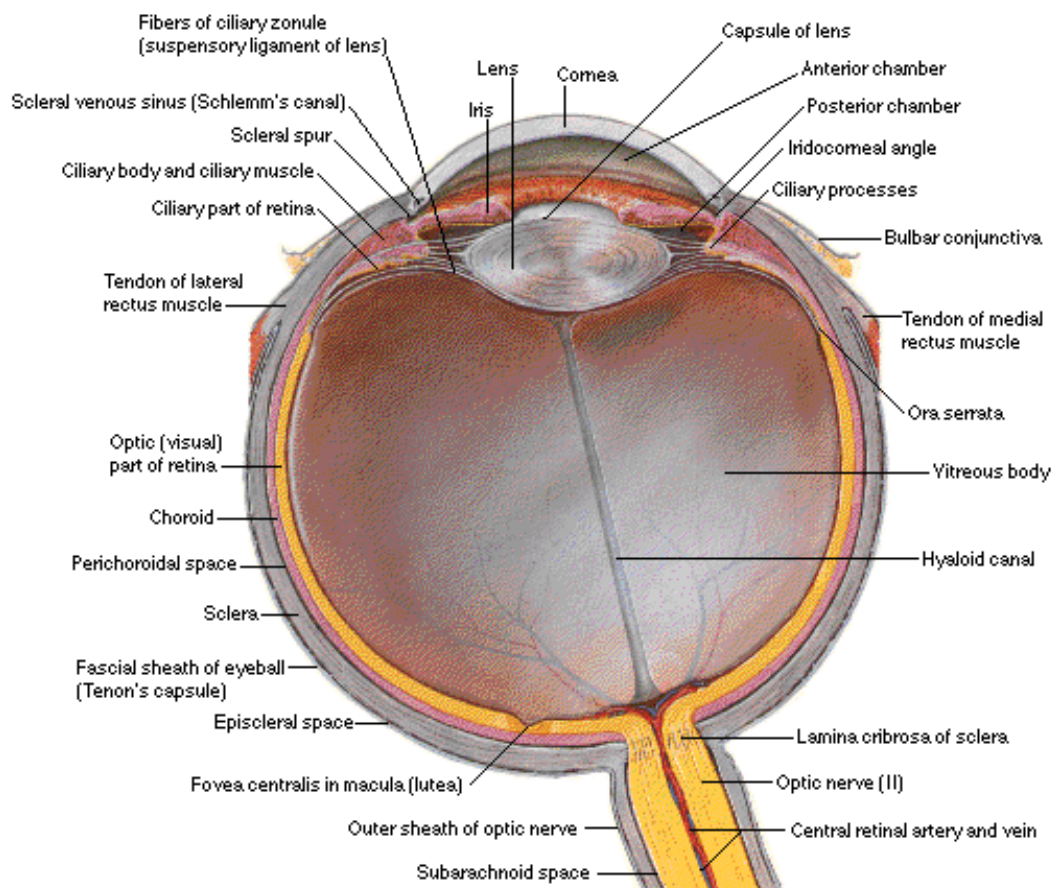


Figure 1.1 - Schematic diagram of the human eye in the horizontal plane. Source: http://www.phys.ufl.edu/~avery/course/3400/vision/eye_human_detail.gif

1.1.2 The Cornea and Sclera

The cornea is the most exposed part of the eye and is also the part with the highest curvature; it has a vertical diameter of 10.6mm which is smaller than the horizontal diameter of 11.7mm (Van Buskirk, 1989). The cornea forms around one sixth of the surface area of the eye (Martola and Baum, 1968), with the remainder being formed by the tough layer called the sclera (Figure 1.1). The cornea's most important features are the high refractive index it provides (the majority of refraction within the eye is caused by the cornea) and its transparency. The transparency comes as a result of the avascularity, the smoothness of the surface and the unique properties of the five layers which form the cornea. The five layers of the cornea in order from the outermost layer inwards are; the corneal epithelium, Bowmans layer, stroma, Descemet's membrane and the endothelium.

On top of the corneal epithelium lies the tear film which consists of three main layers, the meibomian lipid layer (outer layer), aqueous layer (middle layer) and the hydrated mucus layer (inner layer). The tear layer is an important layer that is in contact with the air and functions to maintain a wet surface, create a smooth optical surface and supply nutrients to the cornea.

The tear film also protects the cornea in two main ways, one is by providing antibacterial protection with lysozyme, and the other is the delicate balance of proteinases and proteinase inhibitors which maintain cell turnover and aid repair within the cornea (Remington, 2012).

The sclera forms the remaining five sixths of the eye and provides a tough tissue shell to the eye. It provides resistance to external and internal forces and maintains the eyes shape. The sclera provides attachment points for muscle to join to allow movement of the eye. It is continuous with the cornea but has different properties. The cornea has regularly arranged lamellae which allow the cornea to possess its transparent properties, the sclera however has irregularly arranged lamellae which provide stronger and more flexible properties than the cornea, but the result is that the sclera is opaque.

1.1.3 The Anterior and Posterior Chamber

There are two chambers that lie behind the cornea, the anterior chamber and the posterior chamber (Figure 1.1) within which aqueous humour is produced, held and drained.

Aqueous humour is a transparent fluid which serves two main functions. Firstly, it is the medium through which necessary metabolites are transported to the avascular lens and the cornea and it also serves to remove metabolic products. Secondly it enables maintenance of a stable intra-ocular pressure which results from a balance between rate of production, and drainage of aqueous humour. Aqueous humour is produced and secreted into the posterior chamber (located posterior to the iris and anterior to the lens (Figure 1.1) and is the smaller of the two chambers) from the ciliary processes. Active secretion is responsible for around 80 – 90% of total aqueous humour production with the rest produced through diffusion and ultrafiltration. A total of approximately 2.5µl is produced per minute with a 50% decrease in production at night, following a circadian pattern. Aqueous humour is passed from the site of production through the posterior chamber into the anterior chamber via the pupil.

The anterior chamber lies between the cornea and the iris (and the pupillary part of the lens) (Figure 1.1). It is the larger of the two chambers hosting a total of around 250µl of aqueous humour with a central depth of around 3mm. The anterior chamber is the chamber from which the drainage of aqueous humour occurs. Drainage is either via the “conventional pathway” or the “non-conventional pathway”. The conventional pathway is the main route of exit, responsible for 70-80% of drainage via Schlemm’s canal and the trabecular meshwork. The non-conventional pathway involves aqueous humour passing through intercellular spaces between ciliary muscle fibres and loose connective tissue (Forrester, 2007).

1.1.4 The Ciliary Body

The ciliary body is a ring shaped structure which anteriorly is present in the posterior chamber and posteriorly extends as far as the ora serrata where it terminates.

A large portion of the ciliary body is formed from smooth muscle, which is innervated by both the parasympathetic nervous system for contraction via acetylcholine on muscarinic receptors, and relaxation (inhibition) of the ciliary muscle via noradrenaline acting on $\alpha 1$ and $\beta 2$ -adrenoceptors allowing for lens focussing (accommodation) (Remington, 2012). The supraciliaris is the layer which lays between the ciliary muscle and the sclera. This layer is formed of loose connective tissue and possesses a ribbon like structure which allows the ciliary body to slide against the sclera to prevent tissue detachment from the sclera. The remainder of the ciliary body is taken up by the stroma. This tissue is highly vascularised and contains connective tissue, fibroblasts, melanocytes and some immune cells.

The ciliary body has two main functions; the first is the aiding of lens accommodation via contraction and relaxation of the ciliary muscle, the second is the production of aqueous humour. Aqueous humour is produced by the highly vascularised stroma and ciliary processes. Plasma and macromolecules leak through the permeable capillaries of the stroma and pass through the pigmented epithelial layer (which are joined together by leaky junctions). The non-pigmented epithelial layer contains tight junctions which prevents passive movement into the posterior chamber. This enables this layer to filter unwanted macromolecules. The non-pigmented epithelial layer contains high levels of mitochondria and actively transports ions to enable aqueous humour secretion into the posterior chamber.

1.1.5 The Iris

The iris is a circular structure responsible for controlling illumination levels of the retina. The iris achieves this by having the ability to alter the pupil size. In bright light conditions the pupil can contract to 1mm (miosis), in low light levels the pupil can dilate to 9mm (mydriasis). The iris is approximately 12mm in diameter and cone shaped with the pupillary part lying on the lens anterior to the root of the iris. The iris is thickest at a region called the collarette which is located roughly 1.5mm from the pupil margin (Remington, 2012).

The iris has 4 layers. The outermost layer is the anterior border layer which consist of fibroblasts laying on top of a layer of pigmented melanocytes. The next layer

posterior to this is the stroma and sphincter muscle, which is composed of pigmented (melanocytes and clump cells) and non-pigmented fibroblasts, lymphocytes, macrophages and mast cells with smooth muscle forming the sphincter. The anterior epithelium and dilator muscle lay posterior to the stroma. This layer consists of myoepithelial cells and elongated smooth muscle fibres which form the dilator muscle. The most posterior layer is the posterior epithelium which is formed by a single layer of heavily pigmented columnar epithelial cells (Hogan et al., 1971).

1.1.6 The Lens

The lens is a transparent, avascular elliptic structure whose purpose is to help focus light on the retina. It is composed of two main cell types, lens epithelial cells and lens fibre cells (which differentiate from lens epithelial cells). The lens is biconvex with the posterior surface having a steeper radius of curvature of between 5 - 8 μ m in comparison to the anterior surface which has a radius of curvature of 8 - 14 μ m. The lens has a thickness of between 3.5 and 5mm (measured from the anterior pole to the posterior pole) and a diameter of around 9mm when mature (Remington, 2012). The thickness of the lens increases by around 0.02mm each year due to the formation of new fibres, however the diameter does not change (Dubbelman et al., 2001).

Altering the dioptric power of the lens is achieved by the ciliary muscles which either contract or relax to alter the lens shape. When the eye needs to focus on a distant object, the ciliary muscle relaxes which pulls the zonular fibres tight, and in turn stretches the lens to decrease the refractive power. The opposite occurs when focussing on a near object; the lens accommodates by increasing its refractive power. This happens by the ciliary muscles contracting, loosening the zonular fibres and in turn the lens curvature increases, thus increasing the dioptric power to focus the near object on the retina (Johnson, 1976). Unaccommodated, the lens has a refractive power of 20 dioptres. This is due to a multitude of factors including the refractive index of the lens, change in index between the lens and the aqueous humour, length of the optical path and the surface curvature of the lens.

The transparency of the lens is a key factor in its functioning; the lens needs to be able to refract light but not scatter it. The lens gains its transparency from an absence of blood vessels, minimal cell organelles and an orderly arrangement of fibres

(Remington, 2012). The lens is attached posteriorly to the anterior vitreous face by the hyaloid capsular ligament.

1.1.7 The Vitreous Chamber

The vitreous chamber is the largest section of the eye, occupying around 80% of the total eye volume. The purpose of the vitreous is to provide support for the retina and the eye along with storing essential metabolites for the lens and retina.

It consists mainly of water (98.5 – 99.7%) with a dilute solution of salts, soluble proteins and hyaluronic acid within a meshwork of collagen. The vitreous can be divided into zones depending on its density. There are three main zones within the vitreous; the outer (vitreous cortex) which contains a large amount of tightly packed collagen fibrils, the intermediate zone which consists of fibers that run from the vitreous base to the posterior cortex and the center zone which is surrounded by the intermediate zone and is also known as the hyaloid canal (Figure 1.1).

The vitreous is bound anteriorly to the posterior part of the lens and the ciliary body by the hyloideocapsular ligament. The most extensive attachment of the vitreous is to the basement membrane of the non-pigmented epithelium of the ciliary body and the internal limiting membrane of the peripheral retina. This is held by vitreous fibres which are embedded into the epithelium and membrane (Remington, 2012).

1.2 The Retina

1.2.1 Retinal Function and Anatomy

The retina is the region of the eye responsible for transforming light energy into neuronal signals which are transmitted to the brain, which in turn processes the information enabling vision. This process means that the retina has a high metabolic demand, with the highest oxygen consumption per gram of any tissue within the human body.

To meet this high metabolic demand, the retina has two different blood supplies. The outer retinal layers are supplied by the choroidal capillary bed. Through this path oxygen and metabolites have to diffuse across Bruch's membrane and the RPE to

reach the outer retinal layers. The choroidal pathway has a high flow rate (150 mm/s) but a low oxygen exchange rate (Forrester, 2007) which provides about a third of the retina's total metabolic requirement.

The remainder of the retina is supplied through the central retinal vessels. This pathway starts with the ophthalmic artery passing through the optic disc (Figure 1.2) where it branches into the superior and inferior retinal artery each of which divide further. The vessels ultimately form two capillary networks; the deep capillary network (located in the inner nuclear layer) and the superficial capillary network (located in the nerve fiber layer / and or the ganglion cell layer). This network supplies the remaining two thirds of the retina's total requirements; it has a lower flow rate (25mm/s) but a higher oxygen exchange rate (Forrester, 2007).

The retina is protected by a barrier similar to that of the blood brain barrier known as the blood retinal barrier (BRB). The BRB allows the retina to support the specific environment which is optimal for function (Remington, 2012). The BRB is composed of two parts, the inner BRB (composed of microvascular endothelium cells) and the outer BRB (formed by the RPE) (Campbell and Humphries, 2012). Both the inner and outer BRB possess tight junctions which regulate solute and fluid permeability. The tight junctions are formed from a multitude of transmembrane proteins from the occludin, tricellulin and claudin families along with junctional adhesion molecules all of which are linked to the cell cytoskeleton via zonular occludens.(Runkle and Antonetti, 2011). The tight junctions mean that the permeability of substances across the BRB will vary; this depends on the nature of the substances and is required to allow the access of nutrients and the prevention of toxic substances to the neural retina. This also means that different drugs will possess variable permeability to the BRB which is a consideration to make when developing a drug aimed at targeting the retina.

The retina can be divided into a topographical map of regions along the surface of the retina (Figure 1.2) and also individual layers that run through the retina (Figure 1.3).

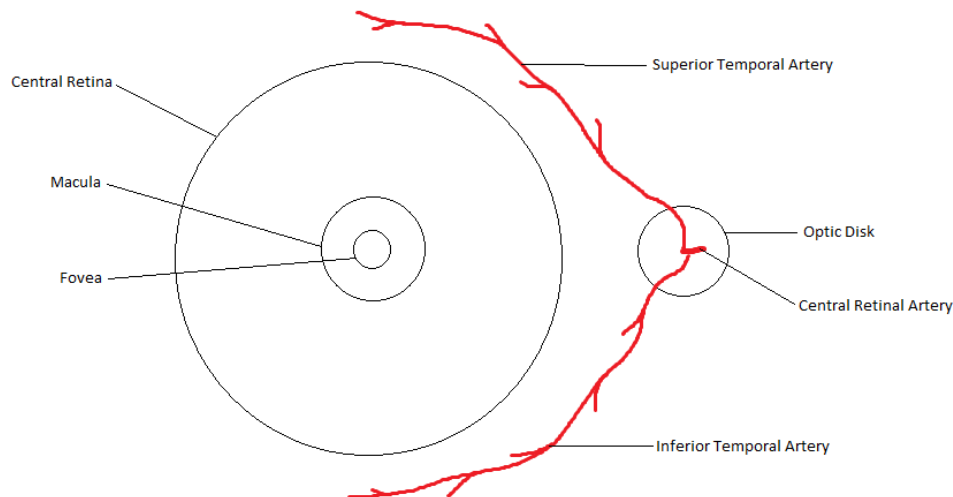


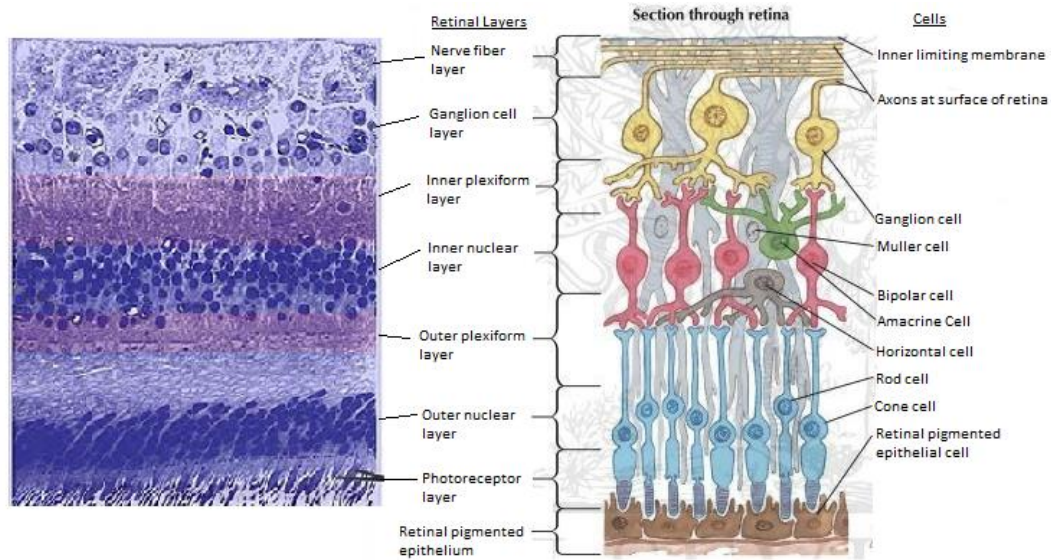
Figure 1.2 - Topographical map of the central retina showing the main arteries

The central retina is the region surrounded by the superior temporal artery and the inferior temporal artery.

At the centre of this area is the macula, an approximate 1.5mm region which is 3mm lateral to the optic disc (Forrester, 2007). It has a distinctive yellow colour in comparison to the rest of the retina due to the pigments zeaxanthin and lutein. The fovea lies at the centre of the macula and is approximately 0.35mm in diameter. It is an avascular depression where light is focussed onto, it is also where cones are at their highest density.

The optic disc is an area where retinal blood vessels pass in and out of the eye and where ganglion cell axons exit to the optic nerve.

The remainder of the retina is named the peripheral retina. It is a region which consists mainly of rods and extends to the ora serrata (the boundary between the retina and the start of the ciliary body) (Forrester, 2007).



A

B

Figure 1.3 - Cross Section of the Human Retina

A Light micrograph of the retinal layers. Source:

<http://webvision.med.utah.edu/images/wv/husect.jpeg>

B Diagram of retinal layers and cell types. Source:

<http://www.netterimages.com/images/vpv/000/000/029/29736-0550x0475.jpg>

The layers in the retina can be seen in Figure 1.3 where a section through the retina is shown. The retina is anatomically divided into 10 layers described below, from the most anterior layer to the most posterior. Following this a description of the different retinal cell types will be given.

1. The internal limiting membrane.

This membrane separates the retina from the vitreous humour. It primarily consists of the endfeet of Müller cells which are covered anteriorly by a basement membrane, consisting of extracellular matrix proteins such as laminin and fibronectin (Russell et al., 1991).

2. The nerve fiber layer.

The nerve fiber layer is a layer mainly consisting of ganglion cell axons which project to the optic disc where they bundle and exit as the optic nerve. This layer also contains retinal vessels and capillaries.

3. The ganglion cell layer.

The ganglion cell layer is a layer dominated by ganglion cells, however other cells and processes are also seen in this area such as some amacrine cells (termed displaced amacrine cells) and Müller cell processes (which separate ganglion cells). In the majority of the retina this layer is one cell thick, however in the macula the layer can become 8 to 10 cells thick (Remington, 2012).

4. The inner plexiform layer

This layer is formed mainly from synaptic connections between bipolar cells and ganglion cells, with invaginating midget bipolar cells synapses being within the inner half and the flat midget bipolar cell synapses in the outer half. Other types of synapse are also present in this layer between amacrine and bipolar cells, amacrine and ganglion cells and also amacrine and interplexiform neurons.

5. The inner nuclear layer.

The inner nuclear layer is a layer consisting mainly of cell bodies from several retinal cells, primarily Müller cells, bipolar cells, horizontal cells, amacrine cells, interplexiform neurons and occasionally displaced ganglion cells. These cells tend to be in the order of amacrine cells, adjacent to the inner plexiform layer, then Müller and bipolar cells, then horizontal cells adjacent to the outer plexiform layer. This layer also contains some deep vascular capillary networks.

6. The outer plexiform layer.

This layer has two main bands within it, the thin band and the wide band. The thin band consists of synapses from rods and cones synapsing with bipolar cells and horizontal cells, and horizontal cells also forming synapses with bipolar cells. The wide band is made of inner fibres of the rods and cones.

7. The outer nuclear layer.

The outer nuclear layer consists of the cell bodies of the rod and cone photoreceptors. These themselves are arranged due to the length of the outer fibres of the photoreceptors. Cones have a short outer fibre which means the cone cell bodies lay very close to the external limiting membrane whereas rod outer fibres are longer and therefore the rods form multiple layers anterior to the cone cell body layer. The thickness of this layer also alters throughout the

retina, with 8 to 9 cell layers nasal to the optic disc and 4 layers temporal to the optic disc (Remington, 2012).

8. The external limiting membrane.

Contrary to its name this layer is not a membrane. This layer is in fact a chain of zonula adherens junctions between the inner layer of photoreceptors and Müller cells and photoreceptors themselves. This layer does have some membrane properties such as the restriction of passage of some large molecules (Remington, 2012).

9. The photoreceptor layer

This layer consists of photoreceptor inner and outer segments with Müller cell projections separating the inner photoreceptor segments.

10. The retinal pigmented epithelium

The retinal pigmented epithelium is a single layer of pigmented cells which interact with the outer segments of photoreceptors.

This section described the different layers of the human retina, next a detailed description of the different cell types of the human retina will be given.

1.2.2 Retinal Pigment Epithelium

The retinal pigment epithelium (RPE) is a single layer of highly pigmented cells which extend from the optic disc to the ora serrata. This layer is located adjacent to the photoreceptors as shown in Figure 1.3. The cells themselves are hexagon shaped and columnar within the centre of the retina (14µm tall, 10 µm wide) and flatter in the periphery (10 - 14µm tall, 60µm wide) (Forrester, 2007).

The basal part of the RPE has numerous infolds and forms a part of Bruch's membrane, with a strong attachment to the chorioid. The apical side of the RPE contains many microvilli which extend into the photoreceptor layer and envelop the rod and cone outer segments. Even though the microvilli envelop the outer segments of the photoreceptors, they do not share any intracellular junctions, which means this whole epithelium is separated from the photoreceptors by the inter-photoreceptor matrix. The RPE is part of the blood retinal barrier and is important in the

maintenance of the correct environment for the photoreceptors. This is achieved by the lateral side of the RPE cells being joined by zonula occludens (Remington, 2012).

The RPE has many roles to maintain correct and efficient retinal functioning. One such role is the absorption of light by melanin to prevent scattering or reflection of light back to the photoreceptors. Another major role of the RPE is the maintenance of the photoreceptors themselves. The RPE achieves this by phagocytosing outermost membranes of rod outer segments (and cone to a lesser extent) in order to turnover damaged photopigment. The RPE is also essential in recycling inactive photoisomerized visual pigment to synthesize an active isomer ready for production of rhodopsin (Sharma et al., 2005). This process known as the visual cycle of retinal involves *trans*-retinal being transported to the RPE, where it is re-isomerized to 11-*cis*-retinal and returned to the photoreceptors (Strauss, 2005). The RPE is responsible for the formation of the interphotoreceptor matrix, the layer of proteins and glycosaminoglycans present between the RPE and the photoreceptors. The RPE performs a vital role in pumping fluid from the sub-retinal space to the choroid. This creates a negative hydrostatic pressure which keeps the retina in contact with the RPE. The RPE also plays an important role in the protection of photoreceptors from oxidative stress. A reduction in RPE cells which can be caused by age related macular degeneration (AMD) or a build-up of toxic substances can lead to a decrease in important anti-oxidants such as α -tocopherol and therefore an increase in ROS (Strauss, 2005).

1.2.3 Photoreceptors

Photoreceptors are the cells responsible for the transduction of light into a neural signal. This is achieved via two types of photoreceptor cell which contain photopigments that absorb and become activated in response to light. Light results in inhibition of neurotransmitter (glutamate) release (in dark conditions glutamate is released). These two photoreceptors are called rods and cones both of which have a relatively similar structure (Figure 1.4).

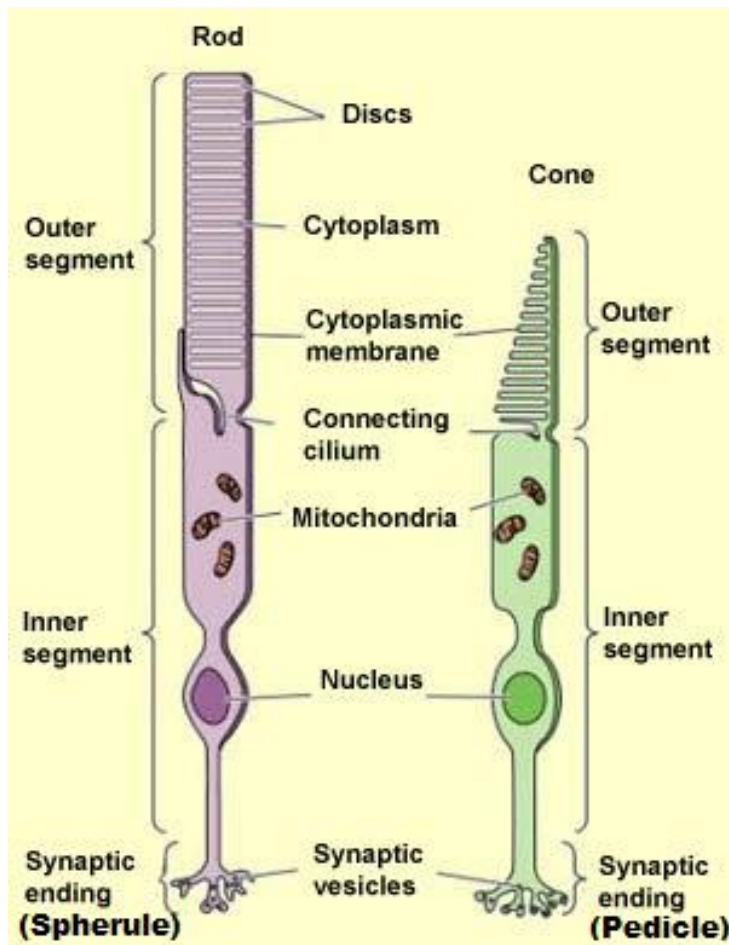


Figure 1.4 - Photoreceptor Structure. Source : http://2.bp.blogspot.com/-PmNqGn4tmI8/Txw3Fh7ehKI/AAAAAAAAAQs/CEIUB7Pak6U/s1600/d_02_m_vis_1a.jpg

The outermost region of the photoreceptor (the part closest to the RPE) contains stacks of membrane disks and is referred to as the outer segment. Each disk contains photopigment enclosed within a membrane sac, which is held within the cell by the plasmalemma (the outer membrane of the outer segment) and separated from each other by an extradisk space. There are major differences between rod and cone outer segments which are explained later.

The cilium is the next part of the photoreceptor. This is a connecting stalk which joins the outer segment to the inner segment. The cilium has an axoneme which is formed from 9 pairs of microtubules. The role of the cilium is the trafficking of proteins for phototransduction from the inner segment into the outer segment ready for use. The cilium achieves this trafficking via a process called intraflagellar

transport (IFT). This method of transport is accomplished via IFT particles binding with motor proteins which transport the IFT (bound with its cargo) along the microtubules either towards the outer segment or towards the inner segment. For anterograde transport of, for example rhodopsin, the IFT particle bound with rhodopsin attaches to the motor protein heterotrimeric kinesin II which then travels along the microtubules of the axoneme. For retrograde transport to the inner segment the IFT particle binds to the motor protein dynein (Ramamurthy and Cayouette, 2009).

The inner segment of the photoreceptors can be further subdivided into further parts. The ellipsoid is the subsection nearest the outer segment and contains high numbers of mitochondria. The myoid is the second subsection closest to the outer fiber and contains the protein synthesis and processing organelles such as the Golgi and the endoplasmic reticulum.

The outer fiber is the section which links the myoid and the cell body together. The cell body is then linked to the inner fiber which is an axonal process with the synaptic terminal at the end. The neurotransmitter for both rods and cones is glutamate (Remington, 2012).

There are many differences between rods and cones. Rods are taller than cones, at around 100 – 120 μ m long and the inner and outer segments are a similar shape (Forrester, 2007). Rods are specialised to work in darker conditions and use the photopigment rhodopsin which has a maximum sensitivity to blue-green light at 496nm (Forrester, 2007). In the outer segment of rods, the plasmalemma (the outer membrane) is separate from the membrane disks and as new disks are formed at the base of the rod outer segment, older disks are pushed further up until eventually phagocytosed by the RPE. There are on average 1000 disks per outer segment in each rod with an average life span of 10 days for each disk before it is phagocytosed at the end of the outer segment. At its opposite end, the rod terminates to synapse forming a spherule (smaller than the cone synapse).

Cones are shorter than rods (on average 60 - 75 μ m) and within the outer segment of cones, basal disks are often wider than the disks at the tip, giving them the conical shape (Forrester, 2007). This however is not always the case, with cones located around the fovea being long and slender and much more tightly packed. The disks

within cones are different to rods; they have a longer lifespan than rods and are not produced from the base up. The plasmalemma runs alongside the disks instead of being separate. Whereas rods are most efficient in dim light, cones work better in brightly lit conditions with each cone possessing one of three photopigments that work at different wavelengths. These are for blue light (420nm), green light (531nm) and red light (588nm) (Remington, 2012). The synaptic connection from the inner fiber of the cone (known as the pedicle) is also different to that of the rod: it is wider and contains more synaptic connections including gap junctions between other photoreceptors.

1.2.4 Bipolar Cells

Bipolar cells are the cells responsible for transmitting the neural signals from photoreceptors to ganglion cells.

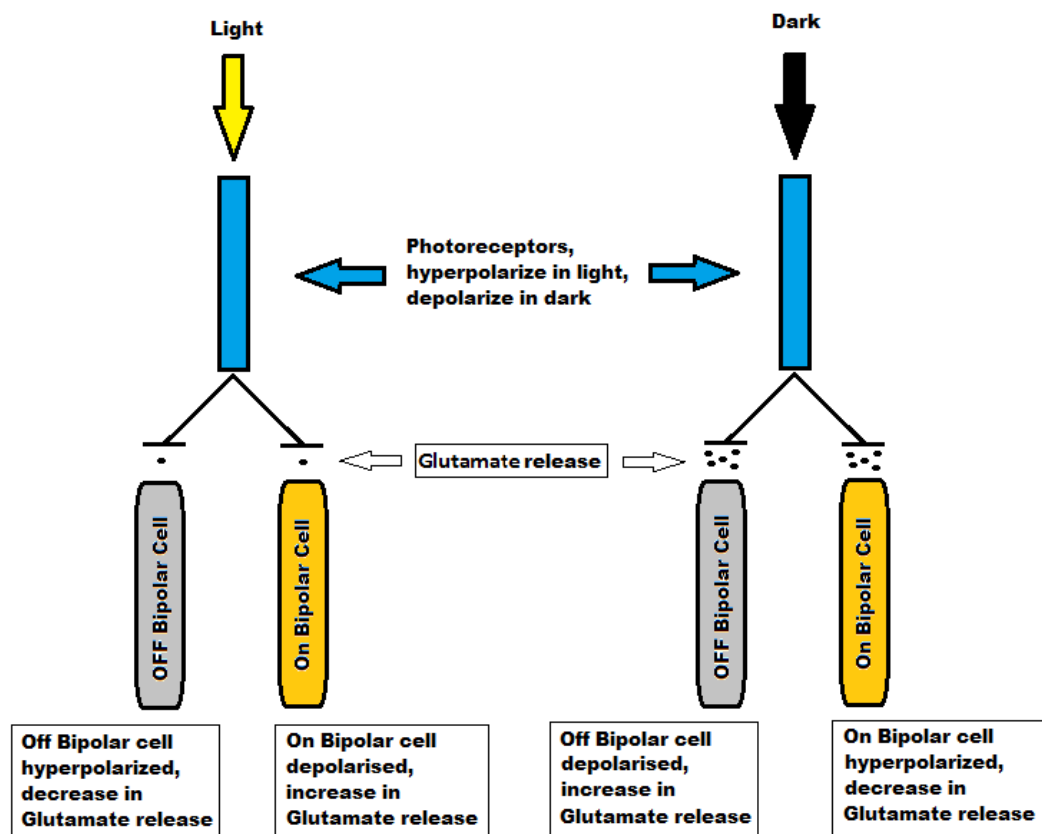


Figure 1.5 - Depolarization and hyperpolarization of ON and OFF bipolar cells

Bipolar cells play a large role in visual acuity, with some foveal bipolar cells synapsing with one cone, and further sending this information directly to one ganglion cell. Within the periphery, bipolar cells synapse with many photoreceptors where sensitivity, not acuity is the main priority. When described on a functional basis, there are two main types of bipolar cell, ON and OFF bipolar cells, both of which respond differently to the same stimulus (glutamate) within the centre of its receptive field. In light conditions when photoreceptors do not release glutamate, ON cells respond by depolarizing whereas OFF cells respond by hyperpolarizing (as shown in Figure 1.5).

This difference in ON and OFF bipolar cell responses is due to different expression of glutamate receptors: ON cells express metabotropic glutamate receptors which initiate an intracellular pathway to increase conductance to depolarize, whereas OFF cells express more ionotropic glutamate receptors which in the absence of glutamate, conductance is decreased and the cells hyperpolarize (Nelson and Connaughton, 1995). As with photoreceptors, the neurotransmitter used by bipolar cells is glutamate. When described morphologically, there are several types of bipolar cell, however only one type is associated with rod cells.

Rod bipolar cells are the only bipolar cells that synapse with rod cells. They are present from approximately 1mm away from the fovea and continue into the periphery. Close to the fovea, each rod bipolar cell makes contact with around 15 – 20 rods, further out into the periphery, each rod bipolar cell can contact up to as many as 80 rods (Kolb et al., 1992).

There are two types of midget bipolar cells, flat and invaginating. Flat bipolar cells differ from invaginating in that they only contact the flat surface of the cone pedicle. Invaginating bipolar cells differ from flat cells because the dendrites are invaginated, surrounding the cone pedicle. Within these invaginations there are triads which consist of a single bipolar cell with two horizontal cell processes on either side which are surrounded by the invagination.

Diffuse cone bipolar cells differ from other bipolar cells in that they are important in converging information from multiple cones with dendrites that span out as far as 100µm and contact as many as 7 cone pedicles (Forrester, 2007).

Blue cone bipolar cells are named so because they appear to only contact cones specifically with pigment sensitive to blue light. There is also a giant cone bipolar cell which gains its name from the size of its dendrites.

1.2.5 Ganglion Cells

Ganglion cells are the last neural cell from the retina in the visual pathway. Ganglion cell axons exit the ganglion cell layer and run along the nerve fiber layer (parallel with the internal limiting membrane), the axons then come together at the optic disc and pass throughout the lamina cribrosa (a sieve like perforation at the posterior of the eye) to form the optic nerve. Beyond the lamina cribrosa the axons become myelinated by oligodendrocytes. There are approximately 1.2 million ganglion cells within the human retina, with an average of around 100 rods and 6 cones to each ganglion cell (Forrester, 2007). Ganglion cells can be classified in two main ways. They can be classified depending on the area within the lateral geniculate nucleus where they terminate. Ganglion cells which terminate in the parvocellular layer are called P cells. There are two types of P cell, P1 and P2. P1 cells are also known as midget ganglion cells and are the most common retinal ganglion cell and only form connections with midget bipolar cells (flat or invaginating). P2 cells terminate within the same layer however their morphology is different with P2 cells having a dendritic tree that spreads horizontally (Remington, 2012). M type ganglion cells are present within the central retina and are named because they project to the magnocellular layer within the lateral geniculate nucleus. When classified morphologically there are 18 types in the human retina

1.2.6 Amacrine Cells

There are many types of amacrine cell, which differ in shape, size and importantly neurotransmitter used. Amacrine cells release many types of neurotransmitter, however the main two are GABA or glycine, both of which are inhibitory neurotransmitters. Amacrine cells possess a single process that branches out and makes multiple connections with bipolar neurons, ganglion cells, interplexiform neurons and other amacrine cells. From this information it is believed that the main

role of these cells is the inhibitory modulation of information to the bipolar cells (Forrester, 2007).

1.2.7 Horizontal Cells

Horizontal cells possess processes that extend horizontally and run parallel with the retinal surface. They are present throughout the retina, but are much smaller in the foveal region (Kolb et al., 1994). The purpose of these cells is to provide inhibitory feedback to either photoreceptors or bipolar cells. There are three types of horizontal cell; HI, HII and HIII. They are differentiated depending on the contacts they make and their morphology. HI cells have dendritic processes that synapse with nearby cones (mainly green and red cones) and a large fan shaped axon that terminates in rod spherules. HII cell dendrites predominantly contact blue cones, whereas the HII cell axon exclusively contacts blue cones. HIII cells have a large dendritic field, however differ from HII cells in that they do not synapse with blue cones (Ahnelt and Kolb, 1994).

1.2.8 Interplexiform Neurons

Interplexiform neurons are found amongst amacrine cells and have processes which descend into the inner plexiform layer and ascend into the outer plexiform layer. The purpose of these cells is to provide “long range” feedback from inner retinal layers to outer retinal layers. Interplexiform neurons can also be divided depending on their neurotransmitters which include glycine, GABA, dopamine and somatostatin. The dopaminergic and glycine interplexiform neurons are believed to be involved in light adaptation. The connections that interplexiform neurons form are both pre-synaptic and post-synaptic to rod and cone cells, however input to the interplexiform cells is still unclear (Jiang and Shen, 2010).

1.2.9 Müller Cells

Müller cells are the most abundant neuroglial cells in the retina, with approximately 10 million present throughout the human retina. The cell bodies of Müller cells are located within the inner nuclear layer and they have extensive processes that span from the inner limiting membrane to the outer limiting membrane. Their primary role is a supportive one, both physically and metabolically. They occupy the majority of the space not occupied by neurons and Müller cell processes ensheath neuronal somata and processes as well as blood vessels, allowing the transport of nutrients, waste, ions, water to support neurones (Reichenbach and Bringmann, 2013).

Müller cells importance in the support of the neural retina is shown by the variety of roles they play, such as the maintenance of the correct environment by, regulating ion and pH levels (Forrester, 2007). They are responsible for the metabolism of glucose to provide neurones with lactate / pyruvate for their oxidative metabolism as well as regulating retinal blood flow and contributing to the maintenance of the blood retinal barrier. Importantly Müller cells also play a role in the neuronal signalling. They achieve this by the rapid uptake of glutamate from the extracellular space and conversion to glutamine ready for neurones to produce glutamate (Bringmann et al., 2006).

Müller cells are also involved with most pathological alterations of the retina by becoming activated (known as Müller cell gliosis). They have the ability to produce proinflammatory cytokines in response to infection and upon activation can influence vasculature and immigration of blood-derived leukocytes (Bringmann et al., 2006).

1.2.10 Retinal Astrocytes

Retinal astrocytes are located within the nerve fiber layer, ganglion cell layer, inner plexiform layer and the inner nuclear layer. Within these layers they lay perpendicular to Müller cells, ensheathing nerve fibers and retinal capillaries. Their role in the retina is similar to Müller cells including isolating the receptive regions of the neurones to prevent interference from active neighbouring neurones (Forrester, 2007).

1.2.11 Retinal Microglia

Retinal microglia are phagocytic immune cells which are evenly distributed throughout the retina (except in the fovea where they are normally absent), but located in two main regions: between the nerve fiber layer and the ganglion cell layer, and between the inner nuclear layer and the outer plexiform layer. When inactive they have the characteristics of a resting macrophage, however when injury or inflammation occurs they then take on the appearance of an active phagocyte (Forrester, 2007).

1.3 Retinal Toxicity

1.3.1 Introduction

According to the Dictionary of Toxicology (2nd Edition Macmillan Reference Ltd, 1998) toxicity is defined as the ability of a chemical to cause a deleterious effect when the organism is exposed to the chemical. Toxicity itself depends on many factors; this is shown by many chemicals / food / drugs that people are exposed to daily which are classed as toxic. A simple example is alcohol: too high a dose or extended periods of exposure can have toxic effects, however low doses have been found to be beneficial in some circumstances. This brings about questions of how to define the toxicity of a substance. The 'Guide to Practical Toxicology, Evaluation, Prediction and Risk' states that some of the determining factors of a compound's toxicity are: dose (including frequency of dose), exposure, species, individuality, receptor presence, absorption, metabolism, protein binding (availability of site, competitive binding), presence of other chemicals which may enhance / inhibit the effect and the physical form of the toxin (Woolley, 2003).

Toxicological studies span a wide variety of areas. Common areas of research include: the establishment of a dose response curve, safety assessment of new chemicals including pesticides, drugs and food additives (which must follow strict government and international guidelines), mechanistic toxicity studies, epidemiological studies and importantly, studies which investigate new methods to assess toxicity (Woolley, 2003).

The need to investigate new methods for toxicity analysis stem from issues involving current testing. Investigation into cell lines is cheaper than investigation into animal models, however there are limitations to a single cell system. Organotypic models contain the multicellular property and the same structural integrity of the tissue of interest. Animal models are still considered the gold standard in that they provide a multi organ system which is currently impossible to replicate in cells, however species difference (if the investigation is about human health must be considered). This makes the development of models using human tissue very appealing since these can be directly related to toxicity in humans.

1.3.2 Drug Development Process

In most industrialized countries any new drug under development must be assessed for its safety to use. The regulations for this testing are variable and depend on the country, however the general aim of these studies is to show that the benefits of the substance outweigh the risks of use (Timbrell, 1995). The research conducted to produce a new drug normally follows a set of common stages.

These stages can be split into three main sections, these are drug discovery, preclinical development and clinical development (as shown in Figure 1.6). Drug discovery involves the selection of a drug candidate depending on the intended target. Preclinical development involves no live human investigations and involves toxicity and pharmacokinetic studies. Clinical development stages are when the compound is tested for its tolerability and side effects within healthy patients, and its effectivity within patients. If the drug is approved by the regulatory agencies, the drug is marketed and continuing surveillance is conducted (H. P. Rang, 2012).

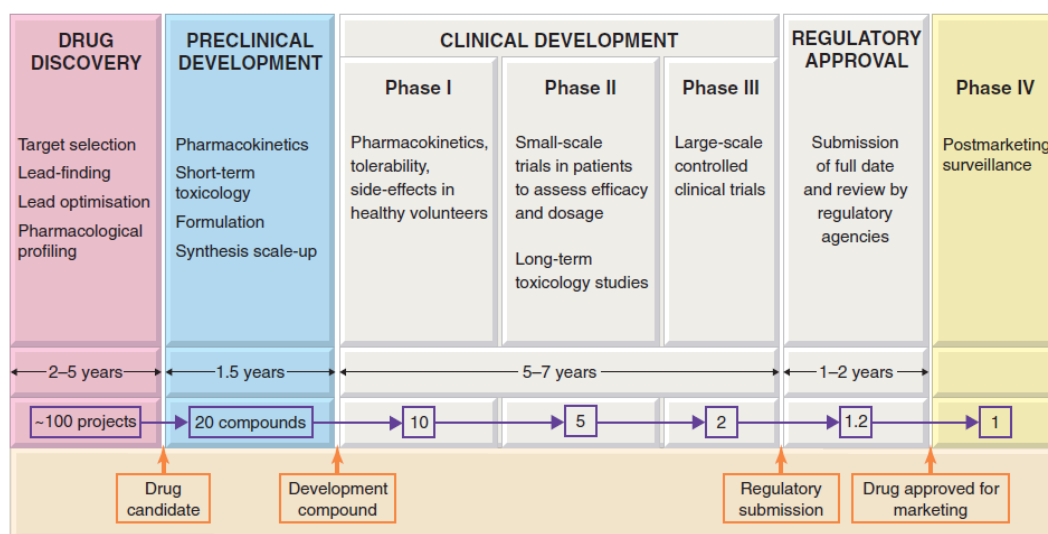


Figure 1.6 - Typical stages of drug development research. Source: (H. P. Rang, 2012).

The process of drug development is time consuming and expensive. It is estimated by 'The Association of the British Pharmaceutical Industry' that the production of a new medicine to a high enough standard of quality, efficacy and safety will take approximately 12 years and 1.15 billion pounds (Industry, 2016). For this reason, models that have the capability to indicate any specific toxicity that may occur in the

early stages of drug development research (drug discovery or preclinical development) are of interest as they have the potential to save time and money.

Retinal toxicity is a major reason of drug development termination. According to Pfizer's internal drug development database, ocular toxicity is responsible for 7% of therapeutic candidate attrition of which 99% were related to retinal toxicity (Huang et al., 2015).

For this reason it is important that available models and methods used to assess retinal toxicity are understood and utilised.

1.3.2 Models and Methods Used to Assess Retinal Toxicity

The assessment of ocular toxicity currently relies on *in vitro* and *in vivo* approaches which are applied mostly within the preclinical development stage of drug development research. *in vitro* toxicity screens may be conducted on cell lines and organotypic models, however *in vivo* models are still required as a pre-clinical safety evaluation step of drug development (Huang et al., 2015).

In vivo approaches to assessing the safety of drugs produced for the treatment of retinal diseases involve a multitude of animal models. Mice and rats provide genetic models of disease for the drug to be tested on, whereas pigs, dogs and cats are used as large animal models. Rabbits are commonly used in retinal toxicity studies, however the gold standard for *in vivo* studies is still nonhuman primates (Penha et al., 2010). In order to assess ocular health within the *in vivo* approaches, common ophthalmologic methods used clinically are utilised in animal studies to assess changes in retinal function / morphology. Examples of these methods are ophthalmoscopic inspection, in which the fundus of the retina can be viewed and photographed (useful if changes over time wish to be observed). Fluorescein angiography, in which fluorescein dye is delivered intravascularly and traced throughout the eye to reveal any defects in vasculature can also be used. Electroretinography (ERG) may be used to assess retinal function by investigation of neuronal activity in response to specific light stimulus and Ocular Coherence Tomography (OCT), which is a non-invasive method of assessing retinal structure by composing a computed tomography of scattered near infrared light from a laser is

also a more recent and useful technique to assess retinal toxicity (W. M. Haschek, 2013).

There are two human retinal cell lines currently available which could be used to assess toxicity; the MIO-M1 cell line and the ARPE19 cell line. The MIO-M1 cell line is an immortalized cell line derived from human Müller cells. Müller cells are the principle glial cells of the retina which provide structural and metabolic support to neurones (Haberecht et al., 1997). The ARPE19 cell line is a human retinal pigmented epithelial cell line from a primary source of retinal pigmented epithelium (Dunn et al., 1996).

Organotypic retinal cultures have been used from a multitude of species, for example rat organotypic cultures have been characterised and show a high degree of tissue viability for up to 17 days (Johnson and Martin, 2008). Rabbit organotypic cultures have also been used and show tissue viability of up to 4 days (Lye et al., 2007). However the problem in using tissue derived from animals is that the retina possesses different properties compared to the human retina. For example the rat retina has many differences compared to that of the human, being less vasculated, with many different retinal features such as no fovea and a high percentage of rods due to the nocturnal nature of the animals.

1.3.4 Known Retinotoxins

In order to develop a new model for the assessment of retinotoxicity, some known retinotoxins must firstly be used to characterise the model and to determine if the results match those found clinically.

There are many different drugs / compounds which are known to cause retinopathy, in this section a number of known retinotoxic drugs and their potential toxic metabolic pathway are discussed.

1.3.4.1 Chloroquine

Chloroquine has been used in the prevention and treatment of malaria since the early 1950's. It also has been used for the treatment of amoebic hepatitis, amoebic abscesses, systemic lupus erythematosus (SLE), discoid lupus erythematosus (DLE), protozoal infections, and most commonly rheumatoid arthritis (RA) (NHS, 2014c). Chloroquine is available as salts in three forms; chloroquine diphosphate, chloroquine sulphate and chloroquine hydrochloride (Verbeeck et al., 2005;Tzekov, 2005).

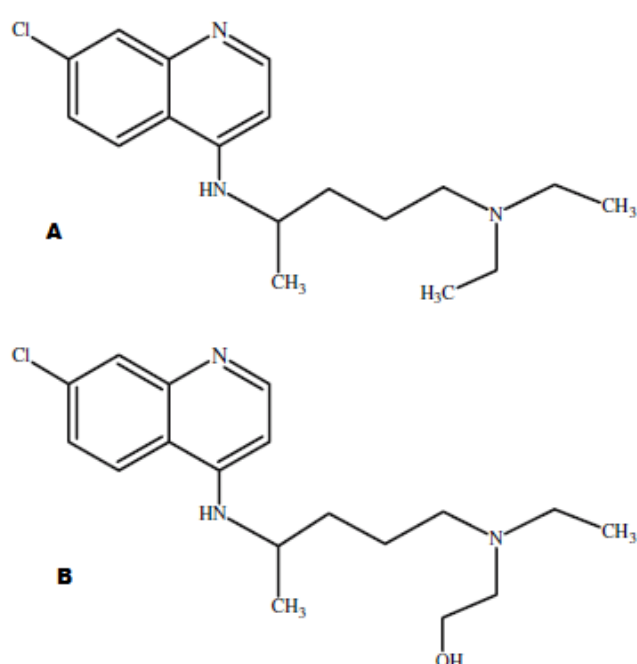


Figure 1.7 - The chemical structure of (A) Chloroquine and (B) Hydroxychloroquine

Source: (Tzekov, 2005)

In the treatment of malaria chloroquine can be administered either orally, or via parenteral administration, although the oral route is most common. When administered orally patients are given a total dose of 25mg/kg over a period of 3 days according to the following protocol:

Day 1: 10mg/kg, followed by 5mg/kg 6 – 8 hours later.

Day 2 and 3: 5mg/kg in a single dose (WHO, 2014).

Chloroquine is readily and rapidly absorbed by the gastro-intestinal tract and although inter-subject bioavailability varies widely, it has an average oral bioavailability of approximately 89% (Verbeeck et al., 2005). A study conducted by Zuluaga-Idarraga (2014) revealed that chloroquine reaches its peak plasma concentration 2 hours after each oral dose, and that throughout the three day treatment of the normal dose described above (25mg/kg), the highest plasma concentration is reached on day 2, with an average plasma concentration of 260.1ng/ml (0.31 μ M) (Zuluaga-Idarraga et al., 2014).

The toxic effects of chloroquine are well documented. The most influential factors which affect the toxicity are dosage, the total amount of time the drug has been taken and the age of the patient. Chloroquine is rarely used now in the treatment of chronic disease due to the availability of the less toxic hydroxychloroquine (see below). However a report by Marks from 1982 states daily doses ranged from 100-1000mg per day (Marks, 1982). A study later summarised older literature and reported that chloroquine can cause retinal toxicity at ≥ 3 mg/kg/day which is at the lower end of the dosage used (Marmor et al., 2002). The cumulative dose of the drug is also positively correlated with toxicity, which is why the total amount of time that the drug is given is important. A cumulative dose of ≥ 200 g has been shown to give a high risk of toxicity (Peponis et al., 2010). Data relating to age is limited, however there is an indication that patients over 60 are more at risk to the toxic effects (Peponis et al., 2010).

Chloroquine retinal toxicity symptoms include that of a loss of vision, either a partial paracentral or complete pericentral ring scotoma (blind spot). These symptoms are not normally noticed until the degeneration caused by chloroquine is advanced (Blomquist, 2011). On ophthalmological examination toxicity caused by the drug is seen on the fundus as granulated pigmentation within the macula region which is surrounded by a ring giving a "bull's eye maculopathy". Although not as common, there are also some cases of visual field loss without the bull's eye maculopathy. This can progress further to give the fundus a spotted appearance (Gaynes et al., 2008).

A study into which cell types are affected by long term exposure to chloroquine was conducted in rhesus monkeys which revealed that ganglion cells were firstly

affected, displaying granulated cytoplasm's, followed by photoreceptor degeneration and eventually RPE deterioration (Rosenthal et al., 1978). More recent studies have utilised OCT and other scanning techniques in the study of chloroquine toxicity in humans and have found that the nerve fibre layer was thinned due to chloroquine treatment, potentially due to a loss of ganglion cells (Pasadhika et al., 2010), (Bonanomi et al., 2006). This data suggesting an initial loss of ganglion cells was re-enforced by data obtained from Costa et al (2007) in which a pair of eyes from a human donor who had received long term chloroquine treatment was obtained and investigated. No differences were found between a control retina and the long term chloroquine treated retina apart from a lack of large sized ganglion cells which may have degenerated due to chloroquine treatment (Costa et al., 2007). In contrast, a study on mice revealed that intraperitoneal administration of chloroquine caused the majority of toxicity to occur in the outer retinal layers, with a marked loss of photoreceptors, thinning of the outer plexiform layer and damage to the RPE (Gaynes et al., 2008). Long term exposure to chloroquine therefore has the potential to affect several cell types of the retina, including the ganglion cells, photoreceptors and the RPE, however the order in which these cells are affected first is still unclear.

There are many theories relating to how chloroquine causes retinal toxicity. One early theory centres around binding to melanin, where it is hypothesised that the high affinity of the drug to melanin leads to accumulation causing toxic levels to be reached in the RPE. This in turn causes the RPE to become unable to phagocytose the photoreceptor outer segments and as a result loss of rods and cones occur (Potts, 1964), (Bernstein et al., 1963). This theory has come under scrutiny, since there has been a lack of evidence to show that melanin binding causes ocular toxicity and chloroquine has been shown to cause retinopathy in albino rabbits, rats and cats (Leblanc et al., 1998).

Another mechanism centres around oxidative stress. An experiment in which male albino rats were treated with chloroquine showed a reduction in retinal glucose-6-phosphate dehydrogenase (G-6-PD) activity and glutathione (GSH) (Toler, 2004). This reduction in GSH concentrations may be due to the reduction in G-6-PD as G-6-PD is involved at two points in the oxidative stage of the pentose phosphate sugar pathway which is important in the production of NADPH and ribulose-5-phosphate (Figure 1.8). A reduction in G-6-PD would inhibit the production of NADPH which

is essential in the reduction of glutathione disulphide (GSSG) to GSH in the glutathione redox cycle (Figure 1.9). This decrease in GSH would cause an increase in oxidative stress which could lead to cell death (Toler, 2004).

Oxidative Stage of Pentose Phosphate Pathway

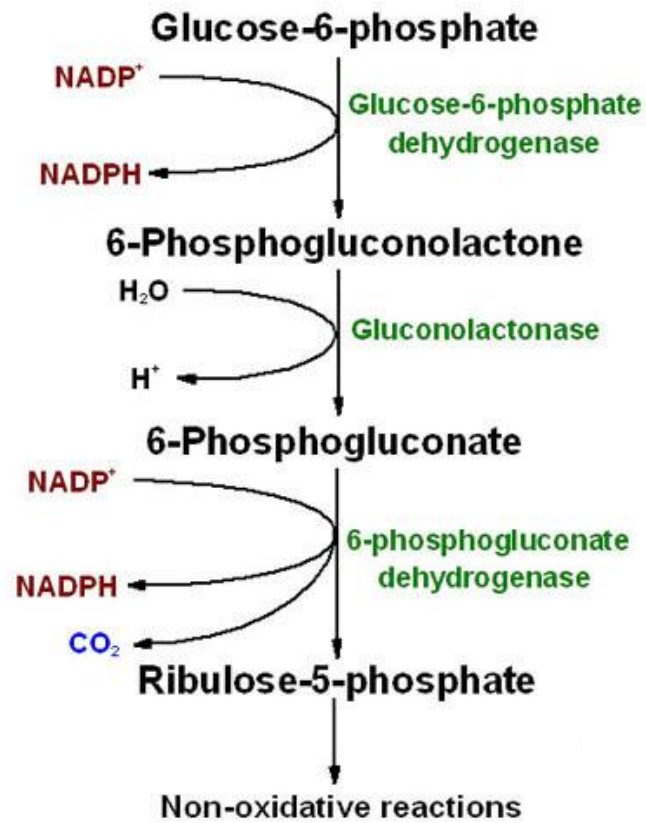


Figure 1.8 - Oxidative stage of the pentose phosphate pathway

Source: <http://themedicalbiochemistrypage.org/pentose-phosphate-pathway.php>

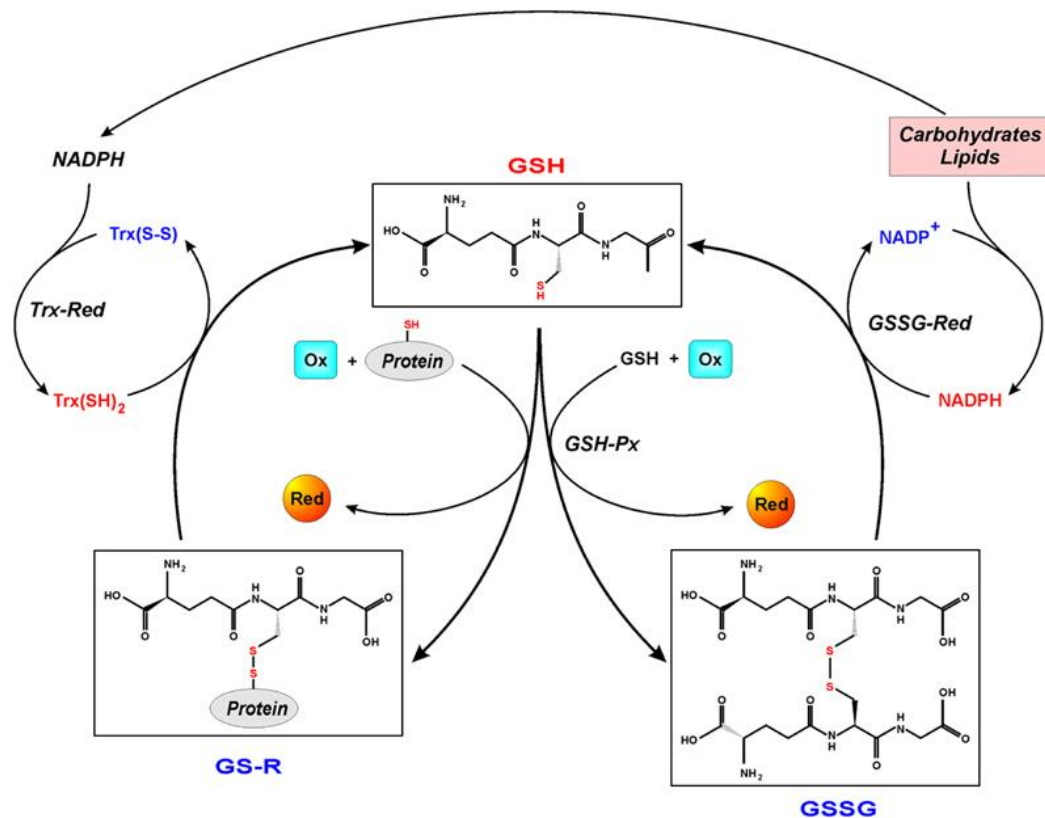


Figure 1.9 - The Glutathione redox cycle. Showing the reduced form of glutathione (GSH) and the oxidized forms of glutathione; GS-R and GSSG. This figure also shows the pathway in which the oxidised forms of glutathione are reduced back to GSH via GSSG-Red or Trx-Red, both of which require NADPH.

Key:

GSH - reduced glutathione

GS-R and GSSG – oxidized glutathione

GSSG-Red - GSSG reductase

Trx-Red – thioredoxin

GSH-Px – Glutathione peroxidase

Source: http://www.nature.com/cdd/journal/v12/n12/fig_tab/4401754f1.html

More recently it has been proposed that the cause of retinotoxicity is due to chloroquine's lysosomotropic properties. This means that chloroquine accumulates in the lysosome, leading to the formation of vacuoles and eventually cell death. This has been extensively studied in RPE cells (Yoon et al., 2010; Chen et al., 2011b).

In an interesting paper, Yoon et al (2010) displayed that caspase dependent cell death appeared not to be the cause of chloroquine induced cell death, as no activation of caspase 3 was detected after chloroquine treatment and a broad range caspase inhibitor z-VAD-FMK did not reduce cell death. This paper also showed that oxidative stress was also unlikely to be the root cause of cell death since the antioxidants (NAC and trolox) failed to reduce cell death (Yoon et al., 2010). In this study, Yoon et al also investigated levels of autophagy and whether this could be responsible for the cell death induced by chloroquine. During autophagy (a process where cellular components are turned over) phagophores are produced (double membranes structure) and cellular components to be degraded are collected within them. Once the components have been sealed in the membrane the structure is known as an autophagosome. The autophagosome then binds with lysosomes to become the autolysosome where the internal components are degraded (Boya et al., 2013). Levels of LC3 proteins are commonly used to assess levels of autophagy since LC3-I is converted to LC3-II in the formation of the autophagosomal membrane. LC3-II is then broken down once the autolysosome has formed (Tanida et al., 2008), (Mizushima and Yoshimori, 2007). Yoon et al (2010) found that LC3-II increased with chloroquine treatment along with p62 (a protein which interacts with LC-3II which is also degraded in the autolysosome) indicating an increase in autophagosome levels. This study also investigated if the increase in LC3-II / p62 was due to inhibition of autophagosome and lysosome binding (to form the autolysosome), and therefore the build up of autophagosomes. This was achieved by looking at the overlap of immunohistochemically stained ARPE19 cells with LC3-II (present in autophagosome membranes) and LAMP1 (present in lysosome membranes). No overlap was found, indicating the build up of LC3-II was due to the inhibition of autophagosome and lysosome binding (Yoon et al., 2010). This occurs because chloroquine is a weak base which concentrates within acidic lysosomes, this in turn causes an increase in lysosomal pH and inhibits optimal functioning of the lysosomal enzymes and inhibits the binding of lysosomes to autophagosomes (Baltazar et al., 2012). This study also showed that when both chloroquine and low concentrations of Bafilomycin A1 were added together, chloroquine did not accumulate within lysosomes to cause lysosomal dysfunction and deformation into vacuoles. This is due to the increased pH caused by Bafilomycin A1, therefore inhibiting chloroquine accumulating in the lysosome. Bafilomycin A1 causes an

increase in lysosomal pH by inhibiting vacuolar-type ATPase and disrupting the vesicular proton gradient causing an increase within the pH of lysosomes (Shacka et al., 2006). Further to this, Yoon also showed that autophagic cellular death does not seem to be a likely cause of chloroquine induced toxicity since the autophagic inhibitor 3-MA (a potent inhibitor of autophagy) also failed to reduce chloroquine induced cellular death (Yoon et al., 2010).

The experiments conducted by Yoon et al indicate the main cause of cell death to be due to a multitude of mechanisms which involve lysosomal dysfunction, whereby an increased accumulation of endocytosed proteins and lipids possess cytotoxic consequences (Yoon et al., 2010).

1.3.4.2 Hydroxychloroquine

Hydroxychloroquine (Figure 2.7) was synthesised in 1964 as a derivative of chloroquine. Since then, it has superseded the use of chloroquine due to a better toxicity profile (Tzekov, 2005). Chloroquine is known to cause retinal toxicity at $\geq 3\text{mg/kg/day}$, whereas this increased to $\geq 6.5\text{mg/kg/day}$ with hydroxychloroquine (Peponis et al., 2010). Hydroxychloroquine is used for the treatment of RA, SLE, DLE and some dermatological conditions caused by sunlight (NHS, 2014a).

Hydroxychloroquine is available commercially as 200mg hydroxychloroquine sulphate tablets (Plaquenil), and due to the toxicity threshold, has a maximum recommended dose of 6.5mg/kg of lean body weight / day (Ophthalmologists, 2009). Standard doses used to treat RA are 200mg to 400mg daily (American College of Rheumatology). For malaria treatment and prevention, the dose of hydroxychloroquine recommended is 400mg as one weekly dose (CDC, 2014).

Hydroxychloroquine is well absorbed within the gastrointestinal tract. After a single 200mg dose of hydroxychloroquine peak plasma concentrations occurs at a mean time of 3.2h post treatment, with a maximum mean plasma concentration of 46ng/ml (0.1 μM) (Tett et al., 1989).

Patients using hydroxychloroquine are screened for ocular side effects in the same way as those who take chloroquine. Both drugs can cause the same clinical

symptoms of visual field defects such as scotomas and are known to cause a change in the appearance of the fundus, with granulated pigmentation and a bull's eye maculopathy (Tzekov, 2005). The method of cell toxicity caused by hydroxychloroquine appears to be the same as that caused by chloroquine; via accumulation within lysosomes (Sundelin and Terman, 2002).

1.3.4.3 Indomethacin

Indomethacin was introduced in 1963 as a non-steroidal anti-inflammatory drug (NSAID) for the treatment of rheumatoid arthritis. It has also been used for other inflammatory conditions due to its anti-inflammatory properties (Graham and Blach, 1988). Indomethacin dosage is variable depending on the degree of pain and inflammation and is available as 25mg and 50mg capsules to be taken orally or 100mg as suppositories. Indomethacin can be used to treat many inflammatory disorders associated with pain including ankylosing spondylitis, bursitis, capsulitis, gout, menstrual problems, osteoarthritis, rheumatoid arthritis, spondylitis, synovitis, tendonitis and tenosynovitis (NHS, 2014b).

Indomethacin is readily absorbed within the gastrointestinal tract. After a 75mg dose the mean peak plasma concentration (measured by HPLC) was at one hour post oral administration showing a concentration of 4.9 μ g/ml (13.7 μ M) (Bechgaard et al., 1982).

Although indomethacin retinopathy cases are rare, it is associated with other reactions such as neutropenia, hepatotoxicity and agranulocytosis (Toler, 2004). Retinopathy symptoms caused by indomethacin include difficulty with night vision, impaired colour vision, photophobia and reduced visual acuity (Peponis et al., 2010). Clinically, the changes seen with indomethacin retinal toxicity are changes in the RPE (granulation) along with occasional changes in electroretinogram (ERG) and electrooculogram (EOG). Graham and Blach (1988) also reported a bullseye maculopathy in a 33 year old patient who suffered arthritis and had been taking 200mg of indomethacin daily for 8 years (in conjunction with no other medication).

Indomethacin is thought to be toxic to the retina via the production of a reactive quinone. This mechanism is also thought to be the cause of toxicity to other tissues

including neutropenia and hepatotoxicity. Figure 1.10 shows the proposed pathway which involves indomethacin being O-dealkylated into O-des-methylindomethacin (DMI). This then undergoes N-deacetylation to produce desmethyl-deschlorobenzoylindomethacin (DMBI) (Toler, 2004). DMBI is a major metabolite of indomethacin (Ju and Utrecht, 1998) and it is DMBI that is believed to form the reactive quinone that can either react with GSH, leading to GSH depletion and consequent oxidative stress, or bind to other macromolecules to cause retinopathy (Toler, 2004).

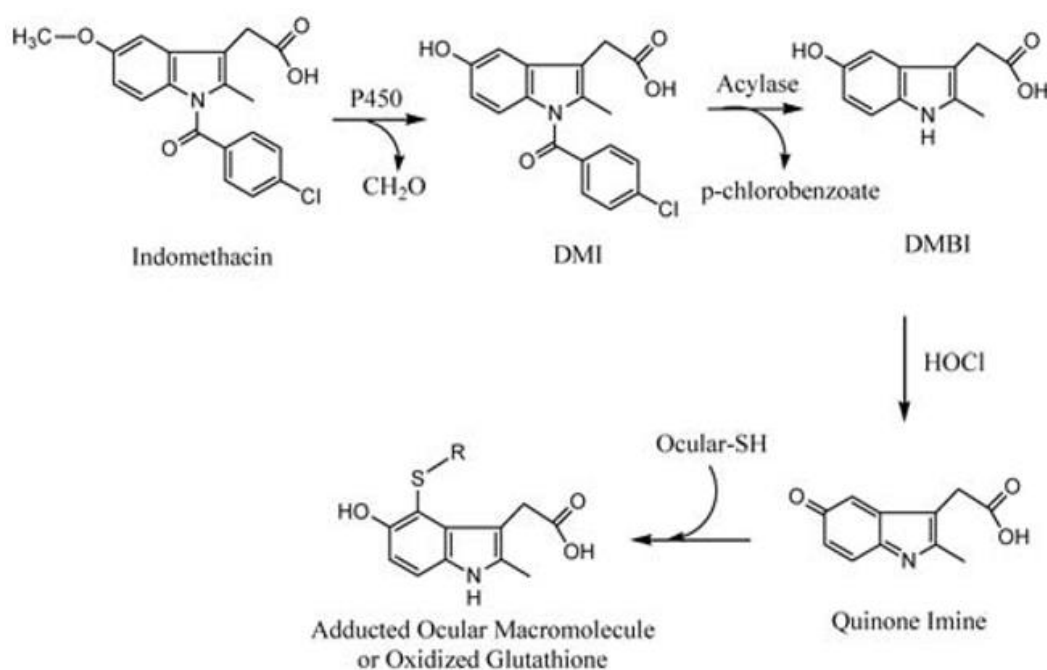


Figure 1.10 - The proposed metabolism of indomethacin to a toxic quinone

Source: (Toler, 2004)

1.3.4.4 Tamoxifen

Tamoxifen is a selective estrogen receptor modulator (SERM) which is used as hormone therapy in the treatment and prevention of hormone responsive breast cancer (Srikantia et al., 2010).

Tamoxifen is available as tamoxifen citrate in 10mg, 20mg and 40mg tablets or a 10mg/5ml oral solution (NHS, 2014d). It is taken as a single daily dose (normally between 20mg and 40mg) (Srikantia et al., 2010).

Tamoxifen citrate is readily absorbed from the GI tract and quickly undergoes hepatic metabolism and excretion of its metabolites (Shin et al., 2006). Tamoxifen pharmacokinetics have been investigated in humans and it was found that the drug reached an initial peak concentration of approximately 167nM in the blood approximately 4h after a single 30mg dose. It was also found that over time, the dose increased until it reached a continuous steady state of approximately 467nM after one month of single 30mg doses (Etienne et al., 1989).

Retinal toxicity is rare from the use of tamoxifen alone (0.6%), but the use of tamoxifen alongside chemotherapy can increase the risk to 10.9% (Srikantia et al., 2010). Although the risk is low, the numbers affected are high due to the large number of patients requiring the treatment. Patients who have tamoxifen induced retinal toxicity often have symptoms of decreased visual acuity and gradual diminution of vision. Clinically, cases of tamoxifen retinal toxicity can present with ocular abnormalities including pigmented retinopathy, macula edema, macula hole and yellow/white spots in the paramacular region (Watanabe et al., 2010; Lazzaroni et al., 1998).

Retinal tamoxifen toxicity normally occurs in patients who have been prescribed the drug for an extended period of time. Early cases of tamoxifen induced retinopathy were seen in patients who took 240-320mg per day. Since then the dose has been reduced to 20-40mg per day (Srikantia et al., 2010). However extended use of the drug leading to a cumulative dose of higher than 16g has been known to induce toxicity (Lazzaroni et al., 1998).

One proposed mechanism of toxicity caused by tamoxifen is implied due to its side effect of neutropenia which is similar to that seen with indomethacin, suggesting that

a similar mechanism may be responsible involving the production of a reactive quinone. The process is shown in Figure 1.11 with tamoxifen being metabolised to 4-hydroxytamoxifen. From this point 4-hydroxytamoxifen can be metabolised through two main pathways, one direct metabolic pathway produces a relatively stable quinone methide. The other pathway can involve the enzyme tyrosinase which can metabolise 4-hydroxytamoxifen to 3,4-dihydroxytamoxifen. This can then be oxidized to produce a reactive ortho-quinone (Zhang et al., 2000) which can oxidise GSH, depleting GSH levels and causing oxidative stress and cell death (Fan and Bolton, 2001). The reactive ortho-quinone could also bind to important macromolecules causing cell disruption and eventually death (Toler, 2004).

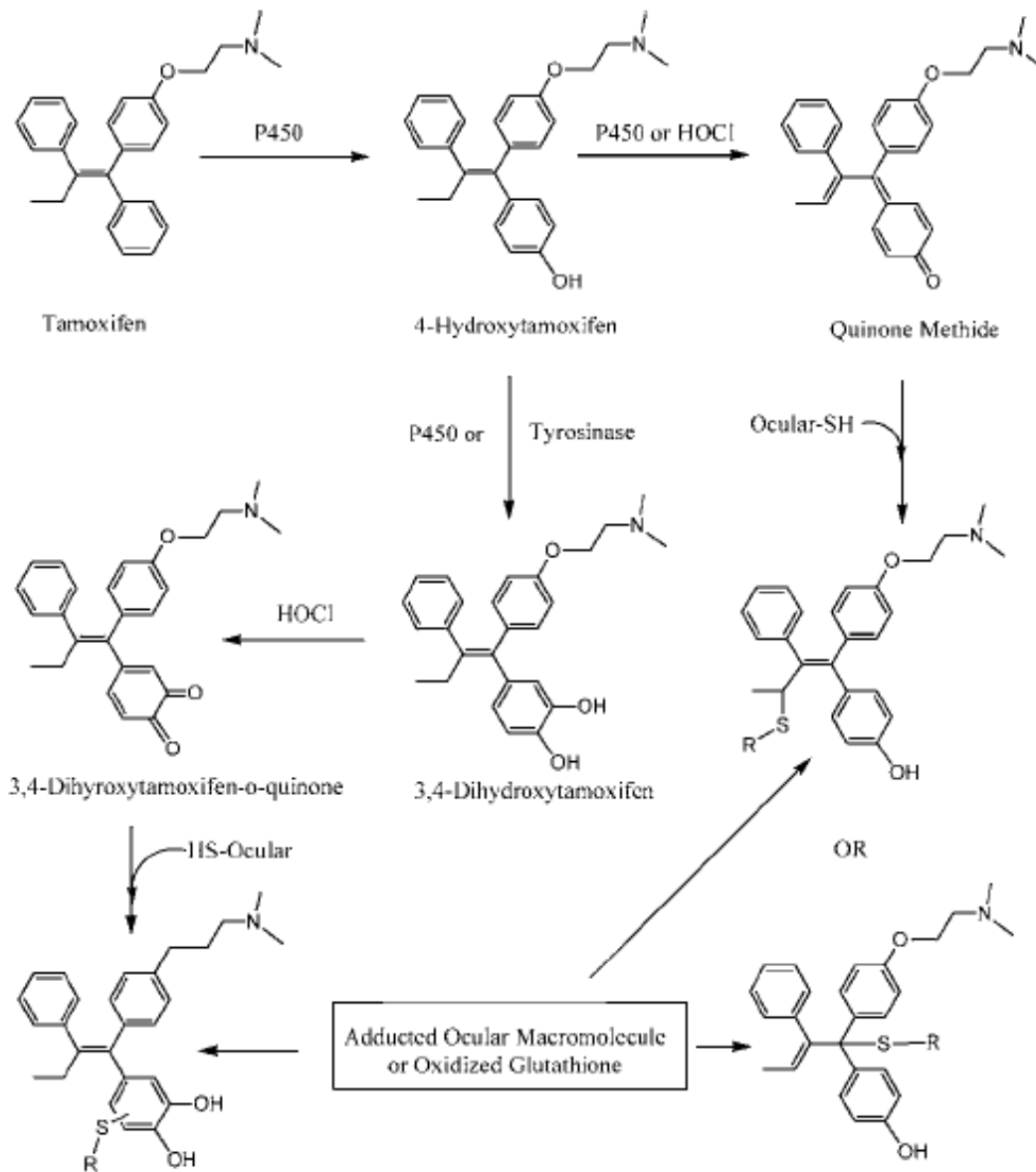


Figure 1.11 - The proposed metabolism of Tamoxifen into a toxic quinone

Source: (Toler, 2004)

Cho et al (2012) have investigated tamoxifen toxicity in RPE (ARPE19) and photoreceptor derived (661W) cell lines and suggested that multiple mechanisms may be responsible for the cell death found. Oxidative stress was found to be involved in tamoxifen induced death, with an increase in ROS and protection by the addition of the antioxidant N-acetyl cysteine (NAC). It was also found that zinc dyshomeostasis may be involved in the oxidative stress caused by tamoxifen, shown by a reduction in ROS and attenuation of cell death with zinc chelation. Cho et al

(2012) also found that autophagic cell death may be involved in tamoxifen induced toxicity, with increased LC3-II levels, and attenuation of cell death with the addition of the autophagic activation inhibitor 3MA, and bafilomycin A1 which inhibits fusion of autophagosomes and lysosomes. Levels of p62 were also investigated (p62 is present within the autophagosome, but is degraded in the autolysosome), showing that binding of the autophagosome and lysosome occurred indicating that tamoxifen upregulated autophagy. Finally it was also found that caspase-3 contributed to tamoxifen toxicity due to the attenuation of cell death with the caspase-3 selective inhibitor DEVD (Cho et al., 2012). A similar study was also carried out by Kim et al (2014) in which it was found that lysosomal destabilisation and cathepsin release occurred before caspase dependent and caspase independent death occurred (Kim et al., 2014).

1.3.5 Aims of Research

Organotypic cultures using human tissue are desirable models to assess retinotoxicity. Human *ex vivo* retinal explants possess the same structural architecture as the *in vivo* retina, allowing the investigation of toxicity to all retinal cell types. The *ex vivo* human retina has not previously been used to assess retinotoxicity and since the retina is known to be particularly susceptible to toxic insult, a model which can measure a drug's potential toxicity to the human retina is of interest. This *ex vivo* human retina model could firstly be used to screen the potential retinotoxicity of a drug, and secondly as a tool, to investigate the cause of the toxicity. It is for this reason that the primary aim of this thesis was to assess human organotypic retinal cultures (HORCS) for the assessment of retinotoxicity.

Previous work using HORCs has shown that they can be used to investigate retinal ganglion cell degeneration. Niyadurupola et al (2011) assessed ganglion cell viability within HORC's over a course of 4 days in different media and no difference in THY1 expression was found when cultured in either DMEM/HamF12 medium or Neurobasal A medium. The study then assessed the effect of OGD (oxygen/glucose deprivation) and NMDA excitotoxicity on ganglion cells and found that a reduction in THY1 mRNA occurred as a result of both OGD and NMDA excitotoxicity,

showing that treatments expected to kill RGC's caused a measurable loss of ganglion cells, indicating the validity of the system (Niyadurupola et al., 2011).

It has also been shown that other markers of ganglion cells (NeuN and β -III Tubulin) that are used in rodents are suitable for the assessment of ganglion cells in the human retina, and that the age of the donor and the post mortem time (within 24h) did not affect ganglion cell number / density (Osborne et al., 2015b).

The specific aims of this research are to firstly characterise the *ex vivo* human retina to gain an understanding of the structure of the retina, and the cell specific markers available to utilise within later research. Secondly a range of known retinotoxins will be applied to two retinal cell lines (ARPE19 and MIO-M1) and the potency of the drugs investigated, this will aid in establishing the retinal cell lines for future use in investigating retinotoxicity. Next one of the known retinotoxins investigated on the retinal cell lines will be applied to the HORC and the response investigated. Once the HORCS response to a known retinotoxin has been investigated, the HORC will then be used to investigate mRNA expression of genes relating to a novel retinotoxin.

Chapter 2

2.0 Methods

2.1 Donor Human Eyes

Donor eyes were provided by the East Anglian Eye bank (Norfolk and Norwich University Hospital, UK) with written consent from the next of kin given for research. The eyes were donated for corneal transplant and following removal of the cornea the remainder of the eye was used for research. The tissue had full ethical approval under the tenets of the declaration of Helsinki, only donated eyes under 24 hours post-mortem were used for research. In the case of living donor tissue, the eye was enucleated during surgery, transported to the lab and the retina dissected within 1h. To ensure no personal information would identify the donor, a donor number was provided. Details of gender, a brief medical history, cause of death and age were provided and any eyes with known retina disease were not used for this research. A database of these details made for the donor eyes used.

Donor eyes were transported from the eye bank in Eagles minimum essential medium (EMEM) (Sigma-Aldrich, Poole, UK) supplemented with the antibiotics gentamicin (50 μ g/ml), penicillin (10,000units/ml), streptomycin sulphate (10,000 μ g/ml), amphotericin B (an antimycotic, 25 μ g/ml) (Invitrogen, Paisley, UK). The lens was removed and used by the lens research group before the retina was dissected.

In total 180 eyes human eyes were used in the research presented in this thesis from donors aged 41 to 92 years old.

2.2 Retinal Dissection

A 10mm incision was made through the sclera and the ciliary body. The sclera and anterior retina was then cut circumferentially below the ora serrata to remove the anterior sclera and all of the ciliary body. The remainder of the sclera was rotated to use the weight of the vitreous to detach the retina from the RPE. At this point the retina's only attachment point to the sclera was the optic nerve, therefore a small cut around the optic nerve head was made. The retina and vitreous was transferred to a

60mm Petri dish (Fisher Scientific, Loughborough, UK). The vitreous was then carefully removed from the retina and discarded. The retina was then flattened by making small incisions from the outer edge of the retina, being careful to avoid areas of the retina needed for experimentation. The macula region was then removed using a 4mm diameter micro-dissecting trephine (Biomedical Research Instruments, MD, USA) and placed into a 35mm petri dish containing 1.5ml serum-free DMEM/HamF12 medium (Fisher Scientific). The remainder of the retina in the 60mm petri dish (Fisher Scientific) was then placed over a template which allowed paramacula explants to be taken at a consistent distance and position from the macula explant (Figure 2.1). Five paramacula explants were taken and placed into one 35mm Petri dish (Fisher Scientific) containing 1.5ml serum-free DMEM/HamF12 medium (Fisher Scientific) to randomise the samples prior to experimentation. Explants were kept in a humidified incubator at 35°C in 95% air, 5% CO₂. Explants were then placed into experimental conditions, or if untreated, prepared for further analysis.

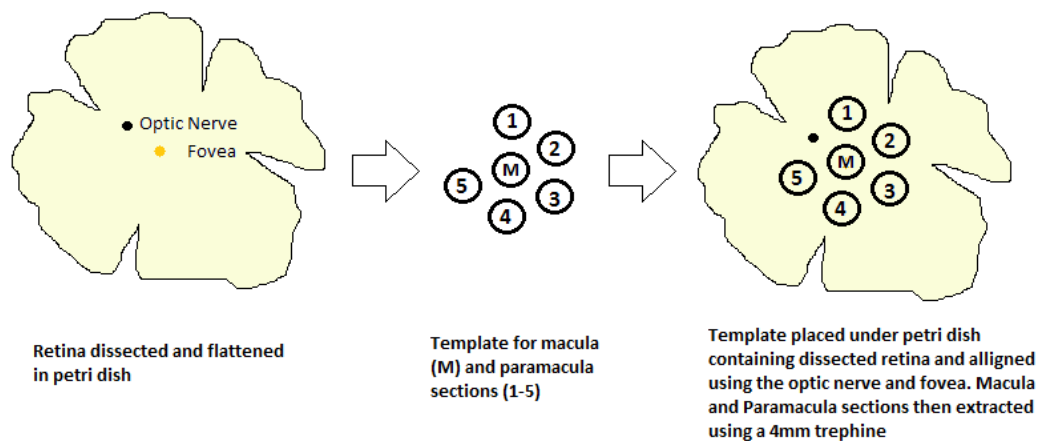


Figure 2.1 - Diagram of Macula and Paramacula Sample Extraction Technique

2.3 Cell Culture

Cell lines were cultured in a humidified incubator at 35°C in 95% air, 5% CO₂ in 75cm² culture flasks (Fisher Scientific). When approximately 90% confluent, cells were passaged. The cell medium was firstly aspirated and the cells washed in 5ml Dulbecco's phosphate buffered saline (DPBS) (Invitrogen). The DPBS was aspirated and 5ml 0.05% Trypsin-EDTA (Life Technologies, Paisley, UK) was applied to the cells and for approximately 3 minutes until the cells were no longer adhered to the

cell culture flask. The Trypsin-EDTA was neutralised through the addition of 10ml 10% foetal bovine serum (FBS) (Invitrogen, Paisley, UK) supplemented medium. This was transferred to a 25ml universal tube (Fisher, UK) and a sample was taken to assess cell number. Cell number was calculated using a haemocytometer (Assistant, Sondheim- Rhön, Germany).

The cell suspension was centrifuged at 90 x G for 10 minutes. The supernatant was aspirated and the cell pellet re-suspended in 5ml 10% FBS medium. The cells were then seeded into 96 well plates or 35mm dishes for experimental use. Another 75cm² culture flask was also seeded to maintain the cell culture.

2.3.1 ARPE-19

ARPE-19 cells are derived from a primary culture of human retinal pigmented epithelial cells (Dunn et al., 1996) and were obtained from the American Type Cell Culture (ATCC, Manassas, VA, USA). The cell line expresses immunohistochemical cell markers for native human RPE cells such as cellular retinaldehyde-binding protein (CRALBP).

The cell line is grown in DMEM/HamF12 medium with 10% FBS, 2mM L-glutamine and 50mg/l Pen-Strep (Invitrogen). Cells were seeded at a density of 4,000 cells per well in a 96 well plate in a volume of 100µl.

2.3.2 MIO-M1

The MIO-M1 cell is a cell line obtained from Professor Astrid Limb (University College London, UK) and is derived from a primary culture of human retinal cells (Limb et al., 2002). The cell line expresses the immunohistochemical markers of native Human Müller cells such as cellular retinaldehyde-binding protein (CRALBP) and Glutamine Synthetase (GS).

The cell line is grown in DMEM GLUTAMAX medium with 10% FBS, and 50mg/l Pen-Strep (Invitrogen). Cells were seeded at a density of 5,000 cells per well in a 96 well plate in a volume of 100µl.

2.4 PCR

2.4.1 Planar Sectioning

Retinal explants were frozen in liquid nitrogen following dissection / experimentation and stored at -80°C until ready for RNA extraction. A frozen block was prepared on which to mount the retinal explant. This involved a chuck being prepared with a layer of frozen optimal cutting temperature (OCT, Sakura Finetek, Zoeterwoude, Netherlands) on top. The chuck had a line drawn down one side for referencing the position within the cryostat. The chuck was then placed in the cryosectioner so that the line from the chuck was directly in line with a mark on the mounting stage. This is performed so that when the sample is sectioned, the position and angle of the mount within the cryostat is the same allowing for level sectioning. The OCT was then cryosectioned so that a flat surface was obtained. This was then stored in the cryostat on the quickfreeze plate at -40°C .

Once the retinal explant was dissected, it was placed into a 35mm Petri dish containing 1.5ml serum-free DMEM/HamF12. The explant was then floated onto a triangular piece of filter paper until directly in the centre of the paper. The paper and explant was then lifted out of the medium and the filter paper with the explant in the centre was placed on top of the cryosectioned OCT on the chuck. OCT was then placed on top of the explant so that the explant lays between two layers of OCT. This was then placed back onto the quickfreeze plate to allow the OCT on top of the explant to freeze. Once frozen, the explant could be cryosectioned (Figure 2.2).

To section the explants, the chuck was placed into the cryostat ensuring the line with the chuck is in line with the mark on the cryostat. The block was then sectioned at $30\mu\text{m}$ sections through the top layer of OCT until the explant was visible. The cryostat was then set to section at $20\mu\text{m}$. As the sample was approaching each new section was placed onto a slide to see if any tissue was present. When the tissue was reached each section was placed into an Eppendorf labelled with sample number and other relevant information and snap frozen in liquid nitrogen.

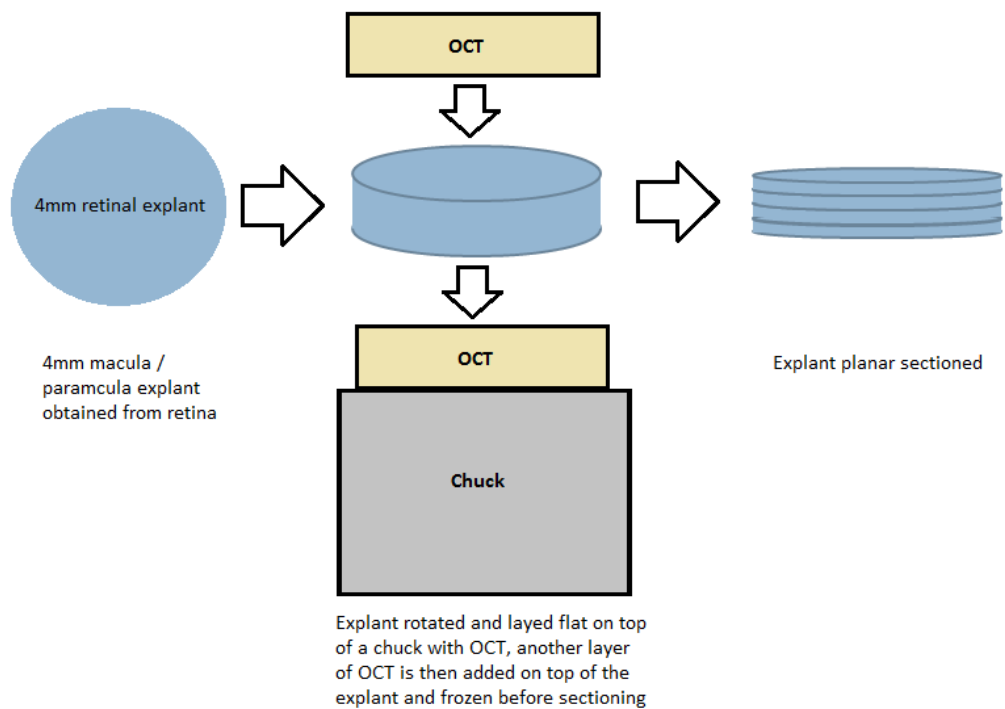


Figure 2.2 - Diagram of the Planar Sectioning Technique

2.4.2 RNA Extraction

The Qiagen RNeasy mini kit (Qiagen, Crawley, UK) was used for RNA extraction of whole retinal explants, and the RNeasy micro kit (Qiagen, Crawley, UK) was used for RNA extraction of planar sections. The protocol provided by Qiagen was followed and is described below. Both protocols are similar, however where differences arise they are highlighted.

To extract the RNA, buffer containing β -mercaptoethanol (Sigma-Aldrich, Poole, UK) was added and the tissue homogenised by passing through a 20-gauge needle 10 times. The lysate was then centrifuged at 12,000g for 3 minutes to remove insoluble debris. The supernatant was then transferred to a separate Eppendorf containing 70% ethanol. Following mixing this was transferred to the RNeasy Minispinn column (RNeasy Minielute for the Micro kit) and centrifuged at 12,000g for 15 seconds. Buffer RW1 was then added and centrifuged at 12,000g for a further 15 seconds. DNA was then digested by adding DNase diluted in RDD buffer (Qiagen, Crawley, UK) to the column and leaving for 15 minutes. The column was then washed in

buffer RW1 twice at 12,000g to remove the DNase.

Following this Buffer RPE (mixed with 100% ethanol) was added to the column and centrifuged for another 15 seconds at 12,000g. Buffer RPE was then added to the column again and centrifuged for 2 minutes at 12,000g to dry the membrane. If using the Micro Kit, 80% ethanol was then added to the column and centrifuged at 12,000g for 2 minutes, before adding the column to a new collection tube and centrifuging at 12,000g for 5 minutes to dry the column. To collect the RNA, 50µl of RNase free water (Qiagen, Crawley, UK) was then added to the Mini kit column, or 14µl to the Micro kit column and centrifuged for 1 minute at 12,000g.

The concentration of RNA was measured in duplicate using a NanoDrop ND-1000 spectrophotometer (NanoDrop Technologies, Wilmington, USA). 260/280 and 260/230 ratios were also measured and a ratio of ≥ 1.8 for each was suitable for use.

2.4.4 RNA Clean-up

RNA clean-up (sodium acetate precipitate method) was performed on RNA extracted samples with either a 260/280 or a 260/230 value of < 1.8 .

During the precipitate stage either 3M sodium acetate or 5M ammonium acetate at pH 4.5 was added at 1/10th of the RNA sample volume. 2.5 X the volume of pre-chilled 100% ethanol was then added and precipitated overnight at -20°C.

The recovery stage began with a 12,000g spin at 4°C for 15 minutes. The Supernatant was then discarded. 0.5ml of ice cold 75% Ethanol was then added and centrifuged at 12,000g at 4°C for 15 minutes. The supernatant was discarded and the RNA sample air dried before being re-suspended in RNase-free water.

2.4.5 cDNA

Before performing PCR, the RNA needs to be converted into complimentary DNA (cDNA) so that PCR can be conducted. Depending on the quantity of RNA extracted, RNA was diluted to either 5ng/µl or 10ng/µl in RNase free water. Random primers (Promega, Southampton, UK) were mixed with dNTP (Invitrogen, Paisley, UK) and added to each sample before being briefly centrifuged to mix the two. The samples

were then placed in a Peltier Thermal Cycler DNA engine (PTC-200, MJ Research, Minnesota, USA) and heated to 65°C for 5 minutes and then chilled on ice. 5x first strand buffer, dithiothreitol (DTT) (Invitrogen, Paisley) and RNase inhibitor (Promega, Southampton, UK) were mixed and added to the samples and incubated for 10 minutes at 25°C and then at 42°C for 2 minutes. Samples were then chilled on ice and Superscript II Reverse Transcriptase (Invitrogen, Paisley, UK) was added. The Eppendorf's were then centrifuged for 15 seconds to mix the contents. The samples were then incubated at 42°C for 50 minutes and then at 70°C for 15 minutes before being stored at -20°C.

2.4.6 PCR

QRT-PCR was conducted using the Applied Biosystems 7500 fast real-time PCR System (Applied Biosystems, Warrington, UK). cDNA was diluted with nucleotide free water to 0.5ng/ml and duplicates of 5ng total cDNA added to each well of the microAmp Optical 96 well reaction plate (Applied Biosystems, Warrington, UK). Mastermix, primers / probes and nuclease free water were all prepared and mixed together so that a total volume of 15µl per well was obtained at a ratio of: Mastermix 8.33µl, primers / probe 1.25µl and nuclease free water 5.42µl. This was then added to each well to bring the total volume of the well to 25µl.

When the plate had been loaded, it was sealed with PCR film (Thermo Scientific, Surrey, UK). The first stage of the PCR reaction involved heating the plate to 50°C for 2 minutes, followed by heating the plate to 95°C for 10 minutes to reduce non-specific amplification. The cDNA was then amplified (40 cycles of heating to 95°C for 15 seconds and cooling to 60°C for 60 seconds) with the heating stage denaturing double stranded DNA and the cooling process allowing new primers to bind to the single strand DNA template.

Table 2.1 – List of Primers / Probes Used

Primer / Probe	Number	Reporter	Source
Topoisomerase (TOP1)		FAM	Primer Design, Southampton, UK
Cytochrome C1 (CYC1)		FAM	Primer Design, Southampton, UK
THY1	Hs00174816_m1	FAM	Applied Biosystems, Warrington, UK
RBFOX3	Hs00876928_m1	FAM	Applied Biosystems, Warrington, UK
AHNAK2	Hs00292832_m1	FAM	Applied Biosystems, Warrington, UK
Protein Kinase C alpha	Hs00925193_m1	FAM	Applied Biosystems, Warrington, UK
Choline acetyltransferase	Hs00252848_m1	FAM	Applied Biosystems, Warrington, UK
Calbindin	Hs01077197_m1	FAM	Applied Biosystems, Warrington, UK
Retinaldehyde Binding Protein 1	Hs00165632_m1	FAM	Applied Biosystems, Warrington, UK
GFAP	Hs00909236_m1	FAM	Applied Biosystems, Warrington, UK
Heat Shock Protein 70	Hs01040501_sh	FAM	Applied Biosystems, Warrington, UK

Recoverin	Hs00610056_m1	FAM	Applied Biosystems, Warrington, UK
Cyclin Dependent Kinase 5	Hs00358991_g1	FAM	Applied Biosystems, Warrington, UK
Cyclin Dependent Kinase 11A/B	Hs02341397_m1	FAM	Applied Biosystems, Warrington, UK
Cyclin Dependent Kinase 16	Hs00178837_m1	FAM	Applied Biosystems, Warrington, UK
Cyclin Dependent Kinase 17	Hs00176839_m1	FAM	Applied Biosystems, Warrington, UK
Cyclin Dependent Kinase 18	Hs00384387_m1	FAM	Applied Biosystems, Warrington, UK

2.4.7 PCR Analysis

Data obtained from PCR was analysed in one of three ways depending on the experiment conducted.

For whole explant data looking at expression levels across the macula and paramacula explants, data obtained from the PCR was quantified based on standard curve values, and then normalised to the housekeeping genes. The housekeeping genes used were; topoisomerase 1 (TOP1) which is involved in the unwinding of DNA (Lodish, 2000) and cytochrome C-1 (CYC1) a mitochondrial transmembrane protein involved in the electron transfer chain (Kokhan et al., 2010). The housekeeping genes were chosen because they showed the least variation between explants and changed the least with time in culture (Sanderson lab, unpublished data).

The delta Ct method was adopted to assess changes in expression with CHQ treatment. This method calculates a fold change in expression by using the following equation (Qiagen, 2016):

$$\Delta Ct1 = Ct (\text{Target A-treated}) - Ct (\text{Ref B-treated})$$

$$\Delta Ct2 = Ct (\text{Target A-control}) - Ct (\text{Ref B-control})$$

$$\Delta \Delta Ct = \Delta Ct1 (\text{treated}) - \Delta Ct2 (\text{control})$$

$$2^{\Delta \Delta Ct} \text{ Normalized target gene expression level} = 2^{\Delta \Delta Ct}$$

In experiments using planar sectioned retina, the level of mRNA was assessed using a standard curve and plotted directly. The standard curve mRNA was prepared from a combination of whole macula and paramacula explants converted to cDNA. 20, 10, 5, 2.5, 1.25 and 0.625ng of cDNA was then loaded into a PCR plate and expression of the gene of interest analysed and the standard curve plotted. The Ct value and ng of cDNA from the standard curve provided a line equation which could in turn be used to obtain a value of “ng cDNA” in future experiments. Data was not normalised to housekeeping genes as these vary in level across the retinal sections.

2.5 Immunohistochemistry

2.5.1 Cryosectioning

Retinal explants were fixed in 4% formaldehyde for 24 hours. They were then dehydrated in 30% sucrose solution for a further 24 hours to prevent freeze damage to the tissue. After this, aluminium foil cups (1 – 2cm in height, 1.5cm in diameter) of OCT were prepared. The explants were then placed vertically into the OCT using forceps, placed onto dry ice to freeze and stored at -80°C. Blocks were mounted onto the chuck using OCT and placed into the cryostat (Bright OTF 5000 Cryostat, Bright Instruments, Huntingdon, UK) and sectioned at 30µm (maximum sectioning thickness) until the retinal sample was 4mm in diameter (middle of the sample), measured using a digital vernier calliper (Clarke, Essex, UK). When the centre of the samples was reached it was sectioned at 13µm and placed onto either Tespa (3-

triethoxysilylpropylamine) coated slides (Sigma-Aldrich, Poole, UK), or superfrost plus slides (Fisher Scientific) with 4 sections placed onto each slide. Sections were not consecutive to make sure that different cells were imaged; after a section was placed onto the slide, the two subsequent sections were discarded before collection of the following section. Slides were stored at -20°C.

2.5.2 Fluorescence Immunohistochemistry

Slides were washed in PBS three times (10 minutes each) to remove the OCT. Retinal sections then had circles drawn around them using a wax pen. Sections were then incubated in blocking solution (5% normal goat serum, 0.2% TritonX-100 (Sigma-Aldrich, Poole, UK) prepared in PBS) for 90 minutes at room temperature. The blocking solution was carefully wiped off avoiding damage to the samples or the wax ring and the primary antibody (Table 2.2), prepared in blocking solution, was added to the sections and incubated for 24 hours at 4°C in a square Petri dish (Fisher, UK) with a damp piece of tissue in the tray to prevent dehydration.

Table 2.2 Primary antibody's used for immunohistochemistry

Target	Antibody Source and Clonality	Dilution	Source
Choline acetyltransferase	Rabbit Polyclonal	1:200	Millipore, Watford, UK
Recoverin	Rabbit Polyclonal	1:500	Millipore, Watford, UK
Calbindin D-28K	Mouse Monoclonal	1:300	Sigma-Aldrich, Dorset, UK
Protein Kinase C	Mouse Monoclonal	1:200	Santa Cruz, Bergheimer, Germany
Thy1	Mouse Monoclonal	1:200	Millipore, Watford, UK

Neuronal Nuclei (NeuN)	Mouse Monoclonal	1:200	Millipore, Watford, UK
Neuronal Enolase	Rabbit Polyclonal	Pre-diluted	Thermo Scientific, Northumberland, UK
Tubulin	Mouse Monoclonal	1:200	Promega, Southampton, UK
Glutamine synthetase	Rabbit Polyclonal	1:200	Millipore, Watford, UK
AHNAK2	Mouse Polyclonal	1:500	Abcam, Cambridge, UK
Glial Fibrillary Acidic Protein (GFAP)	Rabbit Polyclonal	1:500	Dako, Cambridge, UK
Active Caspase 3	Rabbit Polyclonal	1:3000	Abcam, Cambridge, UK

After 24h the primary antibody was removed and three 10 minute washes with PBS performed. Secondary antibody (Table 2.3) prepared in blocking solution was then added to the samples and incubated at room temperature for 2 hours. After incubation the slides were washed in PBS three times (10 minutes each) and then DAPI (Molecular Probes, Leiden, Netherlands) at 0.5 μ g/ml in PBS for 10 minutes. Following this, slides were again washed three times (for 10 minutes each). The slides were then dried and a drop of hydromount added to each sample before sealing with a coverslip. Slides were then allowed to set in the dark for 12 hours before imaging. Fluorescence microscopy was conducted on a wide-field Zeiss Axiovert 200M fluorescence microscope and the images analysed using Zeiss Axiovision 4.8 software.

Table 2.3 – Secondary antibody list

Target	Antibody Source and Fluorophore	Dilution	Source
Mouse IgG (H+L)	Goat AlexaFluor 488	1:1000	Invitrogen, Paisley, UK
Mouse IgG (H+L)	Goat AlexaFluor 568	1:1000	Invitrogen, Paisley, UK
Rabbit IgG (H+L)	Goat AlexaFluor 568	1:1000	Invitrogen, Paisley, UK

2.5.3 Colorimetric Immunohistochemistry

2.5.3.1 Ventana Discovery

The Ventana Discovery (Roche, Burgess Hill, UK) is an automated immunohistochemical and in situ hybridization platform which has the ability to perform multiple immunohistochemical assays at the same time. This platform was used for colorimetric immunohistochemistry with all reagents purchased from Roche (Burgess Hill, UK), the customised protocol input was:

1. Rinse slide with reaction buffer
2. Apply coverslip (DXT)
3. Warm slide to 37°C and incubate for 4 minutes
4. Disable slide heater, incubate for 8 minutes
5. Rinse slide with reaction buffer
6. Apply coverslip (DXT)
7. Warm slide to 37°C and incubate for 4 minutes
8. Rinse slide with reaction buffer
9. Apply coverslip (DXT)
10. Apply one drop of inhibitor CM, incubate for 4 minutes
11. Rinse slide with reaction buffer
12. Apply coverslip (DXT)
13. Apply one drop of primary antibody, incubate for 32 minutes

14. Rinse slide with reaction buffer, then apply coverslip X 3
15. Apply one drop of secondary antibody, incubate for 20 minutes
16. Rinse slide with reaction buffer, then apply coverslip X 3
17. Apply one drop of DAB CM and one drop of H₂O₂ CM, incubate for 8 minutes
18. Rinse slide with reaction buffer
19. Apply coverslip (DXT)
20. Apply one drop of copper CM, incubate for 4 minutes
21. Rinse slide with reaction buffer
22. Apply coverslip (DXT)

2.5.3.2 TUNEL Assay

Terminal deoxynucleotidyl transferase (TdT) dUTP Nick-End Labelling (TUNEL assay) (Roche, Burgess hill, UK) was used to detect cells undergoing apoptosis. Slides underwent the standard protocol for the Ventana Discovery (section 2.5.3.1), in which the primary antibody stage included application of TUNEL label (TUNEL-enzyme 1: 9 TUNEL-label) and was incubated for 1 hour at 37°C. At the secondary antibody stage rabbit anti-FITC (Invitrogen, Paisley, UK) was applied.

2.5.3.3 Colorimetric Imaging

Slides were scanned using the Aperio Scanscope XT (Leica Biosystems, Milton Keynes, UK), and images analysed using Aperio Imagescope software (Leica Biosystems, Milton Keynes, UK). Image analysis involved the quantification of the number of positive pixels (positive pixel count), in which a threshold is set for both positive pixels (antibody of interest) and negative pixels (haematoxylin stain). The number positive pixels (antibody of interest) is expressed as a percentage of all positive and negative pixels (haematoxylin stain), and the result given as a % positive pixel count.

2.6 Western Blot

2.6.1 Protein extraction.

Following experimental conditions, mammalian protein extraction reagent M-PER (Thermo Scientific) with 1:100 of halt phosphatase inhibitor cocktail and 1:100 protease inhibitor cocktail along with 1:100 (0.5M) EDTA (Thermo Scientific, Rockford, IL, USA) was added to the retinal explant. The tissue was lysed using an Eppendorf pestle and lysates spun at 16,000g for 10 minutes at 4°C. The supernatant was collected and transferred to a 0.5ml Eppendorf and stored at -80°C until ready to use.

2.6.2 BCA Assay

A bicinchoninic assay (BCA) was carried out on the tissue lysates to determine the quantity of protein. Protein standards ranging from 0-1000 µg/mL were prepared by diluting bovine serum albumin (BSA) (Sigma-Aldrich) in M-PER. Protein standards were applied to a 96 well plate in triplicate, along with each sample in duplicate. Each well then received ddH₂O and BCA reagents A and B (Thermo Scientific) mixed at a ratio of 10:50:1. The plate was then covered and placed on a shaker for 1 minute before being incubated at 37°C for 1 hour. A BMG Labtech plate reader was used to measure the absorbance at 550nm. The protein concentrations of the unknown samples were calculated from the standard curve.

2.6.3 Sample Preparation

Samples for Western blots were diluted with ddH₂O to the concentration of the lowest sample. Loading Buffer (4% SDS (Melford Laboratories, Ipswich, UK), 0.01% bromophenol blue (Sigma-Aldrich), 30% glycerol (Sigma-Aldrich), 12.5% β-mercaptoethanol (Sigma-Aldrich) and 160mM Tris (Sigma-Aldrich) pH 6.8) was added to each sample and centrifuged at 16,000g for 2 minutes before heating to 100°C for 5 minutes.

2.6.4 SDS-PAGE

10% acrylamide, sodium dodecyl sulphate (SDS-PAGE) gels were made 24h before use. The upper gel consisted of 5% acrylamide (diluted from 40% acrylamide solution (BIO-Rad) in ddH₂O), 4X upper gel buffer (0.5M Tris (Sigma-aldrich), 0.4% w/v SDS (Sigma-Aldrich), pH 6.8), ammonium persulphate and TEMED (Sigma-Aldrich). The lower running gel consisted of 10% acrylamide (via dilution of 40% Acrylamide solution (BIO-Rad) in ddH₂O), 4X lower gel buffer (1.5M Tris, 0.4% w/v SDS, pH 8.8), ammonium persulphate and TEMED.

2.6.5 Gel Electrophoresis

Gels were placed into the electrophoresis tank (Bio-Rad Laboratories, Hercules, CA, USA) filled with running buffer (250mM Tris, 1.92M glycine and 1% SDS (Sigma-Aldrich)). ECL DualVue molecular weight marker (GE healthcare, Buckinghamshire, UK) was loaded into the first well, and samples with loading buffer into the subsequent wells. Electrophoresis was conducted at 4°C with 30 milliamps per gel and was halted once the bromphenol blue dye reached the end of the gel.

2.6.6 Protein Transfer

The SDS-PAGE gels were incubated in transfer buffer (48mM Tris, 39mM glycine (Fisher), 4% w/v methanol (Fisher), 0.0375% w/v SDS, pH 8.3) for 30 minutes. A polyvinylidene difluoride (PVDF) membrane (Perkin Elmer Life Sciences) was activated via submersion in 100% methanol for 30 seconds. Proteins were transferred onto the membranes by sandwiching the gel and the PVDF membrane between thick blotting paper which was placed on a trans-blot semi-dry transfer cell (Bio-Rad) at a constant 15V and a current of 0.03 A per gel for 30 minutes.

2.6.7 Immunoblotting

Post protein transfer the gels were discarded and PVDF membranes washed in PBS (3 times for 5 minutes). Membranes were blocked for 1 hour in PBS-T (5% w/v reduced fat milk powder (Marvel), 0.1% v/v Tween-20 (Fisher) in PBS). PBS-T was removed and membranes were placed into PBS-T containing the primary antibody (Table 2.4) overnight at 4°C. Membranes were then washed in PBS-T (6 times for 5 minutes), and placed in PBS-T containing 1:1000 secondary antibody (Table 2.4) for 1 hour at room temperature. Membranes were washed in PBS-T (6 times for 5 minutes) and then PBS containing 0.1% w/v Tween-20 (once for 10 minutes).

2.6.8 Development

The membranes were immersed in ECL Plus solution (ECL Plus Western Blotting Detection System, GE Healthcare) and kept in the dark for 5 minutes at room temperature. The ECL Plus solution was removed and the membrane placed into a film cartridge and taken to a dark room. In the dark, Amersham Hyperfilm ECL photographic film (GE healthcare) was exposed to the membrane. The photographic film was then passed through Kodak GBX developing solution (Kodak, Rochester, NY, USA), Stop Solution (SB80 photosol, Basildon, UK) and fixing solution (Hypam fixer, Ilford, Cheshire, UK). Bands on the photographic film were scanned and the area of the band measured using Image J (Wayne Rasband, National Institutes of Health, USA). β -actin was used as the loading control. To view multiple antibodies, membranes were stripped by washing twice (15 minutes each) in 200mM NaOH (Sigma-Aldrich) before washing for 5 minutes in PBS. The membrane would then be blocked for one hour in PBS-T before application of the new primary antibody.

Table 2.4 – Antibodies Used for Western Blotting

Antibody	Clonality	Target protein Mw (KDa)	Dilution	Company
Primary antibodies				
Anti-PARP	Rabbit Monoclonal	116, 89	1:1000	Cell Signalling Technology (Danvers, MA, U.S.A)
Anti- β -actin	Rabbit Monoclonal	45	1:1000	Cell Signalling Technology (Danvers, MA, U.S.A)
Secondary antibodies				
Anti-Rabbit HRP Conjugate	IgG Donkey	-	1:1000	GE Healthcare (Buckinghamshire, UK)
Anti-Mouse HRP Conjugate	IgG Sheep	-	1:1000	GE Healthcare (Buckinghamshire, UK)

2.7 LDH Assay

The cytotoxicity detection kit (Roche, Indianapolis, IN, USA) (LDH assay) was performed to detect levels of necrosis. It achieves this by assessing the levels of the cytosolic enzyme Lactate Dehydrogenase (LDH) released into the culture medium when cell membrane integrity is lost. For explants, tissue was first removed from the culture dish and fixed for immunohistochemical analysis. The medium was pipetted

into an Eppendorf and centrifuged for 5 minutes at 16,000g to remove any cell debris. It was then diluted 1:10 in the same medium before placing 100µl into a 96 well plate (Fisher Scientific, Loughborough, UK). For cells, medium was removed from the culture (Fisher Scientific), and 100µl placed directly into a new 96 well plate (Fisher Scientific) for assessment.

Alongside this, 100µl of fresh medium was added to three wells so that the absorbance of the background could be measured and subtracted from the absorbance of the samples. The reaction mixture was then prepared. This consisted of the catalyst (Diaphorase/NAD⁺) and dye solution (Iodotetrazolium chloride (INT) and sodium lactate) mixed at a ratio of 1:45 (catalyst : dye solution). This was added to the samples at a 1:1 ratio. The plate was incubated for 15 minutes at 37°C and readings taken at 490nm and 660nm at 5 minute intervals. The results used for analysis were from the 15 minute time point.

The equation used to calculate total LDH release was:

$$\text{LDH absorbance} = \text{Sample absorbance (490nm)} - \text{background absorbance (660nm)} - \text{background medium absorbance (490, 660nm)}.$$

LDH release data was expressed in one of two ways when analysing cell data. Either a standard curve was run and the data expressed as mU/mL LDH, or one row of cells was lysed using 2% Triton X (Sigma-Aldrich) and the LDH released expressed in comparison to this as % total LDH. Explant LDH release data was measured and expressed as % Control.

2.8 MTS Assay

An MTS assay (96 Aqueous one solution proliferation assay, (Promega, Southampton, UK)) was used to assess cell viability. The MTS assay contains a tetrazolium compound (3-(4,5-dimethylthiazol-2-yl)-5-(3-carboxymethoxyphenyl)-2-(4-sulfophenyl)-2H-tetra-zolium) and an electron coupling reagent (phenazine ethosulphate). Metabolically active cells can reduce the tetrazolium compound into a coloured formazan product (soluble in culture medium) causing a colour change. Therefore the level of colour change can be used to assess viability of the cells. The assay was run in triplicate and applied to cells at a 1:10 dilution (mixed in the

appropriate medium according to the cell type) for 1 hour at 35°C. Absorbance was measured at 490nm using a BMG Labtech plate reader and background readings of medium and MTS were taken. For retinal explants 1.5ml of MTS solution with DMEM/HamF12 medium at a 1:10 ratio was applied to the 35mm culture dish containing the explant and incubated at 35°C for 1 hour. The medium was then extracted and mixed well before being measured at 490nm.

The viability was calculated as follows:

$$\% \text{ cell viability} = ((\text{absorbance treated} - \text{background}) / (\text{absorbance control} - \text{background})) * 100$$

Chapter 3

3.0 Characterisation of retinal cell markers in the human retina

3.1 Introduction

The retina consists of 10 different layers with multiple cell types distributed at different densities throughout these layers. There are three nuclear layers: the outer nuclear layer consisting of the cell bodies of the photoreceptors (Rods and Cones), the inner nuclear layer consisting of the cell bodies of amacrine cells, horizontal cells, bipolar cells and the non-neuronal Müller cells and finally the ganglion cell layer, consisting of the cell bodies of retinal ganglion cells.

To assess location and density of these cells, retinal cell markers may be utilised, and in order to establish the *ex vivo* human retina as a model to assess retinotoxicity, it is important to determine the validity of such markers in the human retina. A general marker of neuronal cells is neuronal specific enolase. Neuronal enolase is an enzyme involved in the glycolysis pathway (Bonner et al., 2000), immunohistochemically it has been studied in the human retina by Li et al (1995) where it was found that the highest density of staining was located within the inner segments of cone photoreceptors. Contrary to this another group which studied neuronal enolase in the retina found staining to be less specific, staining processes of all neurons within the human retina (Molnar et al., 1984).

As a marker of photoreceptors, recoverin may be used. Recoverin is a calcium binding protein involved in the phototransduction of photoreceptors (Dizhoor et al., 1991). Recoverin is known to be expressed in both rod and cone cells (Gunhan et al., 2003) and is therefore a marker for all photoreceptors within the retina.

Commonly used markers of the inner nuclear layer cells; horizontal, bipolar and amacrine are calbindin (a calcium binding protein), protein kinase C α (PKC α , an enzyme involved with the phosphorylation of proteins and cell signalling (Lameirao et al., 2009) and choline acetyltransferase (ChAT, an enzyme involved in the synthesis of acetyl choline) respectively. Chiquet (2005) showed that calbindin stained a multitude of cells in the human retina, with cone cells and horizontal cells being primarily stained and some bipolar cells and amacrine cells (Chiquet et al., 2005), whereas PKC α has been used to immunostain rod bipolar cells (it does

however only mark rod ON bipolar cells) (Haverkamp et al., 2003), (Kolb et al., 1993). ChAT has been used to immunolabel cholinergic amacrine cells and displaced amacrine cells previously (Hutchins and Hollyfield, 1987).

Ganglion cell markers have been extensively investigated in the human retina by the Norwich eye research group, THY1 (a cell surface glycoprotein (Partida et al., 2012)) and NeuN (a neuronal specific nuclear protein (Mullen et al., 1992)) have been used to provide information regarding changes in the number of ganglion cells with oxygen and glucose deprivation and changes with hydrostatic pressure (Osborne et al., 2015a), and NMDA excitotoxicity (Niyadurupola et al., 2011). Recent data published by Osborne et al (2015) has also shown that ganglion cell marker β III Tubulin, a protein within microtubule used in rodent studies is also suitable for the assessment of ganglion cells in the human retina (Osborne et al., 2015b). Ma (2014) has also found with use of a gene array that AHNAK (a scaffold protein (Marg et al., 2010)) and HSP1AB (HSP70, a protein which increases expression in response to elevated temperature (Kayama et al., 2011)) are also expressed at high levels in the human retinal ganglion cell layer, potentially indicating new markers of ganglion cells.

Müller cells may be investigated with the use of glutamine synthetase (an enzyme responsible for the breakdown of excess glutamate), this has been shown in rat retina (Riepe and Norenburg, 1977), pig retina (Oh et al., 2011) as well as other species.

For the *ex vivo* retina to be established as a suitable model for the assessment of retinotoxicity, it is important to compare the *in vivo* retina to the *ex vivo* retina to be aware of any changes which may occur during the post mortem period. In order to make such a comparison, human retina was obtained from eyes that had been removed during surgery. Allowing for the minimum time possible between the functioning retina *in vivo*, to experimental conditions.

Another important factor when establishing a model is the ability to compare treated samples to a control, for this all samples must be equivalent at the start. QRT PCR can be used to investigate the expression levels of cell specific mRNA, if samples possess the same expression values across all samples, any change in expression during culture with a retinotoxin may be attributed to the treatment.

The aim of the research presented in this chapter is to build a cellular profile of the human retina, throughout the nuclear layers of the retina and across the macula and paramacula region, determining the mRNA expression profiles of cell specific marker genes of the major retinal cell types and localization of marker proteins by immunohistochemistry. A comparison between the post mortem donors and living donors will also be made to investigate any differences. This characterisation sets the baseline characteristics of the model prior to development of the model for investigation of retinotoxicity.

3.2 Results

3.2.1 Immunohistochemical analysis of retinal cell marker proteins in the human retina

In initial experiments the morphology of the retina was shown using antibodies to immune label specific cells within each layer, starting with the photoreceptor layer and ending with the ganglion cell layer. All retinal samples were processed directly following dissection.

3.2.1.1 Neuronal Specific Enolase

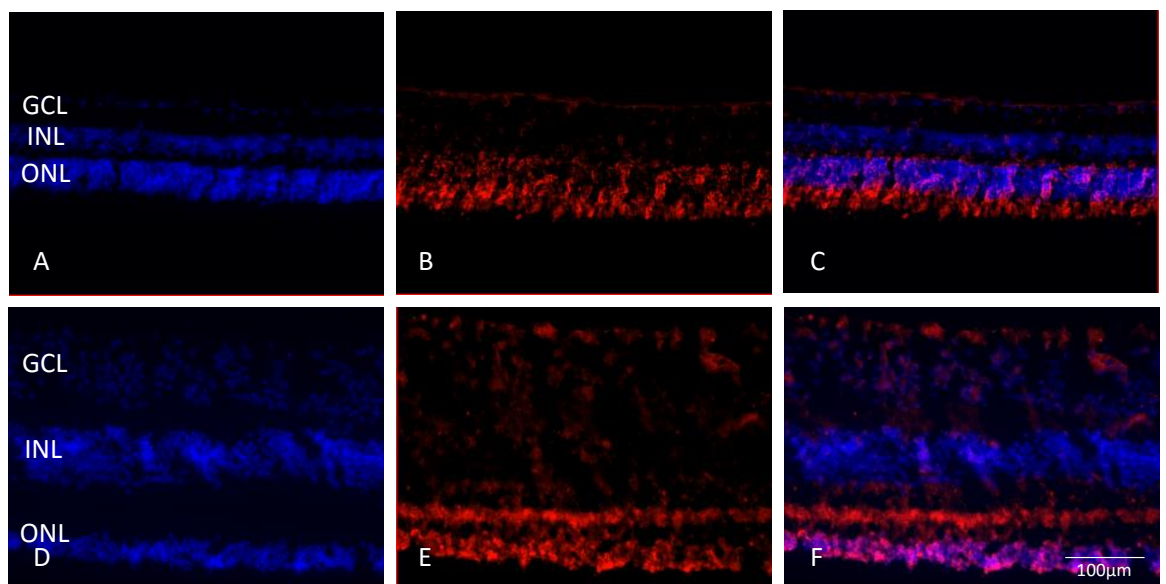


Figure 3.1 - Neuronal Specific Enolase Presence in the Live and Post Mortem Human Paramacula Retina

Cross section of the paramacula human retina immunostained for neuronal specific enolase (red). Fig 3.1 A - C shows immunostaining from a cross section of retina from a living donor. Fig 3.1 D - E shows the immunostaining from a cross section of retina from a post mortem donor (pre-24h).

Neuron specific enolase was selected as a marker of neurons in the human retina. Figure 3.1 A-C show staining in the living human retina from neuron specific enolase. Staining can be found in the ganglion cell layer and the inner nuclear layer,

however the highest intensity of staining was seen in the photoreceptor layer. Figure 3.1 D-E displays staining from a post mortem donor in which a similar pattern of staining was found.

3.2.1.2 Recoverin

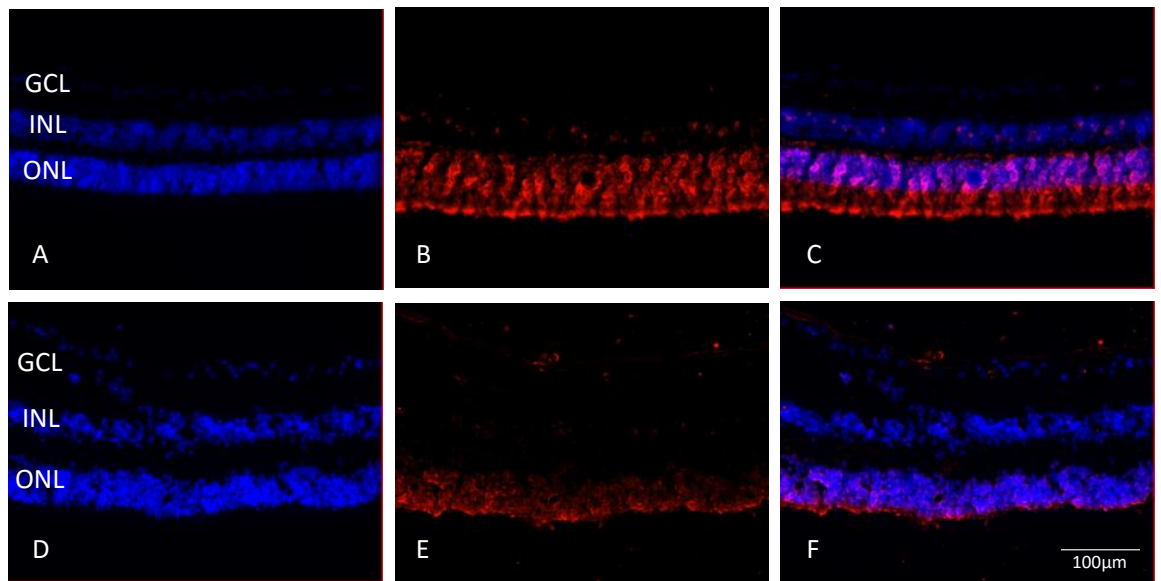


Figure 3.2 - Recoverin Presence in the Live and Post Mortem Human Paramacula Retina

Cross section of the paramacular human retina immunostained for Recoverin (red). Fig 3.2 A - C shows the immunostaining from a cross section of retina from a living donor. Fig 3.2 D - E shows the immunostaining from a cross section of retina from a post mortem donor (pre-24h).

Recoverin was used as an immunohistochemical marker of photoreceptor cells.

Figure 3.2 showed recoverin to stain the photoreceptor layer, including cell bodies in the outer nuclear layer and photoreceptor outer segments. This was similar in both the living donor (Figure 3.2 A-C) and the post mortem donor (Figure 3.2 D-F), however more outer segments can be seen in the retina of the live donor.

3.2.1.3 Calbindin

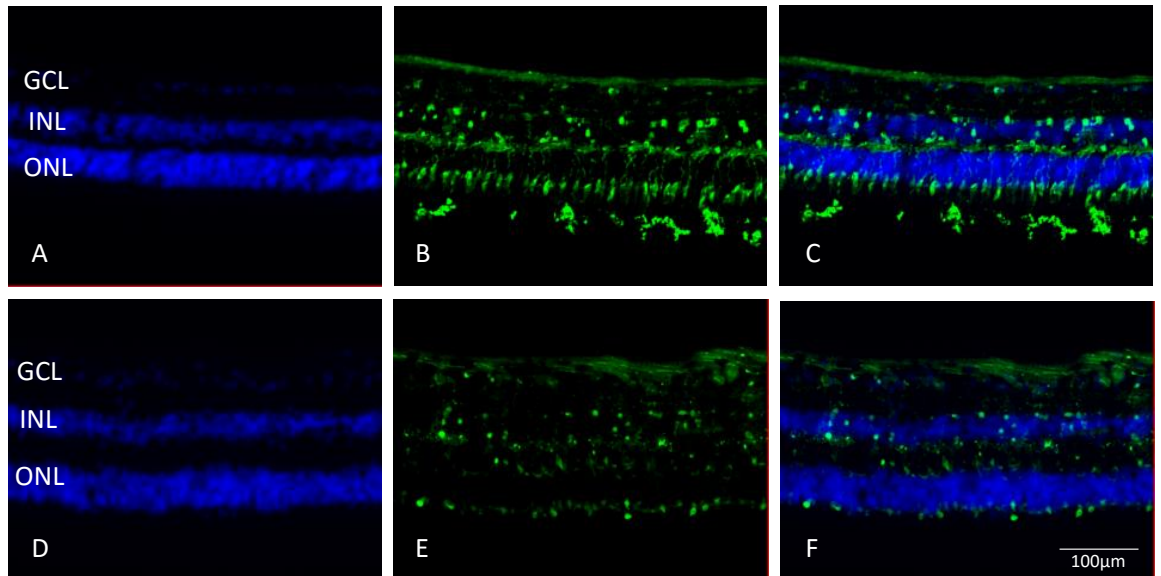


Figure 3.3 - Calbindin Presence in the Live and Post Mortem Human Paramacula Retina

Cross section of the paramacular human retina immunostained for Calbindin D-28K (green). Fig 3.3 A - C shows the immunostaining from a cross section of retina from a living donor. Fig 3.3 D - E shows the immunostaining from a cross section of retina from a post mortem donor (pre-24h).

Calbindin was selected as an immunohistochemical marker of horizontal cells. Calbindin identified multiple cells in both the living donor and the post mortem human retina (Figure 3.3). Remnants of some photoreceptor outer segments were stained in the living donor as well as the post mortem donor, however interestingly, no cell bodies were stained in the outer nuclear layer. Both donors displayed staining of cell bodies in the inner nuclear layer, and to a lesser extent cell bodies in the ganglion cell layer, the nerve fibre layer also displayed staining in both.

3.2.1.4 Protein Kinase C α

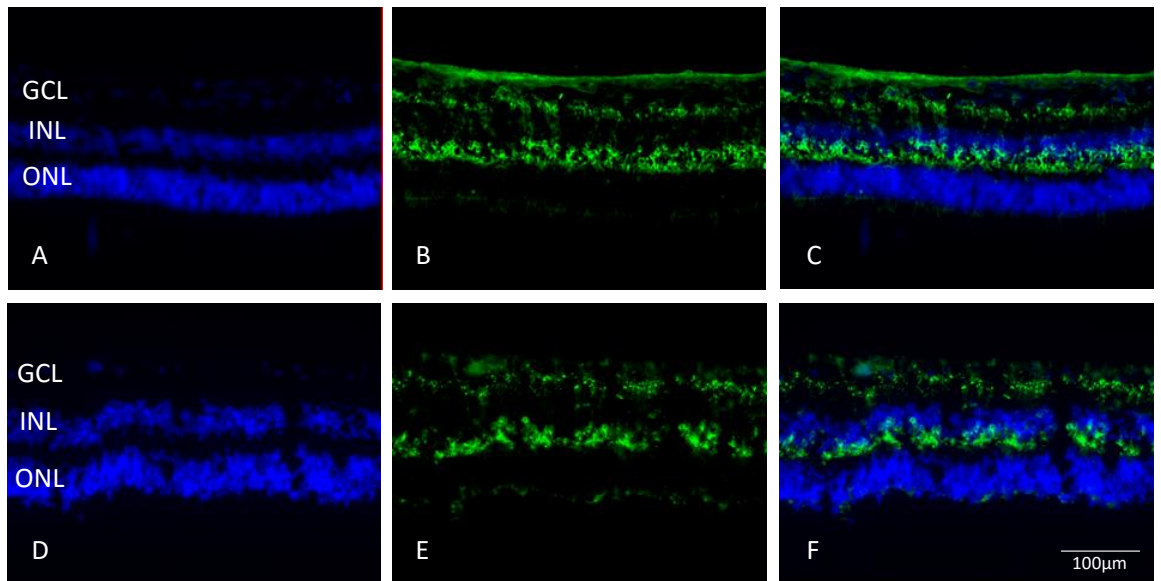


Figure 3.4 - Protein Kinase C α Presence in the Live and Post Mortem Human Paramacula Retina

Cross section of the paramacular human retina immunostained for PKC α (green). Fig 3.4 A - C shows the immunostaining from a cross section of retina from a living donor. Fig 3.4 D - E shows the immunostaining from a cross section of retina from a post mortem donor (pre-24h).

PKC α was selected as a marker of bipolar cells within the inner nuclear layer (Figure 3.4). It identified a specific subset of cells in the inner nuclear layer of both the living donor and the post mortem donor, processes which extend from the inner nuclear layer to the ganglion cell layer can also be seen.

Supplementary data 1 (SPD 1) also shows PKC α staining across a macula explant, staining was found to be in the inner nuclear layer throughout the macula explant apart from the fovea where PKC α was absent.

3.2.1.5 NeuN

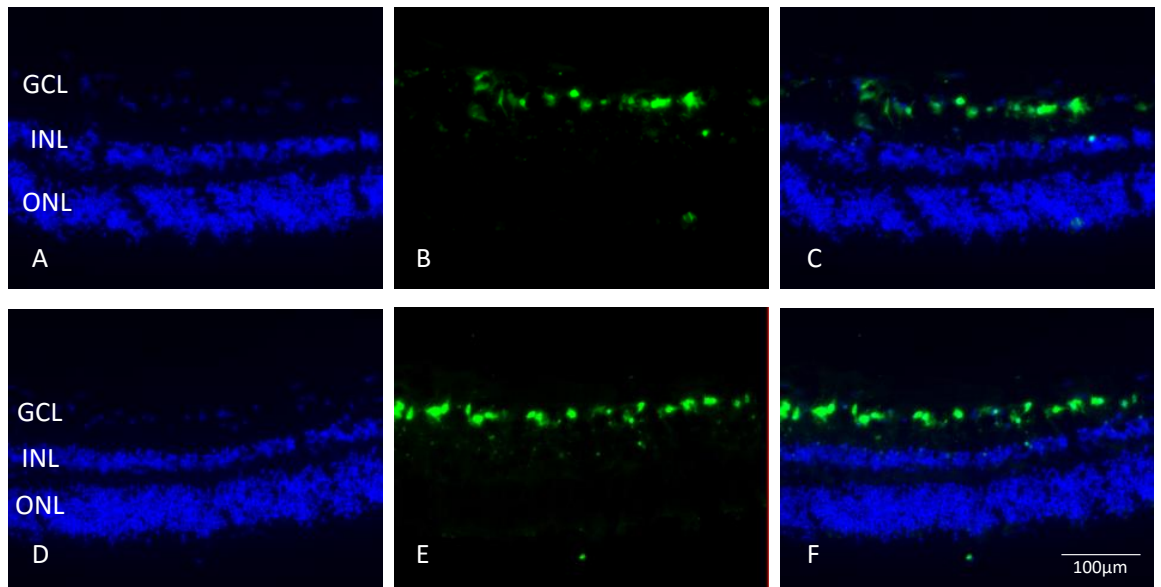


Figure 3.5 - NeuN Presence in the Live and Post Mortem Human Paramacula Retina

Cross section of a paramacular human retina immunostained for NeuN (green). Fig 3.5 A - C shows the immunostaining from a cross section of retina from a living donor. Fig 3.5 D - E shows the immunostaining from a cross section of retina from a post mortem donor (pre-24h).

NeuN was selected to identify retinal ganglion cells in the ganglion cell layer. NeuN immunostained cell bodies within the ganglion cell layer of both the living donor and the post mortem donor. Some cell bodies were also stained in the inner nuclear layer, although these were infrequent.

3.2.1.6 THY1

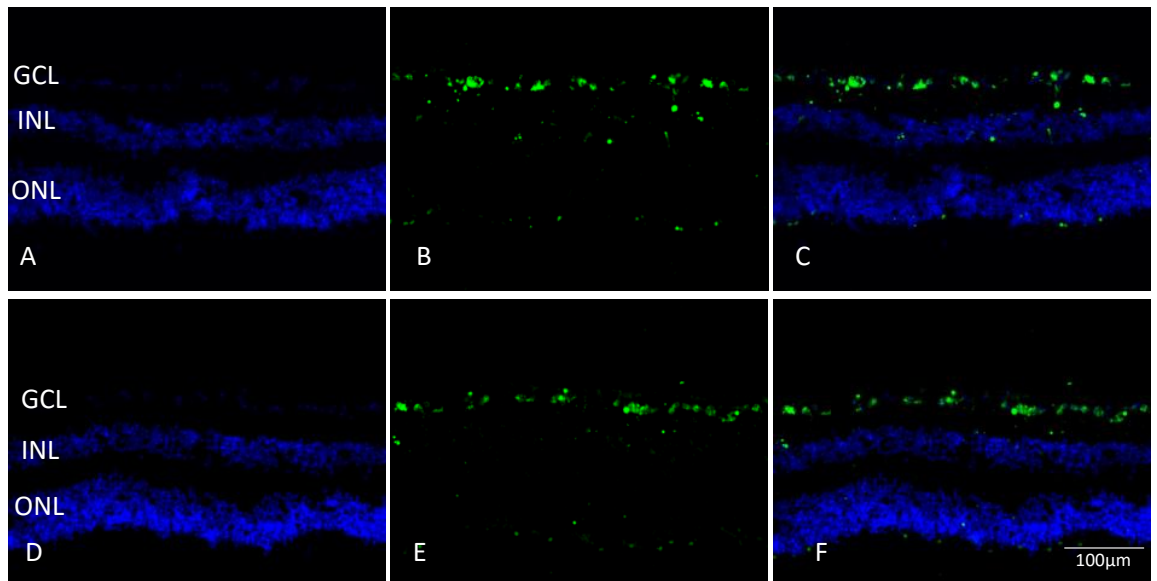


Figure 3.6 - THY1 Presence in the Live and Post Mortem Human Paramacula Retina

Section of a paramacular human retina immunostained for THY1 (green). Fig 3.6 A - C shows the immunostaining from a cross section of retina from a living donor. Fig 3.6 D - E shows the immunostaining from a cross section of retina from a post mortem donor (pre-24h).

THY1 was also selected as a retinal ganglion cell marker. THY1 staining was seen in the retinal ganglion cell layer of both the living donor and the standard donor.

3.2.1.7 β III Tubulin

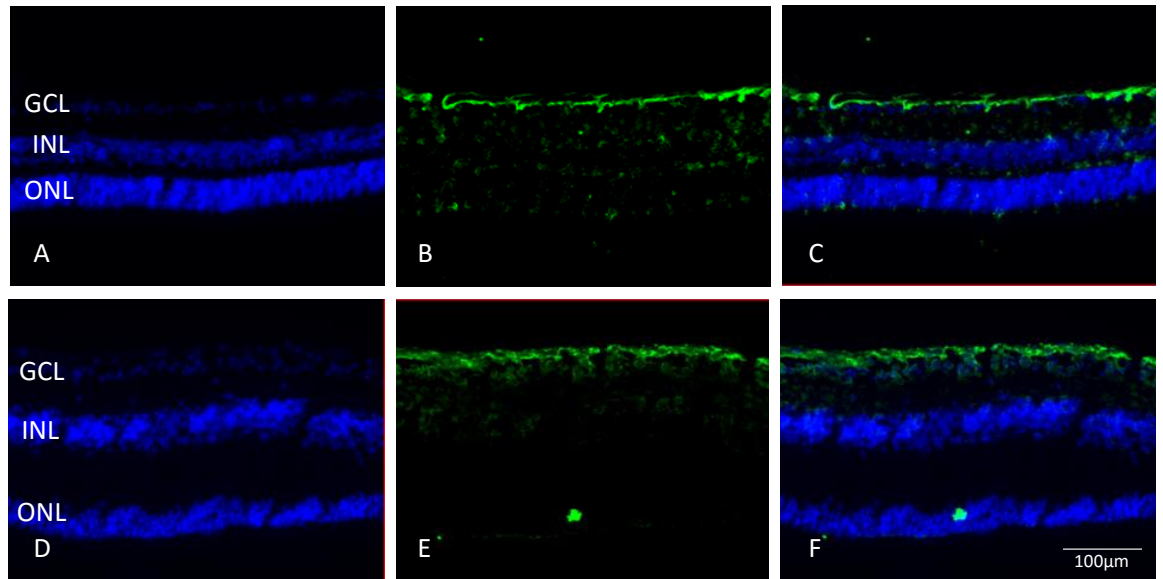


Figure 3.7 - β III Tubulin Presence in the Live and Post Mortem Human Paramacula Retina

Cross section of the paramacula human retina immunostained for Tubulin (green). Fig 3.7 A - C shows the immunostaining from a cross section of retina from a living donor. Fig 3.7 D - E shows the immunostaining from a cross section of retina from a post mortem donor (pre-24h).

β III Tubulin was also selected as a retinal ganglion cell marker. Tubulin immunostaining was present within cell bodies of the ganglion cell layer, and within the nerve fibre layer. This was consistent between the living donor and the post mortem donor as shown in Figure 3.7.

3.2.1.8 Glutamine Synthetase

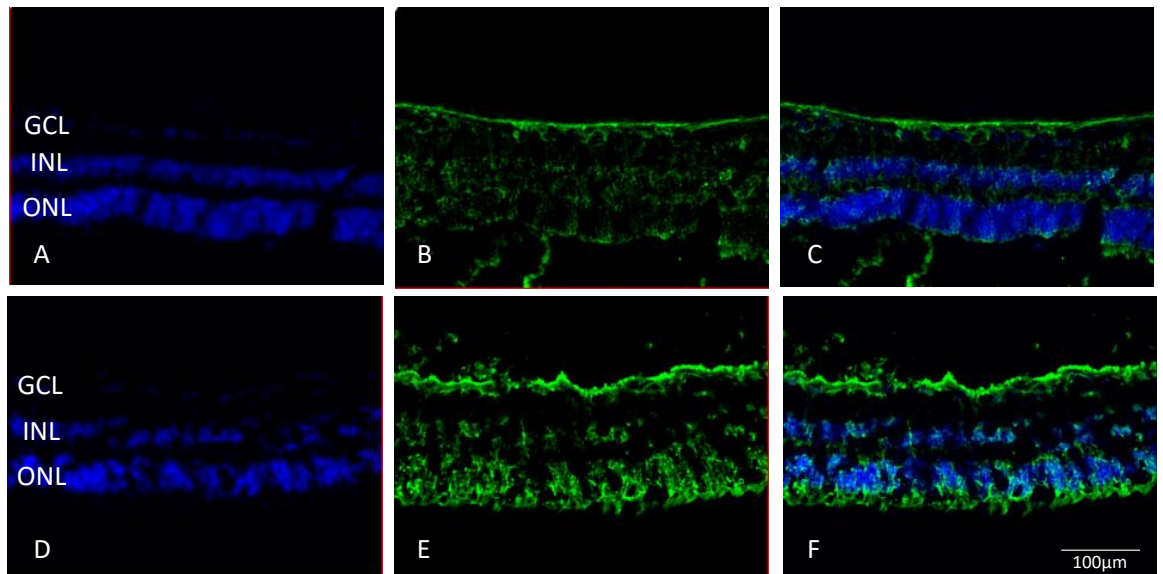


Figure 3.8 - Glutamine Synthetase Presence in the Live and Post Mortem Human Paramacula Retina

Cross section of the paramacula human retina immunostained for Glutamine Synthetase (green). Fig 3.8 A - C shows the immunostaining from a cross section of retina from a living donor. Fig 3.8 D - E shows the immunostaining from a cross section of retina from a post mortem donor (pre-24h).

Glutamine synthetase was selected as a marker of Müller cell presence within the human retina. Throughout the retina of the living donor (Figure 3.8 A-C) a distinct staining was seen in the inner retina corresponding to the area where the Müller cell end feet would be found. Müller cell bodies were also stained within the inner nuclear layer and the processes from these can be seen extending into the outer nuclear layer. A similar staining pattern was found in the retina of the post mortem donor (Figure 3.8 D-E), however the staining appeared to be stronger in the outer nuclear layer.

3.2.1.9 AHNAK2

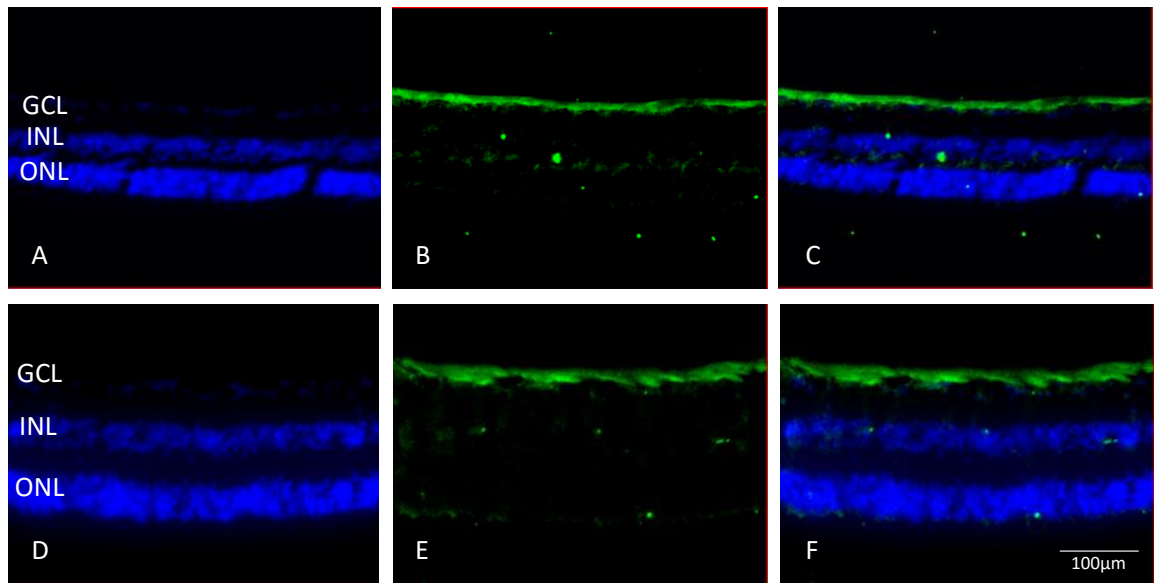


Figure 3.9 - AHNAK2 Presence in the Live and Post Mortem Human Paramacula Retina

Cross section of the paramacula human retina immunostained for AHNAK2 (green). Fig 3.9 A - C shows the immunostaining from a cross section of retina from a living donor. Fig 3.9 D - E shows the immunostaining from a cross section of retina from a post mortem donor (pre-24h).

AHNAK2 was selected as a marker of the inner retina. AHNAK2 was found to strongly stain the nerve fibre layer in both the post mortem donor and the living donor, ganglion cell bodies were also stained with both donors. A small amount of staining was also apparent in the outer plexiform layer of the living donor.

3.2.1.10 Heat Shock Protein 70

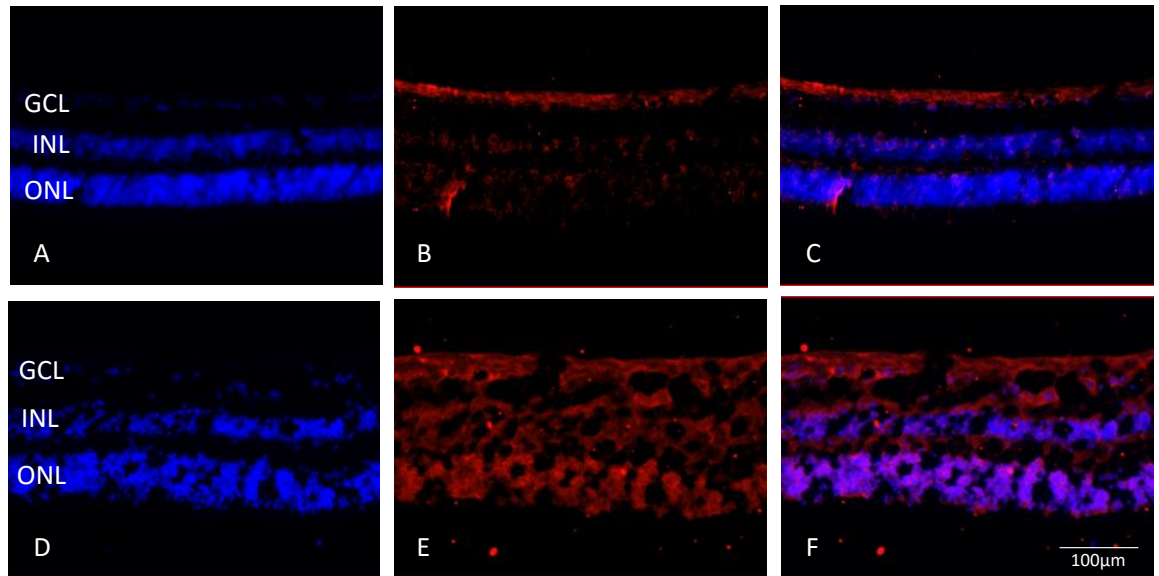


Figure 3.10 - Heat Shock Protein 70 Presence in the Live and Post Mortem Human Paramacula Retina

Cross section of the paramacula human retina immunostained for Heat Shock protein 70 (Red). Fig 3.10 A - C shows the immunostaining from a cross section of retina from a living donor. Fig 3.10 D - E shows the immunostaining from a cross section of retina from a post mortem donor (pre-24h).

Heat Shock Protein 70 (HSP70) was also investigated due to data obtained by Ma et al (2012) which indicated high levels of HSP70 mRNA in the ganglion cell layer. The living donor (Figure 3.10 A-C) showed HSP70 to be present in all nuclear layers, however the strongest staining was found to be in the ganglion cell layer, whereas the post mortem donor (Figure 3.10 D-E) displayed widespread staining throughout the retina.

3.2.2 mRNA Expression of Cell Specific Markers Within Whole Macula and Paramacula Samples

Distribution of the mRNA of key cell specific markers was investigated throughout the five paramacula samples and the macula sample in order to investigate the density and distribution of cell specific markers throughout the human retina.

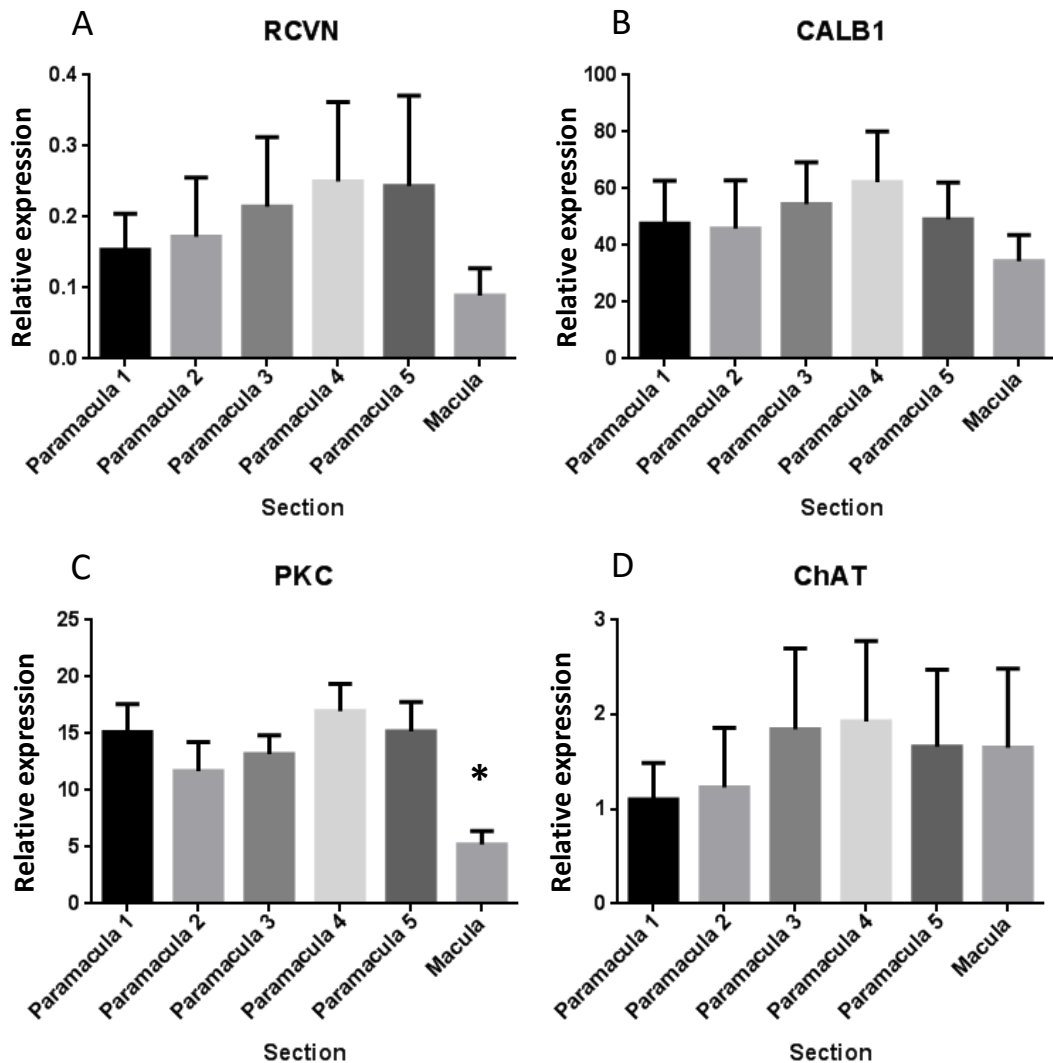


Figure 3.11 - Expression of Outer and Inner Nuclear Layer Markers in Whole Explants. Expression of outer nuclear layer cell marker *RCVN* and inner nuclear layer markers *CALB1*, *PKC* and *CHAT* within paramacula samples 1 -5 (mean + SEM n=5) and macula samples (mean + SEM n=4) relative to the housekeeping genes *TOP1* and *CYC1*. * Indicates a significant difference between the sample and all other samples ($P < 0.05$) (One-way ANOVA with Tukeys post hoc test)

Expression of the outer nuclear layer cell marker *RCVN* and inner nuclear layer markers *CALBI*, *PKC α* and *CHAT* was investigated within the 5 paramacula and the macula samples (Figure 3.11) to investigate the distribution and density of photoreceptor cells, horizontal cells, bipolar cells and amacrine cells (respectively) within these regions.

RCVN is a marker of photoreceptors. *RCVN* showed a trend of increasing expression from paramacula sample 1 to paramacula sample 5. A trend of lower expression within the macula compared to all paramacula samples was also seen, however variability was high and no significant differences were seen.

CALBI was used as a marker of horizontal cells. *CALBI* showed even distribution throughout all 5 paramacula samples and the macula sample.

PKC α is a marker of rod on bipolar cells. *PKC α* displayed even distribution throughout the 5 paramacula samples and significantly lower expression within the macula compared to the paramacula samples.

CHAT is a marker for amacrine cells. *CHAT* showed similar levels of expression throughout the five paramacula and macula samples although it was noted that variation between samples for different donors was high.

Expression of the ganglion cell markers *THY1*, *BRN3A*, *AHNAK2* and *RBFOX3* (NeuN) were investigated within the 5 paramacula samples and the macula sample (Figure 3.12) to explore the distribution and density of ganglion cells within these regions. It was interesting to compare different markers for one cell type to determine which might be the most appropriate for use in the human retina.

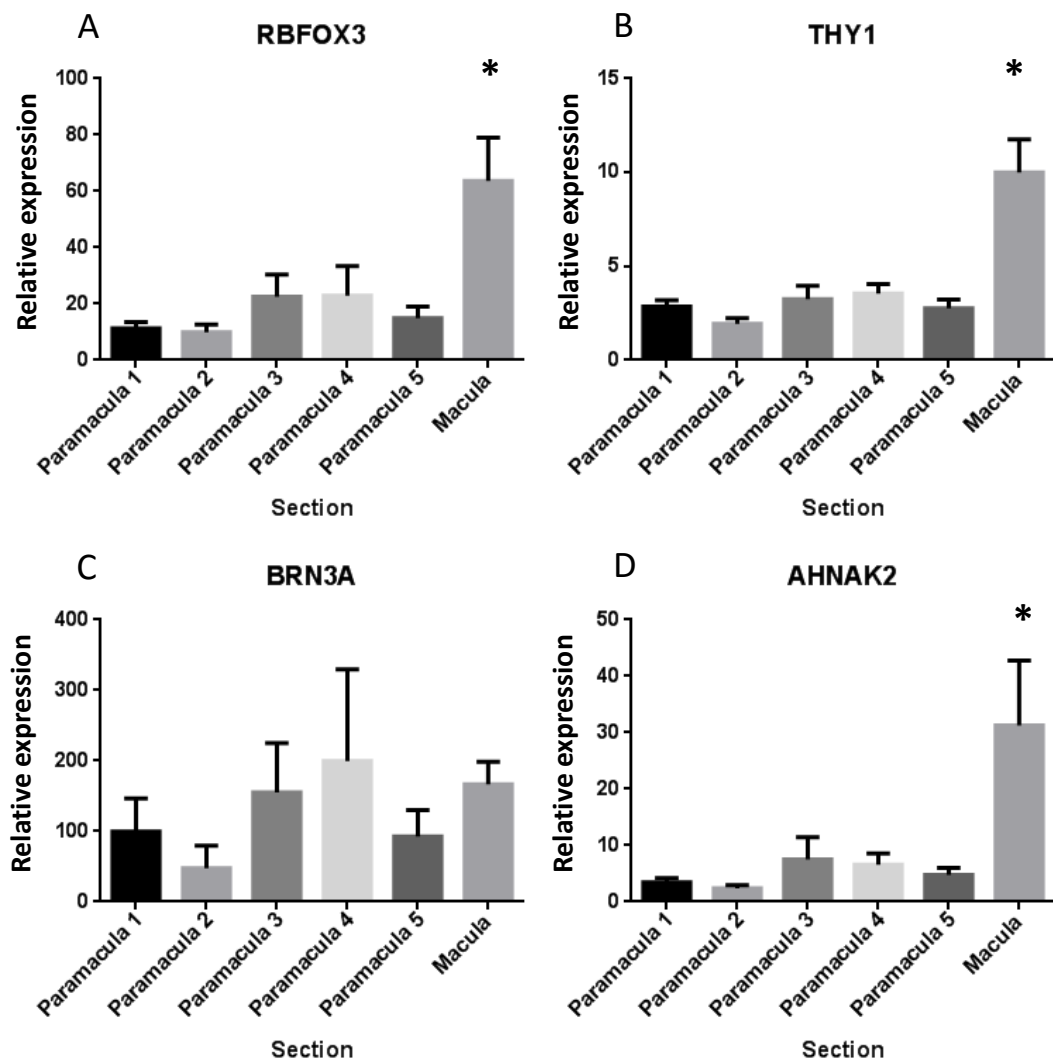


Figure 3.12 - Expression of Ganglion Cell Layer Markers in Whole Explants.

Expression of known ganglion cell markers: *RBFOX3*, *THY1*, *BRN3A* and *AHNAK2* within paramacula samples (mean + SEM n=5) and macula samples (mean + SEM n=4) relative to the housekeeping genes *TOP1* and *CYC1*. * Indicates a significant difference between the sample and all other samples (P<0.05) (One-way ANOVA with Tukeys post hoc test)

THY1, *AHNAK2* and *RBFOX3* all showed a significantly higher level of expression in the macula compared to the paramacula as would be expected for markers of

retinal ganglion cells. *BRN3A* did not show typical ganglion cell expression, with variable expression throughout the paramacula and macula samples.

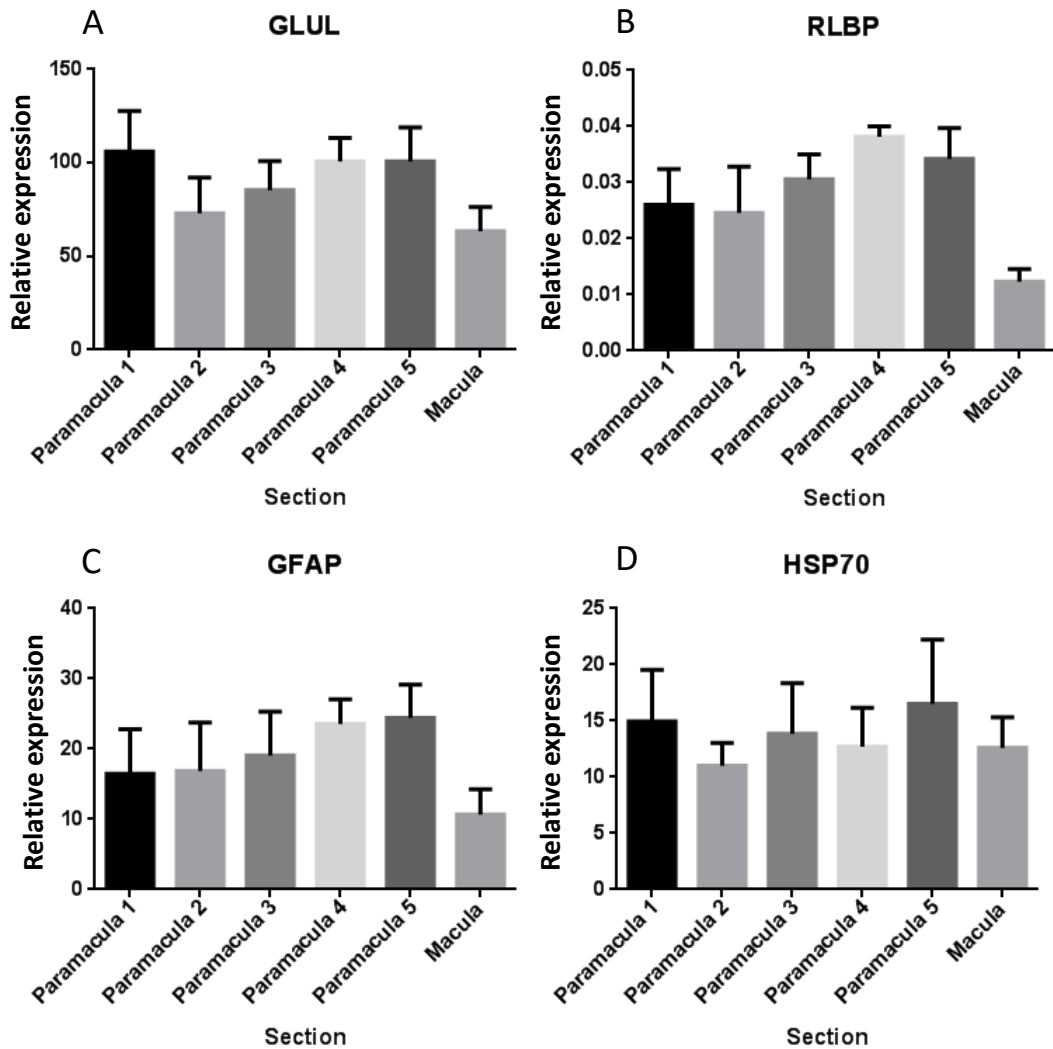


Figure 3.13 - Expression of Müller Cell Markers in Whole Explants. Expression of known Müller cell markers: *GLUL*, *RLBP* and *GFAP*, and the cell stress marker *HSP70* within paramacula samples 1 -5 (mean + SEM n=5) and macula samples (n=4) relative to the housekeeping genes *TOP1* and *CYC1*. * Indicates a significant difference between the sample and all other samples (P<0.05) (One-way ANOVA with Tukeys post hoc test)

Expression of the Müller cell markers *GLUL*, *RLBP*, *GFAP* and the cell stress marker *HSP70* were also investigated in the 5 paramacula and the macula samples (Figure 3.13).

The Müller cell markers *GLUL*, *RLBP* and *GFAP* displayed similar trends in expression, with lower expression in the macula compared to paramacula samples. This lower expression in the macula was significant for *RLBP* expression. *HSP70* (a cell stress marker) differed to the other Müller cell markers in that expression was similar throughout all paramacula and macula sections.

3.2.3 mRNA Profiling of Retinal Cell Markers in the Human Retina

Planar sectioning allows the analysis of mRNA expression throughout the different layers of the retina to be conducted. The expression profile of cell specific markers throughout the different layers of the retina was investigated in the retina, comparing macula and paramacula regions and also retina from post mortem and living donors. This will provide information about the location and strength of expression of the cell specific markers throughout the retina in the macula and paramacula regions as well as any differences that may occur as a result of post mortem changes.

3.2.3.1 mRNA Profiling of Retinal Cell Markers in the Post Mortem Macula

The post mortem macula was first investigated to determine the expression profile of the cell specific markers *THY1*, *AHNAK2*, *RBFOX3*, *CHAT*, *RLBP*, *PRKCA*, *CALB1* and *RCVRN* (Figure 3.14).

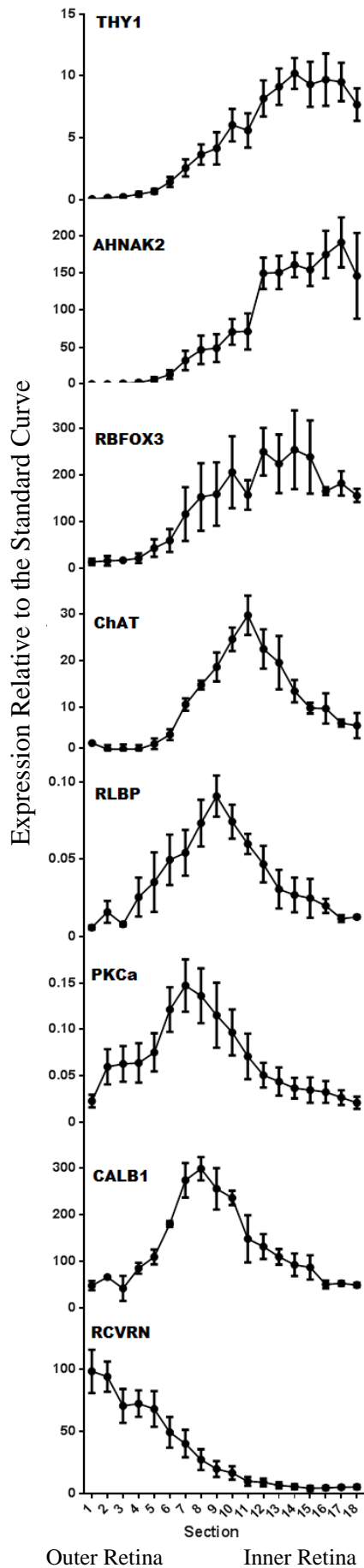


Figure 3.14 - Planar Sectioned Macula Explant From a Post Mortem Donor

Expression profile of *THY1*, *AHNAK2*, *RBFOX3*, *CHAT*, *RLBP*, *PRKCA*, *CALB1*, *RCVRN* mRNA in macula sections of post mortem human retina (mean + SEM; n=4).

mRNA analysis of the planar sectioned macula samples revealed the location of peak expression of the cell specific marker being investigated.

The outermost retina displayed peak expression of *RCVRN*. The highest level of expression was in sections 1 and 2, which was followed by small a decrease in expression at section 3. Expression plateaued from section 3 to section 5 which was followed by a gradual decrease in expression until baseline expression was reached at section 14.

The mid-section, corresponding to the inner nuclear layer displayed peak expression of the markers *CALB1*, *PRKC α* , *RLBP* and *ChAT*.

CALB1 expression displayed baseline expression in the outer retina until section 3, followed by an increase in expression until peak expression was reached at section 8. This was followed by a decrease in expression until baseline expression was reached again in the inner retina at section 16.

PRKC α displayed low levels of expression in the outer retina at section 1, this was followed by a gradual increase in expression until peak expression occurred at section 7. This peak was followed by a gradual decrease in expression towards the inner retina at section 16.

RLBP expression displayed low levels of expression in the outer retina until section 3, this was followed by an increase in expression until peak expression was reached in section 9. This peak expression was followed by a decrease in expression until section 17 where baseline expression was reached in the inner retina.

CHAT expression was baseline within the outer retina until section 6 where a gradual increase in expression followed until peak expression was reached at section 11. A decrease in expression then occurred until section 16.

The inner retina displayed peak expression of the markers *RBFOX*, *AHNAK2* and *THY1*. *RBFOX3* expression was baseline in the outer retina until section 4 where a gradual increase in expression occurred until a plateau of peak expression was reached from section 12 -15. This was then followed by a slight decrease in expression in sections 16 – 18.

AHNAK2 expression was baseline in the outer retina until section 4. This was followed by a gradual increase in expression until section 11 where there was a sharp increase in expression. Expression then remained high and peaked at section 17.

THY1 expression was baseline from section 1 – 4 followed by a gradual increase to peak expression at section 14. Expression then remained high until section 17 followed by a slight reduction in expression at section 18.

3.2.3.2 mRNA Profiling of Retinal Cell Markers in the Living Donor Macula

The expression profile of the live donor Macula sample was then investigated (Figure 3.15), allowing a comparison between the expression profiles of the standard donor, and the live donor to be made.

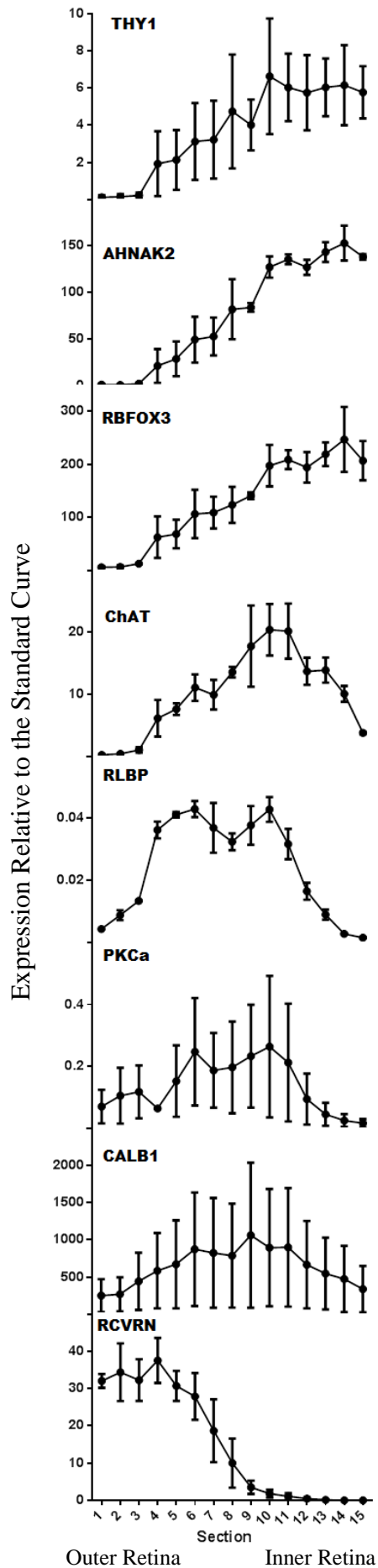


Figure 3.15 - Planar Sectioned Macula Explant from a Living Donor

Expression profile of *THY1*, *AHNAK2*, *RBFOX3*, *CHAT*, *RLBP*, *PRKCA*, *CALB1*, *RCVRN* mRNA in macula sections of a living donor (mean + SEM, n=2).

Planar PCR data from the macula region of a living donor (Figure 3.15) showed the same pattern of expression as the post mortem human retina (Figure 3.14).

The outer retina displayed peak expression of *RCVRN*. This was shown by peak expression occurring in sections 1 – 4. A gradual decrease in expression then followed.

The central region sections displayed peak expression of the following markers *CALB1*, *PRKC α* , *RLBP* and *ChAT*. *CALB1* displayed peak expression in the inner nuclear layer in the macula of the post mortem donor (Figure 3.14), however within the macula of the live donor there were variable results. This is likely due to the small number of repeats available.

PRKC α displayed peak expression within the inner nuclear layer between section 6 and section 10. There was also some variability seen with *PRKC α* expression due to the small number of repeats.

RLBP displayed a low level of expression at section 1. This was followed by a gradual increase in expression to section 3 where a sharp increase in expression occurred to display peak expression at section 6. There was a slight decrease in expression which was followed by another peak in expression at section 10 and then a decrease to basal expression at section 15.

ChAT expression was baseline within the outer retina until section 3, this was followed by a gradual increase in expression until peak expression was reached at section 10. A decrease in expression was then found from section 12.

The ganglion cell layer displayed peak expression of the ganglion cell markers *RBF3*, *AHNAK2* and *THY1*. These all displayed a similar pattern of expression of baseline expression in the outer retina until section 3, followed by a gradual increase in expression until peak expression is reached at approximately section 9 until section 15.

3.2.3.3 mRNA Profiling of Retinal Cell Markers in the Post Mortem Paramacula

Whole section analysis of cell specific mRNA displayed differences between paramacula sections and macula sections, reflecting a difference in cell density between the two regions.

To build a comprehensive profile of cell specific mRNA, the potential differences that may also occur within the distribution of cells throughout the nuclear layers of the retina was investigated between planar sectioned macula and paramacula sections.

For this reason the expression profile of cell specific mRNA was then investigated within standard donor paramacula sections (Figure 3.16).

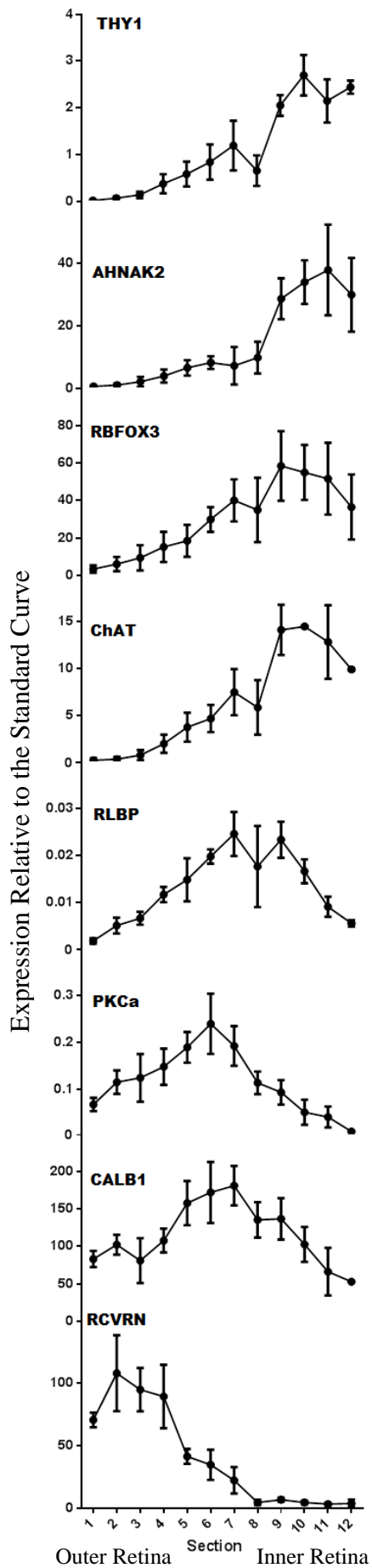


Figure 3.16 - Planar Sectioned Paramacula Explant from a Post Mortem Donor

Expression profile of *THY1*, *AHNAK2*, *RBFOX3*, *CHAT*, *RLBP*, *PRKCa*, *CALB1* and *RCVRN* mRNA in paramacula sections of a post mortem human retina (mean + SEM n=4).

The expression profile of cell specific marker genes from planar sectioned paramacula samples was similar to the expression profile of planar sectioned macula samples. The main difference being the number of sections, there were more sections available from the macula due to the tissue being thicker at this region.

The outer retina displayed peak expression of *RCVRN*. This peak expression occurred at section 2, and high levels of expression were maintained until section 4. A decrease in expression then occurred until basal expression levels were reached at section 8.

The inner regions displayed peak expression of the following markers *CALBI*, *PRKCA*, *RLBP* and *CHAT*.

CALBI expression was low in the outer retina, expression then increased from section 3 where peak expression was reached at section 7. A gradual decrease then followed this until section 12.

PRKCA expression was low in the outer retina and gradually increased until peak expression was reached at section 6, this was followed by a gradual decrease in expression.

RLBP expression was low in the outer retina. Expression gradually increased until section peak expression was reached at section 7. High expression levels were present until section 9 where a decrease in expression occurred to section 12.

CHAT expression was baseline in the outer retina. Expression then gradually increased until section 8 where a large increase in expression occurred until section 11.

The ganglion cell layer displayed peak expression of the markers *RBFOX3*, *AHNAK2* and *THY1*. These markers followed a similar expression pattern of baseline expression in the outer retina, followed by a gradual increase until peak expression was reached from sections 9 – 12.

3.2.3.4 mRNA Profiling of Retinal Cell Markers in the Living Donor Paramacula

Analysis of planar sectioned paramacula sample (Figure 3.17) was performed to ensure the pre-24 hour post mortem retina possesses the same expression properties as the live donor.

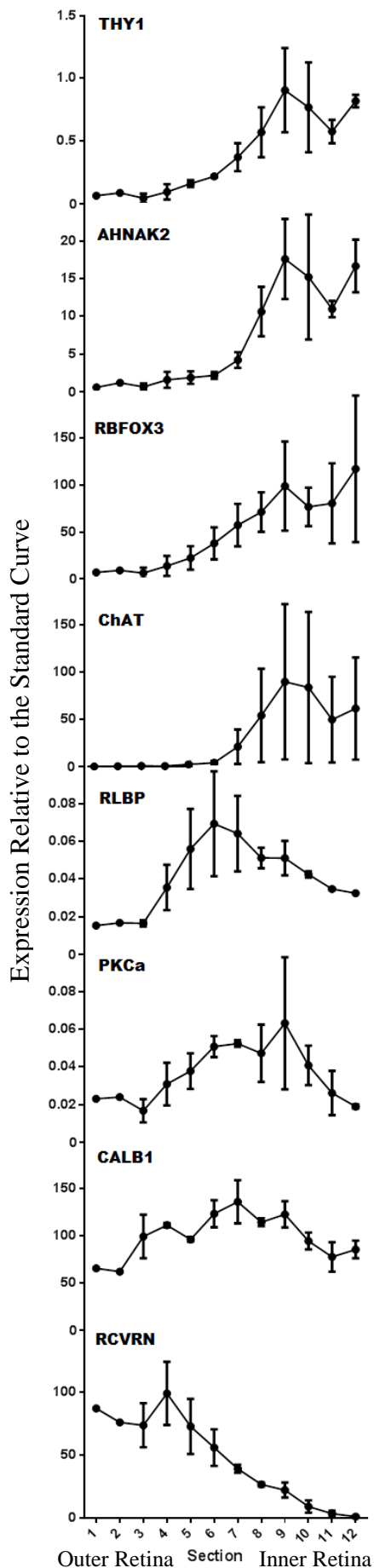


Figure 3.17 - Planar Sectioned Paramacula Explant from a Living Donor

Expression profile of *THY1*, *AHNAK2*, *RBFOX3*, *ChAT*, *RLBP*, *PRKCa*, *CALB1* and *RCVRN* mRNA in paramacula sections of a retina from a living human donor (mean + SEM, n=2).

As in the macula region, the paramacula retina from the living donors possessed very similar expression properties to the post mortem donor.

The outer retina possessed peak expression of *RCVRN*. High expression began at section 1, however peak expression was not reached until section 4. A decrease in expression then followed through to section 12.

The inner regions of the retina displayed peak expression of the markers *CALBI*, *PRKCα* and *RLBP*

CALBI expression was low in the outer retina. Expression gradually increased and reached peak expression at section 7, this was followed by a gradual decrease until section 12.

PRKCα expression was low in the outer retina, an increase in expression was seen from section 3 until peak expression was reached at section 9. The peak at section 9 was found to possess some variability (due to the small number of repeats) and therefore may be a false peak, whereas the peak at section 6 displayed little variability. This peak was then followed by a gradual decrease in expression.

RLBP expression was baseline in the outer retina. Expression gradually increased until peak expression was reached at section 6, this was followed by a decrease in expression.

ChAT expression was baseline in the outer retina until section 6, expression then increased and reached peak expression at section 9 and remained high.

The inner retina displayed peak expression of the markers *RBFOX3*, *AHNAK2* and *THY1*. These markers displayed similar expression patterns of baseline expression in the outer retina, followed by an increase to peak expression at section 9, high expression levels remained until section 12.

3.3 Discussion

Before any investigation into the toxicity of compounds on the human retina can be performed, three important factors must be considered.

The first is the profile of the various cell types within the human retina. This profile will prove useful when investigating the effect of retinotoxins by helping identify the cell types affected by such compounds. This was investigated using both immunohistochemistry and QRT-PCR.

The second is whether changes take place in terms of structure and expression as a result of the retina being taken from post mortem material. This is important as any changes that may occur due to the tissue being post mortem could have the potential to hide the effect of any retinotoxin being investigated. The immunohistochemical properties of the living donor retina and the post mortem retina were therefore investigated to find any differences that may occur. Alongside this, mRNA expression profiles of cell specific marker genes were investigated, again comparing the profile of the live retina to that of the standard retina.

Finally, when investigating the distribution of mRNA expression, the equivalence of expression throughout the five paramacula samples needs to be considered. This will aid in the development of the *ex vivo* model to assess retinotoxicity in that if the samples are found to possess equivalent expression throughout the five paramacula samples, then one paramacula sample may be used as a control, whilst the effect of varying concentrations of a retinotoxin on expression of the other four paramacula samples can be analysed.

Neuronal specific enolase is an enzyme which is involved in the glycolysis pathway in neurons (Kirino et al., 1983) (Bonner et al., 2000). The immunohistochemical results show staining was present throughout the retina, however it can be seen to mark the outer plexiform layer and the photoreceptor cell bodies most strongly (Figure 3.1). A slight difference was found between the live donor and the post mortem donor in that the outer plexiform layer was labelled more clearly in the post donor than in the live donor. Although this marker was interesting to use, it did not stain all neurons equally and therefore is not a good marker of all neuronal cells of the retina.

Recoverin binds specifically to a 23-kilodalton calcium binding protein which regulates the activation of guanylate cyclase, an enzyme which is stimulated during bright conditions via a decrease in cytosolic calcium in the photoreceptor outer segments (Dizhoor et al., 1991). It was seen to clearly immunostain photoreceptor cell bodies and the photoreceptor outer segments where this enzyme is most present (Figure 3.1). Whole explant mRNA analysis of recoverin showed equivalent expression throughout the five paramacula samples and a trend of lower expression in the macula sample (Figure 3.11A), and planar analysis revealed peak expression in the outer retina. Previous data has indicated that recoverin is expressed in both rods and cones (Gunhan et al., 2003), however data obtained here indicates that recoverin may be more highly expressed in rods than cones, with the higher density of cones in the macula causing the lower expression of recoverin compared to the paramacula regions. Overall recoverin was a good marker of photoreceptors and will prove to be useful in further studies involving photoreceptor investigations.

Calbindin-28k is a protein consisting of six E-helix-loop-F-helix-hand motifs (of which only four are active). This protein binds to Ca^{2+} to act as a calcium buffer to help maintain fluctuations with intracellular Ca^{2+} (Mojumder et al., 2008). The antibody for Calbindin-28k effectively marked the cone outer segments along with horizontal cells and to a lesser extent some amacrine cells (Figure 3.3). There is a slight difference between the live donor and the standard donor with calbindin in that more cone outer segments were immunostained within the photoreceptor layer of the live donor, however this is most likely due to the retinal extraction process.

Photoreceptor outer segments are particularly delicate and can easily become detached during retinal dissection. During removal of the retina, the retina becomes detached from the RPE and due to the engulfed outer segments the outer segments can break off from the photoreceptor cell bodies at any point between the external limiting membrane and the end of the outer segments. Therefore variance in number of outer segments varies between donors. Whole sample mRNA analysis of calbindin revealed similar expression throughout the five paramacula sections and the macula sample, indicating even distribution of the cells which express calbindin. Planar sectioning revealed calbindin to be most highly expressed in the inner nuclear layer, with peak expression occurring in the outer parts of the INL, indicating that horizontal cells may be responsible for the high expression. Although calbindin

proved to be an effective marker of inner nuclear layer cells, it also stained other cells not in the inner nuclear layer, therefore is not a marker exclusive enough for further investigation of inner nuclear layer cells.

PKC is a family of enzymes which are involved in cell signalling pathways downstream of second messengers (Lameirao et al., 2009). PKC- α specifically identified rod ON bipolar cells within the inner nuclear region of the retina (Figure 3.4). Further to this, a whole macula image of a PKC α immunostained section was performed and is shown in supplementary data 1 (SPD1), in this image it can be seen that stained bipolar cells become less dense towards the fovea, where there are no stained bipolar cells. This is in line with other research which has shown that Rod ON bipolar cells only appear approximately 1mm away from the fovea (Lameirao et al., 2009). Whole explant mRNA analysis of PKC α showed expression equivalence throughout the five paramacula samples, and significantly lower expression within the macula. This significantly lower expression of PKC α in the macula re-enforces data showing that PKC α marks rod ON bipolar cells. Planar analysis also revealed that peak expression occurs within the inner nuclear layer. PKC α is therefore a good marker of the inner nuclear layer and may be used further to investigate rod on bipolar cells in the inner nuclear layer.

ChAT has previously been used to immunolabel cholinergic amacrine cells and displaced amacrine cells in the human retina (Hutchins and Hollyfield, 1987). These experiments were attempted to be replicated, however the antibody showed no specificity towards any cells and therefore the images were not included. Whole explant analysis of ChAT mRNA expression showed that expression was equivalent throughout the paramacula sections and the macula, whereas planar sectioning revealed a difference between the expression pattern in paramacula and macula. Macula peak expression was found within the inner nuclear layer, whereas the paramacula was more associated with with the ganglion cell layer. This difference may be due to the higher presence of displaced amacrine cells within the ganglion cell layer in the paramacula region. This is re-enforced by previous studies which have shown that only 3% of central retinal cells are displaced amacrine cells, whereas ~80% of cells present within the peripheral retina are displaced amacrine cells (Curcio and Allen, 1990). Overall, ChAT would be useful for further

investigation of amacrine cells through mRNA, however investigation of amacrine cells through the ChAT antibody used in this research would not be viable.

Neuronal nuclei (NeuN) is a neuron specific nuclear protein which is expressed in most neuronal cell types within vertebrates (Mullen et al., 1992). Within the retina, NeuN is an effective ganglion marker in the post mortem donor and the living donor (Figure 3.5). Whole section mRNA analysis of *RBFOX3* (NeuN) displayed equivalent expression throughout the five paramacula sections and significantly increased expression in the macula. Planar sectioning analysis of NeuN revealed peak expression in the ganglion cell layer in both macula and paramacula samples. The significantly higher expression of NeuN in macula whole explants compared to paramacula explants can be explained by the macula's thick ganglion cell layer. The thick ganglion cell layer contains high numbers of ganglion cells and provides a low photoreceptor to ganglion cell ratio. This (in particular the fovea where the majority of light is focussed) leads to a high visual acuity in the macula, whereas in the paramacula region there is a thinner ganglion cell layer, and therefore fewer ganglion cells. This increases the photoreceptor to ganglion cell ratio and decreases visual acuity, but increases sensitivity to light in the peripheral retina. Overall, NeuN is a good marker of ganglion cells and would prove to be a useful in future studies of ganglion cells.

THY1 is a glycosylphosphatidylinositol anchored protein (Partida et al., 2012) which is expressed within approximately 80% of retinal ganglion cells (Chauhan et al., 2012). Figure 3.6 showed THY1 stained the ganglion cell layer of the retina to a similar degree in both the living donor and the post mortem donor. Like NeuN, THY1 expression in whole explants showed equivalent expression through the five paramacula sections and significantly higher expression within the macula section. Planar analysis also showed THY1 expression peaked within the ganglion cell layer. THY1 is also a good marker of ganglion cells and could be useful for future studies of human retinal ganglion cells.

Beta III tubulin is a core protein within microtubules. The antibody for tubulin marked the nerve fibre layer and the ganglion cell bodies (Figure 3.7), a region which has a high density of microtubules. Beta III tubulin expression was not investigated in whole explants due to the use of other ganglion cell markers, however

in a recent paper by Osborne it has been shown to be a suitable marker of ganglion cells (Osborne et al., 2015b).

The AHNAK family is a family of scaffold PDZ proteins which have multiple cellular process functions such as membrane repair (Marg et al., 2010). AHNAK2 possessed similar marking to beta III tubulin, it also marked the nerve fibre layer and some ganglion cells (Figure 3.8). Whole section analysis of AHNAK2 showed similar expression properties as the other ganglion cell markers NeuN and THY1, with equivalent expression throughout the five paramacula sections and significantly higher expression within the macula section. Planar sectioning also revealed peak expression of AHNAK2 to reside within the ganglion cell layer. AHNAK2 is not known as a marker of human retinal ganglion cells, however this research and previous research by Ma (2012) has shown that it is a good marker, it is however not as specific as NeuN or THY1 (shown by the incorporation of the nerve fibre layer in the immunohistochemical results).

BRN3A has been shown to be a suitable marker of retinal ganglion cells in rats and mice (Nadal-Nicolas et al., 2009). Whole explant mRNA expression was analysed, and unlike the ganglion cell markers THY1, AHNAK, and RBFOX3, BRN3A did not show consistent expression throughout the five paramacula samples or significantly higher expression in the macula and therefore does not appear to be an appropriate ganglion cell marker to be used within the human retina.

Glutamine synthetase is the primary enzyme responsible for the breakdown of excessive glutamate to prevent excitotoxicity from glutamate. It is normally present within Müller cells of the retina and is in high concentrations in regions which surround glutamergic synapses (Moreno et al., 2005). The immunohistochemical images obtained showed the antibody against glutamine synthetase marked Müller cell end feet to the highest degree and Müller cell bodies to a lesser extent (Figure 3.8).

Müller cell mRNA expression was also investigated using the known markers GLUL, RLBP and GFAP (Hollborn et al., 2011). All of the Müller cell markers displayed equivalent expression throughout the 5 paramacula samples and lower expression within the macula sample. This may be due to the lower number of Müller cells in the foveal region, which overall reduces the number of these cells in

the macula sample. Only RLBP expression was investigated using planar sectioning as this gave the clearest results in whole explant analysis. Peak expression of RLBP was found to reside in the inner nuclear layer, re-enforcing this as a useful marker of Müller cells.

Heat shock protein 70 (Hsp70) is named so because of its molecular weight (70kDa) (Kayama et al., 2011), they are also named this because of their increase in expression with elevated temperature. The role of these proteins is the maintenance of the health of the cell, they aid in cellular processes such as the folding of proteins and the disposal of irreversibly damaged proteins (Urbak and Vorum, 2010). HSP is not only increased due to hyperthermia, it can also become increasingly expressed due to other stressors such as ischemia, osmotic and oxidative stress (Urbak and Vorum, 2010). Another vital role that HSP's play is the prevention of apoptosis. Hsp70 can achieve this by interfering with; the translocation of Bax and the Apaf-1 apoptosome (Urbak and Vorum, 2010). Hsp70 was stained to the highest extent in the nerve fibre layer of the live donor and to a lesser extent throughout the rest of the retina. Within the post mortem donor Hsp70 immunostaining was high throughout the retina (Figure 3.10). Since Hsp70 is increased due to stressors, this protein may naturally be at higher levels within post mortem tissue due to expression changes after death. Expression of HSP70 mRNA was also investigated and displayed similar levels of expression throughout macula and paramacula samples. As an mRNA investigator, Hsp70 may be useful as an indicator of stress, however immunohistochemically it would be hard to investigate any changes in Hsp70 levels due to the strong presence in post mortem tissue.

The immunohistochemistry results provided by this research have given information regarding the location and density of cells within the retina. Importantly no major differences were found between the living donor and the pre-24 hour post mortem retina. This indicates that the *in vivo* human retina possesses the same structural and immunohistochemical properties as the post mortem retina, and therefore the pre-24 hour post mortem retina is a useful tissue. This data will be helpful when using the retina as a model to assess retinotoxicity, allowing the investigation into specific cell sensitivities to retinotoxic compounds, for example, through the use of co-localisation with cell death markers such as TUNEL or cleaved caspase 3.

Whole explant PCR analysis allowed investigation into the density and distribution of retinal cells throughout paramacula and macula samples. The differences in expression between the macula and paramacula samples shows that expression levels of cell specific markers can be used as a measure of cell density / population.

Another important factor determined from whole explant analysis was the equivalent expression throughout the 5 paramacula sections. This enables the cell specific markers to be used within a toxicity study, by using one control paramacula sample, and applying varying concentrations of a retinotoxic compound to the remaining 4 paramacula samples. Any changes in cell specific marker expression may reflect a decrease in that cell type, and the relative sensitivities of specific cell types to the retinotoxins to be determined.

It should be noted that a different method of analysis was used when investigating mRNA expression throughout planar sections. Previously planar data had been normalised to the highest value, leading to the highest expression always being 1 (Osborne et al., 2015b), however this would not allow for further investigation into the effect of retinotoxins on expression due to the fact the highest value will always be 1. This new method of analysis opens up opportunities to investigate the effect of retinotoxins on expression by looking into raw expression values. This new method of analysis does not distort the pattern of expression and each nuclear layer is still well represented by peaks of expression related to cell specific markers with little variability.

3.4 Conclusion

This chapter gives evidence supporting the use of this model in relation to three important areas. Firstly the similarity between the living donor and the post mortem donor as shown by the immunohistochemical and PCR results, providing good evidence on the suitability of the post mortem retina for use in subsequent experiments.

Secondly, expression equivalence throughout the five whole paramacula samples enables this method of cell density / population analysis to be used when

investigating the retinotoxicity of compounds on the retina. For example one of the five paramacula samples can be used as a control and varying concentrations of a potential retinotoxic compound can be applied to the remaining four paramacula samples. Expression of the cell specific markers can then be investigated and the sensitivity of specific cell types to the retinotoxins determined.

Finally, data from planar sectioned macula and paramacula samples provided confirmation of the location of expression and the cell type associated with expression. The new method of mRNA expression analysis of planar sections also opens opportunities to use this method for the investigation of cell sensitivities to retinotoxins and genes related to retinotoxins.

Chapter 4

4.0 The Effect of Known Retinotoxins on Retinal Cell Lines

4.1 Introduction

Cell lines are commonly used in initial studies of drug development where lead compounds are sought. During this, many compounds can be screened on cell lines in search of a compound which matches the specific activity sought (Woolley, 2003). Cell lines may also be utilised in later toxicology studies for investigations of a single endpoint, such as; does compound x induce autophagy, and / or induce cell death via apoptosis.

In this research two retinal cell lines were used: ARPE19 cells, a cell line derived from a primary culture of human RPE cells (retinal pigmented epithelium cells) which exhibit similar characteristics to native RPE cells (Dunn et al., 1996). And MIO-M1 cells, a cell line derived from a primary culture of human retinal cells which also exhibit similar characteristics to native Müller cells (Limb et al., 2002). These cell lines were exposed to a variety of retinotoxins to obtain information regarding the relative toxicity of the compounds.

Chloroquine and hydroxychloroquine are known retinotoxins. They are anti-malarial agents which also possess therapeutic properties in the treatment of other diseases including systemic lupus erythematosus and rheumatoid arthritis. Cases of chloroquine retinotoxicity are well documented with clinical effects such as a “bulls eye maculopathy” (Gaynes et al., 2008). Hydroxychloroquine causes fewer side effects and is less toxic and therefore is used more commonly than chloroquine as an anti-malarial agent.

Tamoxifen is a selective oestrogen receptor modulator (SERM) used in the treatment of hormone responsive breast cancer. It is also a known retinotoxin which can cause retinopathy and retinitis pigmentosa (Watanabe et al., 2010; Lazzaroni et al., 1998).

Indomethacin is a non-steroidal anti-inflammatory drug (NSAID) which is commonly used within the treatment of rheumatoid arthritis. Indomethacin is not

commonly known for its retinotoxic properties, however it has been recorded in one patient (Graham and Blach, 1988).

It is useful to compare the effects of the retinotoxins to a positive control which is known to cause cell death. The positive control used here is the reactive oxygen species (ROS) hydrogen peroxide (H_2O_2), a chemical compound which is a strong oxidizer and is created as a by-product of metabolism in mitochondria (Giorgio et al., 2007). Cells possess defence mechanisms against ROS, such as antioxidants (e.g. glutathione) and the enzymatic conversion of ROS to a less reactive product. However damage occurs to cells when an imbalance in favour of pro oxidants (ROS) occurs which may eventually lead to cell death. Cell death induced by H_2O_2 has been studied in ARPE19 cells and it was found that low levels of H_2O_2 induced apoptosis whereas high concentrations of H_2O_2 induced necrosis (Kim et al., 2003). Many retinal diseases are associated with oxidative stress, where an imbalance between pro oxidants such as H_2O_2 and anti-oxidants occurs. One example of this is age related macular degeneration (AMD) in which necrosis occurs in RPE cells as a result of oxidative stress (Hanus et al., 2013). Diabetic retinopathy is also associated with oxidative stress, and it has been found that Lutein (an anti-oxidant) prevented the neurodegenerative effect of diabetes within mice (Sasaki et al., 2010).

The aim of the research in this chapter is to establish retinal cell lines for use alongside an *ex vivo* retina as models to assess retinotoxicity. This will be achieved by firstly investigating the effect of specific retinotoxins on the two retinal cell lines ARPE19 cells and MIO-M1 cells.

4.2 Results

4.2.1 ARPE19 Cells Response to Retinotoxins

Initial experiments were conducted on ARPE19 cells. The effects of retinotoxins on the ARPE19 cell line were assessed with two assays, one to assess levels of cell death (the LDH assay), and the other to assess cell viability (the MTS assay).

4.2.1.1 Hydrogen Peroxide

The positive control was firstly investigated (H_2O_2) and Figure 4.1 displays the effect of increasing concentrations of H_2O_2 on levels of cell death (A) and cell viability (B) on ARPE19 cells.

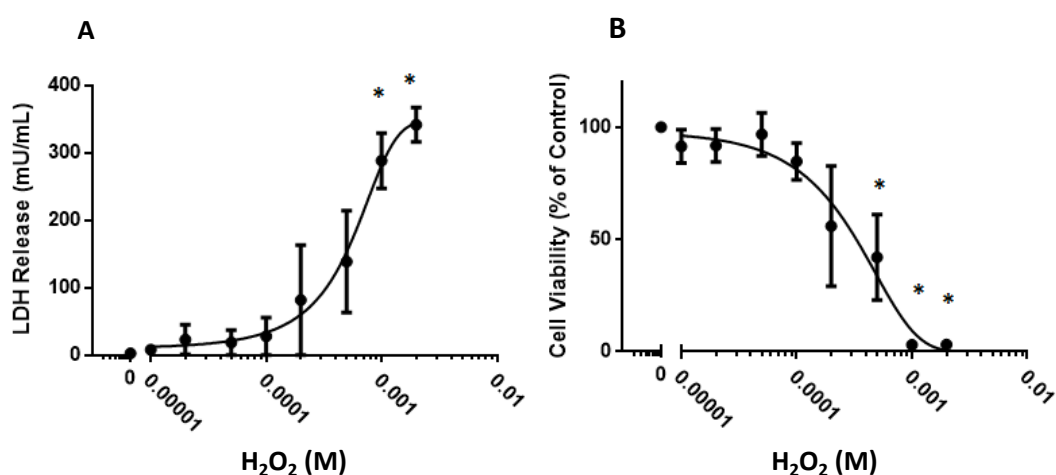


Figure 4.1 - ARPE19 cell death / viability in response to H_2O_2 - (A) Cell death (LDH release) and (B) cell viability (MTS assay) in response to varying concentrations of H_2O_2 (10 μ M-2mM) in ARPE19 cells (n=4) \pm SEM. * indicates significance (P<0.05) using one way ANOVA with Dunnetts post-hoc test.

Hydrogen peroxide caused a dose dependent increase in cell death as measured by LDH release and decrease in cell viability. A significant increase in cell death was found from 1mM (A) and a significant decrease in cell viability found from 500 μ M (B).

4.2.1.2 Indomethacin

ARPE19 cells were exposed to varying concentrations of indomethacin to reveal the effect of a relatively unknown retinotoxin on levels of cell death (A) and cell viability (B) of the retinal pigmented epithelial cell line.

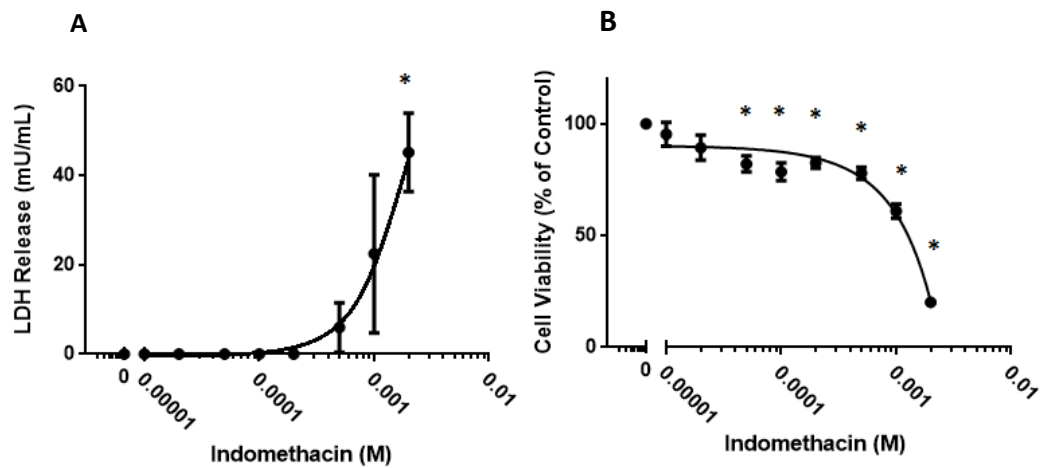


Figure 4.2 - ARPE19 cell death / viability in response to Indomethacin - (A) Cell death (LDH release) and **(B)** cell viability (MTS assay) in response to varying concentrations of Indomethacin (10 μ M-2mM) in ARPE19 cells (n=4) \pm SEM. * indicates significance (P<0.05) using one way ANOVA with Dunnett's post-hoc test.

Figure 4.2 shows a dose dependent increase in LDH release / decrease in cell viability with increasing concentrations of indomethacin. A significant increase in cell death was found at the highest concentration (2mM) (A) whereas a significant decrease in levels of cell viability was found at 50 μ M (B).

4.2.1.3 Tamoxifen

ARPE19 cells were exposed to varying concentrations of tamoxifen to reveal the RPE cells response to a well-documented retinotoxin.

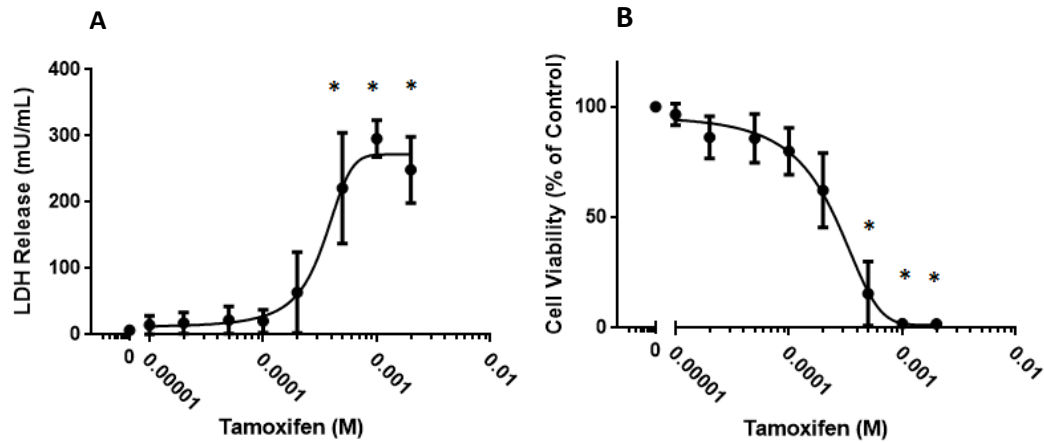


Figure 4.3 - ARPE19 cell death / viability in response to Tamoxifen - (A) Cell death (LDH release) and **(B)** cell viability (MTS assay) in response to varying concentrations of Tamoxifen (10 μ M-2mM) in ARPE19 cells (n=4) \pm SEM. * indicates significance (P<0.05) using one way ANOVA with Dunnetts post-hoc test.

Figure 4.3 shows a dose dependent increase in LDH release (A), and a decrease in cell viability (B) with increasing concentrations of tamoxifen. A significant increase in levels of cell death was found from 500 μ M and a significant decrease in cell viability from 500 μ M.

4.2.1.4 Chloroquine

ARPE19 cells were exposed to varying concentrations of chloroquine to provide an understanding of the retinal cells response to a well-documented retinotoxin.

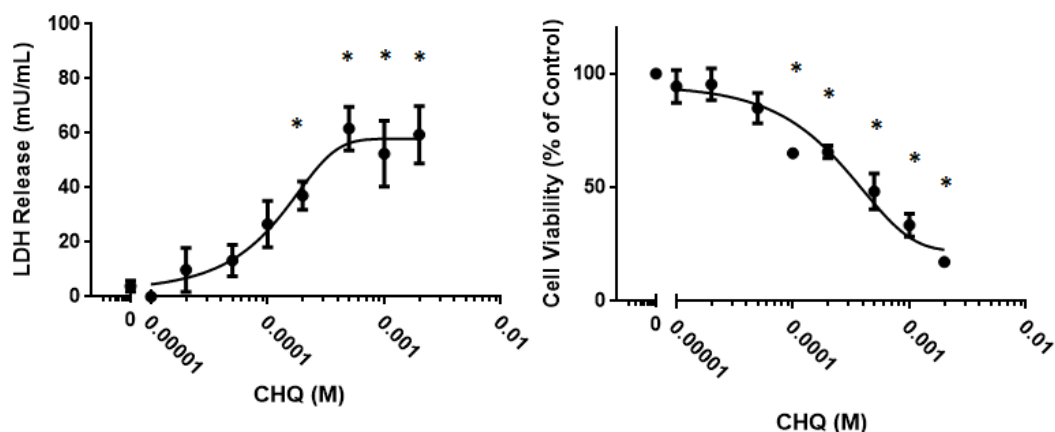


Figure 4.4 - ARPE19 cell death / viability in response to CHQ - (A) Cell death (LDH release) and **(B)** cell viability (MTS assay) in response to varying concentrations of chloroquine (10 μ M-2mM) in ARPE19 cells (n=4) \pm SEM. * indicates significance (P<0.05) using one way ANOVA with Dunnetts post-hoc test.

Figure 4.4 shows a dose dependent increase in LDH release (A), and a decrease in cell viability (B) with increasing concentrations of chloroquine. A significant increase in cell death was found from 200 μ M (A) and a significant decrease in cell viability from 100 μ M (B).

ARPE19 cells responded to all of the compounds in a dose dependent manner. The LD50 values and the concentration from which there is a significant difference from the control value are summarised in Table 4.1

A - LD50 Values

	LDH	MTS	Average LD50
H ₂ O ₂	439 μ M	257 μ M	348 μ M
Indomethacin	900 μ M	~1mM ^{\$}	950 μ M
Tamoxifen	335 μ M	~290 μ M ^{\$}	312.5 μ M
Chloroquine	~150 μ M ^{\$}	~350mM ^{\$}	250 μ M

B – Significant From Values

	LDH	MTS	Average
H ₂ O ₂	\geq 1mM	\geq 500 μ M	\geq 750 μ M
Indomethacin	\geq 2mM	\geq 50 μ M	\geq 1.025mM
Tamoxifen	\geq 500 μ M	\geq 500 μ M	\geq 500 μ M
Chloroquine	\geq 200 μ M	\geq 100 μ M	\geq 150 μ M

Table 4.1: Summary of data obtained from treated ARPE19 cells. A - LD50 values, B – significant from values. ^{\$} indicates value calculated by hand.

The LD50 values were initially calculated by Graphpad Prism (A). However, some of the LD50 values calculated in this way did not correspond well with the dose response shown by the ARPE19 cells. For this reason LD50 values were also calculated by hand (indicated by ^{\$}). If the LD50 calculated by hand was similar to that of the Graphpad calculation, the Graphpad value was used. The value from which the response became significant was also calculated for all drugs (B).

This data revealed that chloroquine was the most potent retinotoxic drug assessed on the ARPE19 cell line, with an average LD50 of 250 μ M and a significant increase in LDH release occurring from \geq 200 μ M and a significant decrease in cell viability occurring at \geq 100 μ M (overall an average significant increase from 150 μ M).

Tamoxifen appeared to be the second most potent drug on the ARPE19 cell line, with an average LD50 of 312.5 μ M and a consistent increase in cell death / decrease in cell viability at \geq 500 μ M.

H₂O₂ was the third most potent compound assessed, producing an average LD50 of 348µM and an average significant increase in cell death / decrease in cell viability of ≥750µM.

Indomethacin was the least potent drug assessed and displayed an average LD50 of ≥950µM. Contradictory results were found regarding the significant increase in LDH release and significant decrease in cell viability, with a significant increase in LDH release occurring at 2mM, whereas a significant decrease in cell viability occurred much earlier at ≥50µM. This overall produced an average significant increase of ≥1.025mM.

4.2.2 MIO-M1 Cells Response to Retinotoxins

MIO-M1 cells were then exposed to the same retinotoxins as the ARPE19 cell line, to investigate the differences in the sensitivity of the two cell lines to the retinotoxins.

4.2.2.1 Hydrogen Peroxide

MIO-M1 cells were firstly exposed to varying concentrations of H₂O₂, to gain an understanding of the cells response to oxidative stress

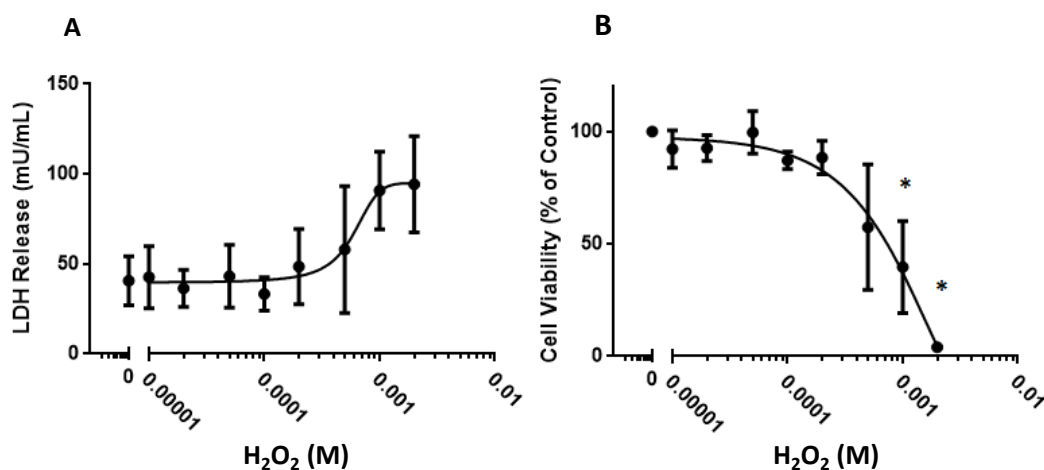


Figure 4.5 - MIO-M1 cell death / viability in response to H₂O₂ - (A) Cell death (LDH release) and (B) cell viability (MTS assay) in response to varying concentrations of H₂O₂ (10 μM-2 mM) in MIO-M1 cells (n=4) ± SEM. * indicates significance (P < 0.05) using one way ANOVA with Dunnett's post-hoc test.

Figure 4.5 shows a dose dependent increase in LDH release (A), and a decrease in cell viability (B) with increasing concentrations of H₂O₂. No significant increase in levels of cell death were found, however a significant decrease in levels of cell viability was found from 1 mM.

4.2.2.2 Indomethacin

MIO-M1 cells were exposed to varying concentrations of indomethacin to show the response of the Müller cell line to a relatively unknown retinotoxin.

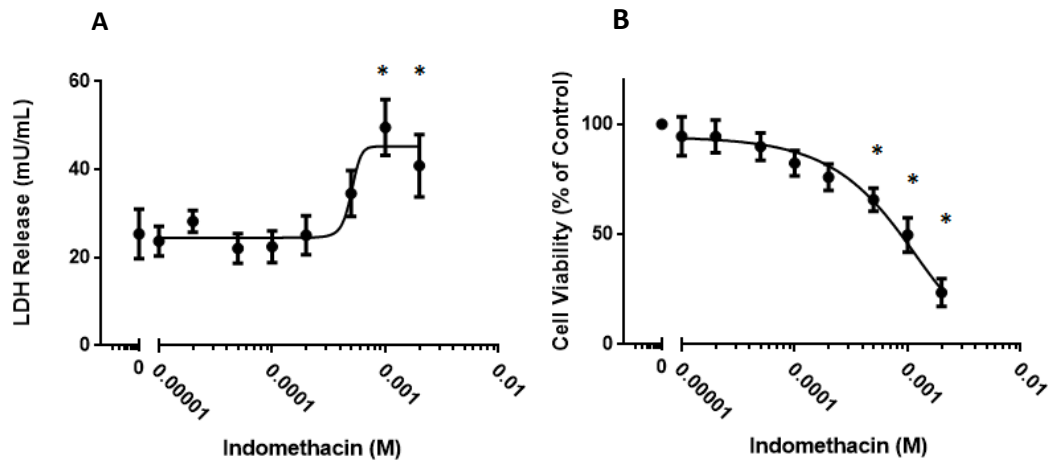


Figure 4.6 - MIO-M1 cell death / viability in response to Indomethacin - (A) Cell death (LDH release) and **(B)** cell viability (MTS assay) in response to varying concentrations of indomethacin (10 μ M-2mM) in MIO-M1 cells (n=4) \pm SEM. * indicates significance (P<0.05) using one way ANOVA with Dunnett's post-hoc test.

Figure 4.6 shows a significant increase in LDH release from 1mM, with a steep dose response curve (A). A dose dependent decrease in cell viability was found with increasing concentrations of indomethacin, and a significant decrease was found from 500 μ M (B).

4.2.2.3 Tamoxifen

MIO-M1 cells were then exposed to varying concentrations of tamoxifen.

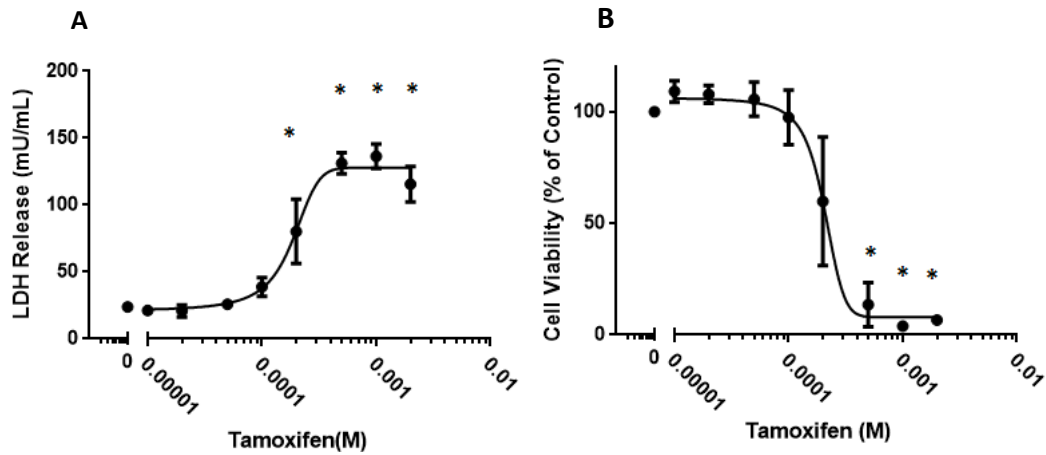


Figure 4.7 - MIO-M1 cell death / viability in response to Tamoxifen - (A) Cell death (LDH release) and **(B)** cell viability (MTS assay) in response to varying concentrations of tamoxifen (10 μ M-2mM) in MIO-M1 cells (n=4) \pm SEM. * indicates significance (P<0.05) using one way ANOVA with Dunnett's post-hoc

Figure 4.7 shows a dose dependent increase in LDH release (A), and a decrease in cell viability with increasing concentrations of tamoxifen (B). A significant increase in LDH levels were found from 200 μ M (A) and a significant decrease in cell viability was found from 500 μ M (B).

4.2.2.4 Chloroquine

MIO-M1 cells were exposed to varying concentrations of chloroquine to show the response of the Müller cell line to a well-documented retinotoxin.

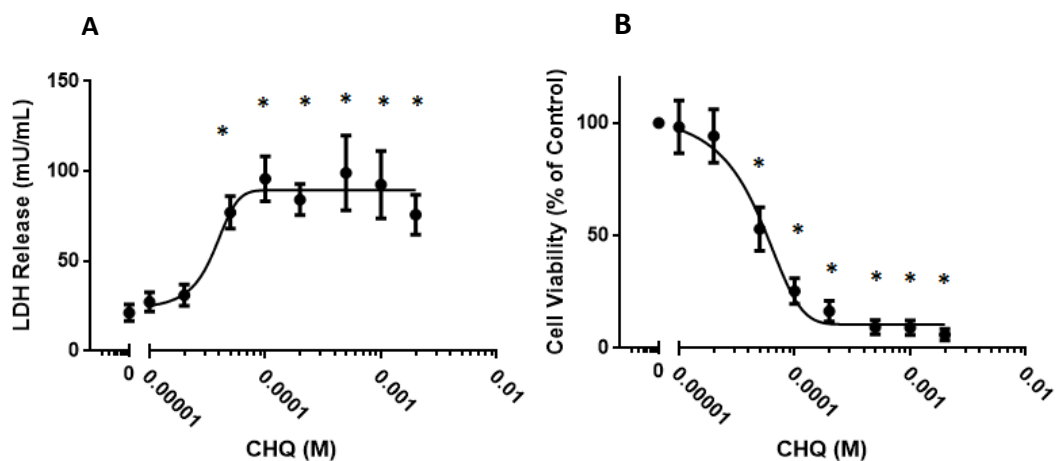


Figure 4.8 - MIO-M1 cell death / viability in response to CHQ - (A) Cell death (LDH release) and (B) cell viability (MTS assay) in response to varying concentrations of chloroquine (10 μM-2 mM) in MIO-M1 cells (n=4) ± SEM. * indicates significance (P < 0.05) using one way ANOVA with Dunnett's post-hoc test.

Figure 4.8 shows a dose dependent increase in LDH levels (A), and a decrease in cell viability (B) with increasing concentrations of chloroquine. A significant increase in LDH release and decrease in cell viability was found from 50 μM.

MIO-M1 cells responded to all compounds in a dose dependent manner, the LD50 values of the compounds calculated from LDH and MTS results are shown in Table 4.2

A - LD50 Values

	LDH	MTS	Average LD50
H ₂ O ₂	591 μ M	~700 μ M ^{\$}	645.5 μ M
Indomethacin	N.A	~800 μ M ^{\$}	800 μ M
Tamoxifen	183 μ M	204 μ M	193.5 μ M
Chloroquine	35 μ M	40 μ M	37.5 μ M

B – Significant From Values

	LDH	MTS	Average
H ₂ O ₂	N.A	\geq 1mM	\geq 1mM
Indomethacin	\geq 1mM	\geq 500 μ M	\geq 750 μ M
Tamoxifen	\geq 200 μ M	\geq 500 μ M	\geq 350 μ M
Chloroquine	\geq 50 μ M	\geq 50 μ M	\geq 50 μ M

Table 4.2: Summary of data obtained from treated MIO-M1 cells. A - LD50 values, B - significant from values. ^{\$} indicates value calculated by hand.

As with the data regarding the ARPE19 cells, the LD50 values were initially calculated by Graphpad Prism (A). However, some of the LD50 values calculated in this way did not correspond well with the dose response shown by the ARPE19 cells. For this reason LD50 values were also calculated by hand (indicated by ^{\$}). If the LD50 calculated by hand was similar to that of the Graphpad calculation, the Graphpad value was used. The value from which the response became significant was also calculated for all drugs (B).

The MIO-M1 cell line displayed a similar pattern of sensitivity as the ARPE19 cell line with chloroquine being the most toxic drug investigated. Chloroquine displayed an average LD50 of 37.5 μ M and a significant increase in LDH release / decrease in cell viability both occurring from 50 μ M.

Tamoxifen was also the second most potent drug, with an average LD50 of 193.5 μ M, and an average significant difference from 350 μ M.

Indomethacin and H₂O₂ required high concentrations to cause a significant difference in LDH release / decrease in cell viability which was matched by high LD50 values.

4.2.3 ARPE19 Cells Response to 24, 48 and 72h Chloroquine and Hydroxychloroquine Exposure

Results suggested that chloroquine was the most potent retinotoxic drug in both the RPE and the Müller cell lines (ARPE19 and MIO-M1). Chloroquine has been superseded by hydroxychloroquine on the basis that hydroxychloroquine is less toxic, therefore the difference in toxicity between CHQ and HCQ on ARPE19 cells was investigated. It was also interesting to determine toxicity at longer time points, therefore experiments were conducted at 24, 48 and 72h time points.

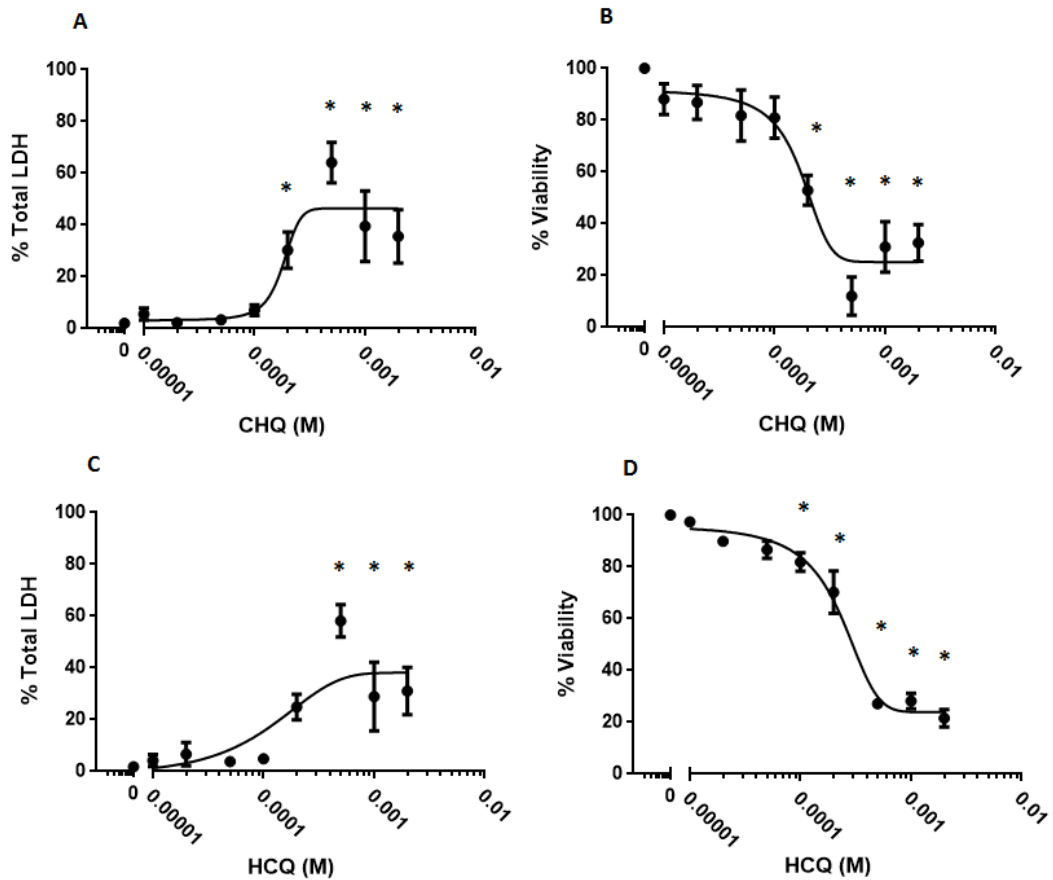


Figure 4.9 - ARPE19 cell death / viability in response to 24h CHQ / HCQ. Cell death (LDH release) (A, C) and cell viability (B, D) in response to differing concentrations of CHQ and HCQ (10 μ M-2mM) in ARPE19 cells after 24h exposure (n=4) \pm SEM, * indicates significance (P<0.05) using one way ANOVA with Dunnett's post-hoc test.

Exposure to chloroquine for 24 hours (Figure 4.9 A, B) caused a significant increase in cell death / decrease in cell viability from approximately 200 μ M.

Hydroxychloroquine caused a gradual increase in LDH release from 200 μ M, with a significant increase occurring at 500 μ M. Hydroxychloroquine also caused a dose dependent decrease in cell viability, with a significant decrease occurring from 100 μ M (Figure 4.9 C, D).

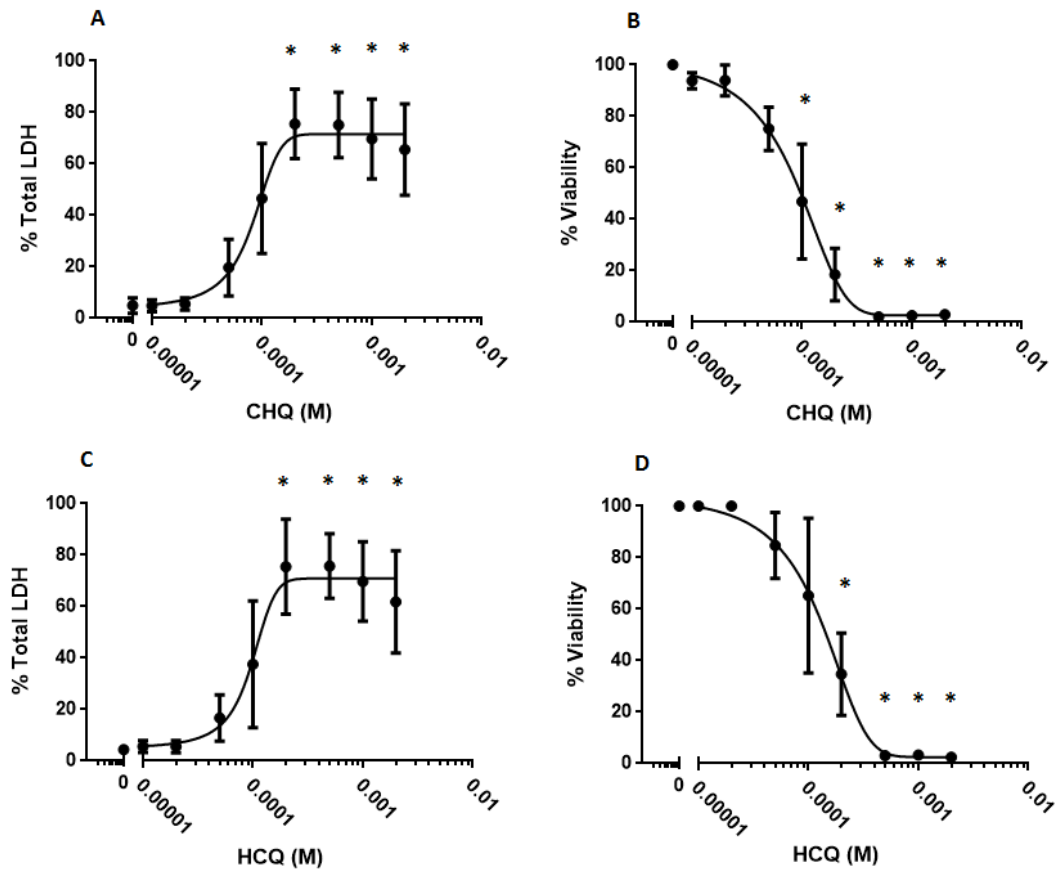


Figure 4.10 - ARPE19 cell death / viability in response to 48h CHQ / HCQ. Cell death (LDH release) (A, C) and cell viability (B, D) in response to differing concentrations of CHQ and HCQ (10 μ M-2mM) in ARPE19 cells after 48h exposure (n=4) \pm SEM * indicates significance (P<0.05) using one way ANOVA with Dunnett's

Exposure to chloroquine for 48 hours (Figure 4.10 A, B) caused gradual increase in cell death (LDH) / decrease in cell viability from approximately 50 μ M. A significant increase in cell death was not found until 200 μ M and a significant decrease in cell viability at 100 μ M.

48 hours of exposure to hydroxychloroquine (Figure 4.10 C, D) caused gradual increase in cell death from approximately 50 μ M and a gradual decrease in cell viability from 100 μ M. A significant difference in both cell death and cell viability occurred at 200 μ M treatment.

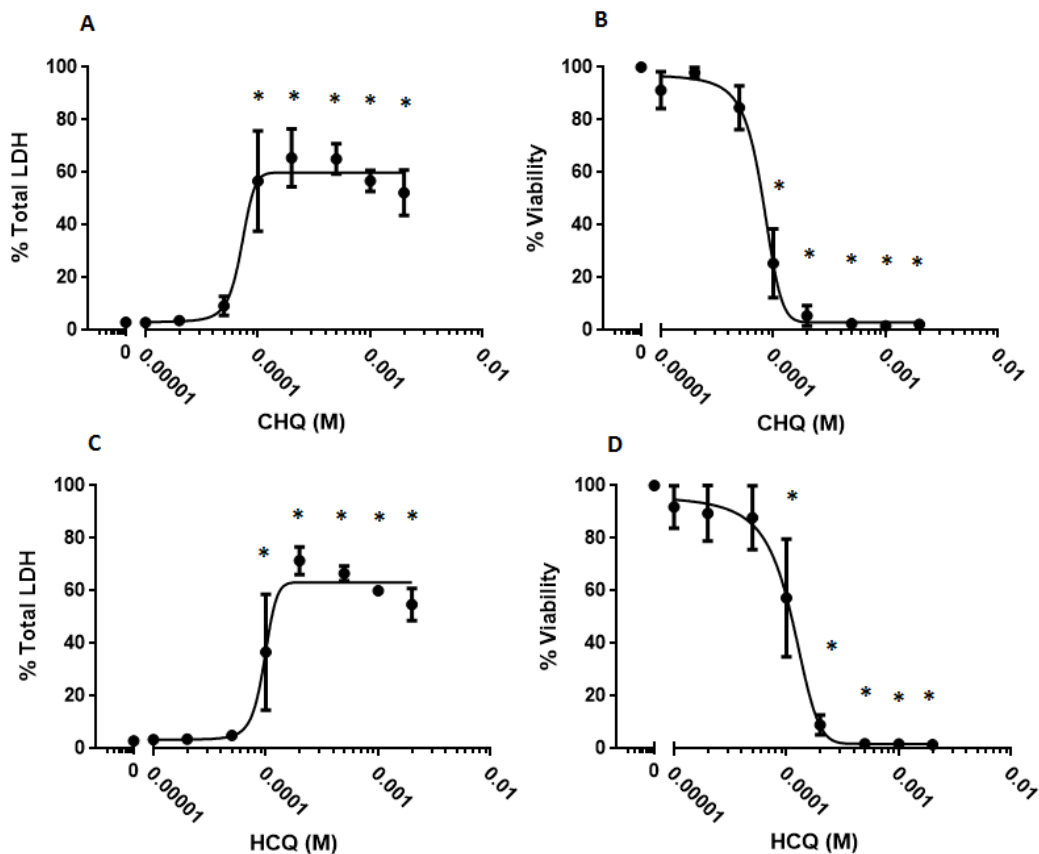


Figure 4.11 - ARPE19 cell death / viability in response to 72h CHQ / HCQ. Cell death (LDH release) (A, C) and cell viability (B, D) in response to differing concentrations of CHQ and HCQ (10 μ M-2mM) in ARPE19 cells after 72h exposure (n=4) \pm SEM, * indicates significance (P<0.05) using one way ANOVA with Dunnett's post-hoc test.

Exposure to chloroquine for 72 hours (Figure 4.11 A, B) caused a sudden increase in cell death (LDH) / decrease in cell viability with significant differences occurring with 100 μ M treatment.

Hydroxychloroquine exposure for 72 hours (Figure 4.11 C, D) also caused a sudden increase in cell death (LDH) / decrease in cell viability again, with significant differences occurring with 100 μ M treatment.

ARPE19 cells responded to chloroquine and hydroxychloroquine in a dose dependent manner, with increasing concentrations of both causing an increase in

LDH release and a decrease in cell viability. ARPE19 cells also showed a difference in response with the length of time exposed to the toxins with LD50 values decreasing with increasing time (Table 4.3).

A - LD50 values of 24, 48 and 72h CHQ and HCQ Treated ARPE19 cells

Cell Line	Exposure to Drug	LDH LD50 (M)	MTS LD50 (M)	Average LD50
ARPE 19	24h CHQ	181 μ M	170 μ M	175.5 μ M
ARPE 19	48h CHQ	~90 μ M ^{\$}	~100 μ M ^{\$}	95 μ M
ARPE 19	72h CHQ	71.3 μ M	80.4 μ M	75.85 μ M
ARPE 19	24h HCQ	170 μ M	~350 μ M ^{\$}	188.5 μ M
ARPE 19	48h HCQ	96 μ M	78.4 μ M	87.2 μ M
ARPE 19	72h HCQ	97 μ M	110 μ M	103.5 μ M

B - Significant Difference's of 24, 48 and 72h CHQ and HCQ Treated ARPE19 cells

ARPE19	CHQ			HCQ		
	LDH	MTS	Average of LDH and MTS	LDH	MTS	Average of LDH and MTS
Time Exposed						
24h	$\geq 200\mu$ M	$\geq 200\mu$ M	$\geq 200\mu$ M	$\geq 500\mu$ M	$\geq 100\mu$ M	$\geq 300\mu$ M
48h	$\geq 200\mu$ M	$\geq 100\mu$ M	$\geq 150\mu$ M	$\geq 200\mu$ M	$\geq 200\mu$ M	$\geq 200\mu$ M
72h	$\geq 100\mu$ M	$\geq 100\mu$ M	$\geq 100\mu$ M	$\geq 100\mu$ M	$\geq 100\mu$ M	$\geq 100\mu$ M

Table 4.3: Summary of data obtained from 24, 48 and 72h treated ARPE19 cells. A- LD50 values of CHQ and HCQ treated ARPE19 cells. **B –** Significant differences of CHQ and HCQ treated ARPE19 cells. ^{\$} indicates value calculated by hand.

ARPE19 cells displayed a time dependent response of increased LDH release and decreased cell viability with increasing time exposed to CHQ and HCQ. This is shown by the decreasing LD50 with increasing time exposed to both drugs. CHQ possessed a lower LD50 at the 24 and 72h time points, but not the 48h timepoint, displaying CHQ's higher toxicological properties over HCQ.

The data regarding the value from which there is a significant difference from the control also indicates that CHQ was slightly more toxic to the ARPE19 cells than HCQ, as shown by the lower concentration causing a significant difference in cell death / cell viability at 24 and 48h treatment. With 72h treatment, this data indicated that CHQ and HCQ were equally toxic as each other.

4.2.4 MIO-M1 cells response to 24, 48 and 72h Chloroquine and Hydroxychloroquine exposure

The time course experiments investigating the toxicity of chloroquine and hydroxychloroquine in ARPE19 cells were repeated using MIO-M1 cells

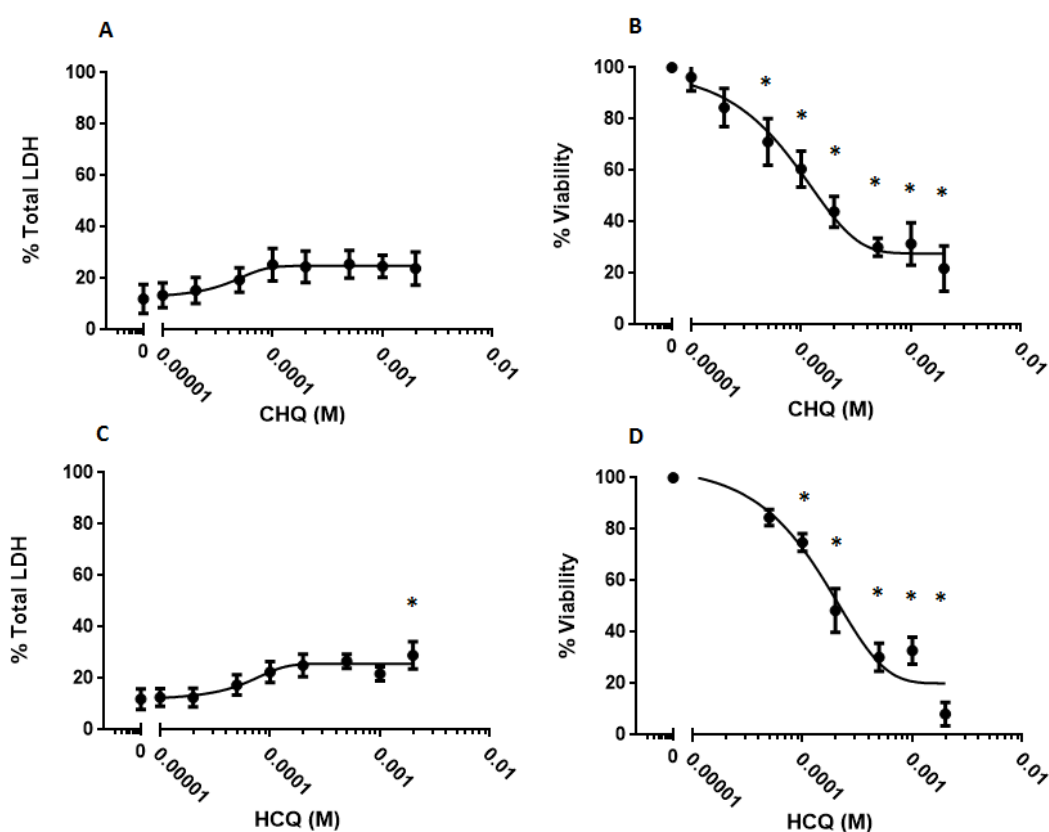


Figure 4.12 - MIO-M1 cell death / viability in response to 24h CHQ / HCQ. Cell death (LDH release) (A, C) and cell viability (B, D) in response to differing concentrations of CHQ and HCQ (10 μ M-2mM) in MIO-M1 cells after 24h exposure (n=4) \pm SEM, * indicates significance (P<0.05) using one way ANOVA with Dunnett's post-hoc test.

Exposure to CHQ for 24 hours (Figure 4.12) caused a trend of increased LDH release (cell death), however no significant difference was found compared to untreated cells. A gradual decrease in cell viability began from approximately 20 μ M CHQ, with a significant decrease occurring from 50 μ M.

24 hours exposure to HCQ also caused an increase in LDH release, with a significant increase occurring at 2mM. A trend of decreased cell viability was found from 50µM HCQ, with a significant difference occurring from 100µM.

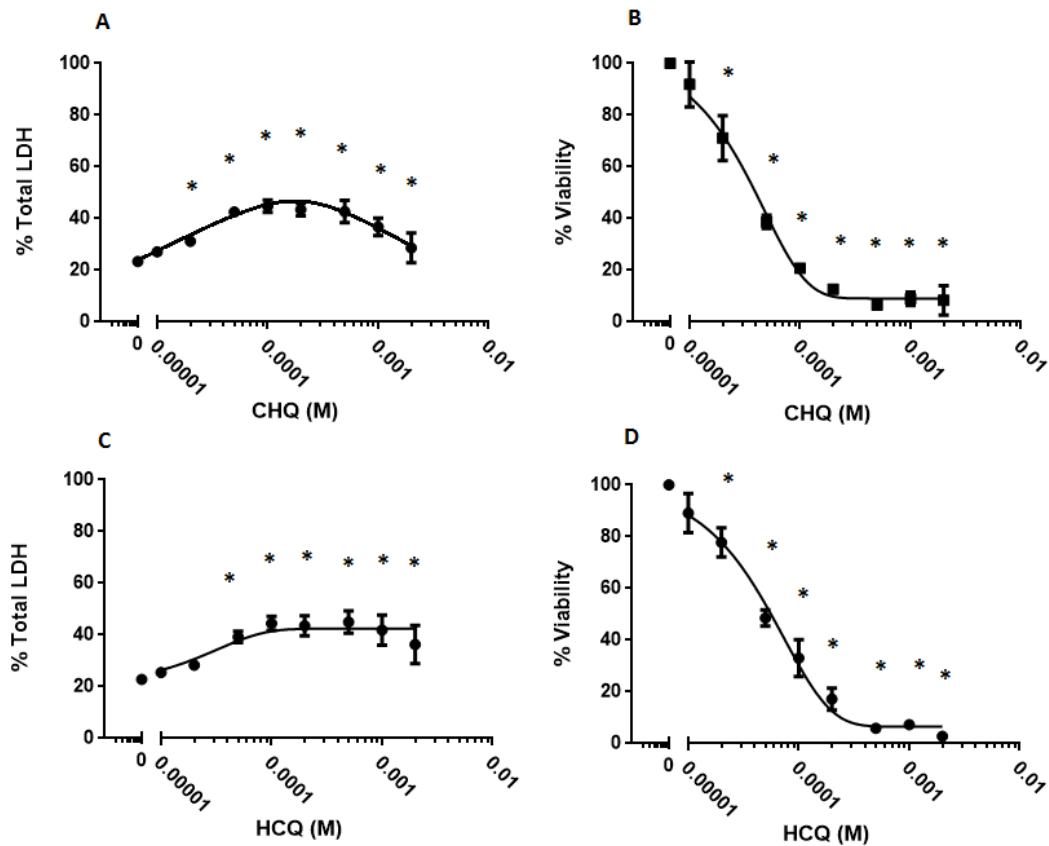


Figure 4.13 - MIO-M1 cell death / viability in response to 48h CHQ / HCQ. Cell death (LDH release) (A, C) and cell viability (B, D) in response to differing concentrations of CHQ and HCQ (10µM-2mM) in MIO-M1 cells after 48h exposure (n=4) ± SEM, * indicates significance (P<0.05) using one way ANOVA with Dunnett's post-hoc test.

Exposure to CHQ for 48 hours (Figure 4.13) caused an increase in LDH release (cell death) with a significant increase in LDH release found from 50µM. At higher concentrations there also appeared to be a small decrease in LDH release. A gradual decrease in cell viability began from approximately 10µM, with a significant difference occurring at 20µM CHQ.

48 hours of exposure to HCQ also caused an increase in LDH release, with a

significant increase occurring at 50 μ M. A trend of decreased cell viability was seen from 10 μ M HCQ, with a significant decrease occurring at 20 μ M.

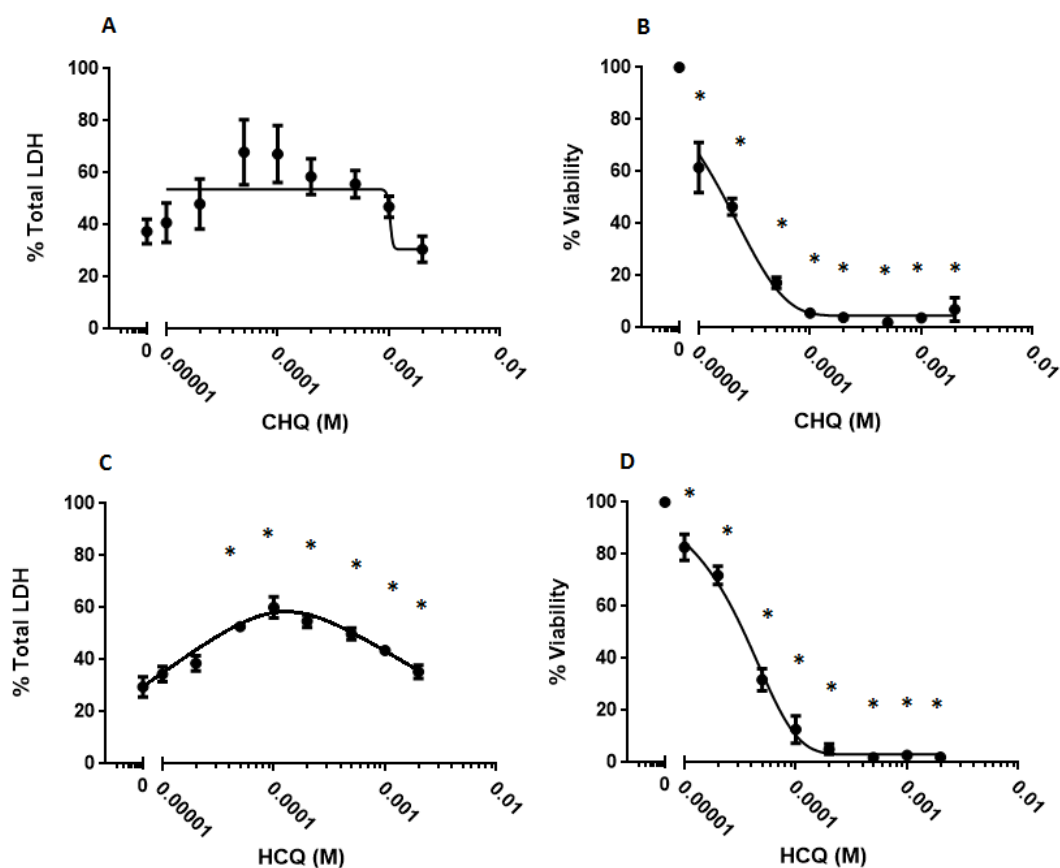


Figure 4.14 - MIO-M1 cell death / viability in response to 72h CHQ / HCQ. Cell viability (LDH release) (A, C) and cell viability (B, D) in response to differing concentrations of CHQ and HCQ (10 μ M-2mM) in MIO-M1 cells after 72h exposure (n=4) \pm SEM, * indicates significance (P<0.05) using one way ANOVA with Dunnett's post-hoc test.

72 hours exposure to CHQ (Figure 4.14) caused little change in LDH release with no significant difference found, however a significant decrease in cell viability was found from 10 μ M CHQ.

72 hours exposure to HCQ caused an increase in LDH release, with a significant increase occurring from 50 μ M. The LDH release started to decrease from the peak release (at 200 μ M) to 2mM. A significant decrease in cell viability was also found from 10 μ M HCQ.

MIO-M1 cells responded to CHQ and HCQ in a dose dependent manner when assessed with the MTS assay, whereas the LDH assay provided variable results. MIO-M1 cells also displayed a correlation of decreasing cell viability with increasing time exposed to CHQ and HCQ, the results of which are summarised in Table 4.4.

A – LD50 values for 24, 48 and 72h CHQ and HCQ Treated MIO-M1 cells

Cell Line	Exposure to Drug	LDH LD50 (M)	MTS LD50 (M)	Average LD50
MIO-M1	24h CHQ	N.A	~150 μ M [§]	150 μ M
MIO-M1	48h CHQ	N.A	43.7 μ M	43.7 μ M
MIO-M1	72h CHQ	N.A	~20 μ M [§]	20 μ M
MIO-M1	24h HCQ	N.A	~200 μ M [§]	200 μ M
MIO-M1	48h HCQ	N.A	~60 μ M [§]	60 μ M
MIO-M1	72h HCQ	N.A	~40 μ M [§]	40 μ M

B – Significant Differences for 24, 48 and 72h CHQ and HCQ Treated MIO-M1 cells

MIO-M1	CHQ			HCQ		
Time Exposed	LDH	MTS	Average of LDH and MTS	LDH	MTS	Average of LDH and MTS
24h	N.A	$\geq 50\mu$ M	$\geq 50\mu$ M	≥ 2 mM	$\geq 100\mu$ M	≥ 1.05 mM
48h	$\geq 50\mu$ M	$\geq 20\mu$ M	$\geq 35\mu$ M	$\geq 50\mu$ M	$\geq 20\mu$ M	$\geq 35\mu$ M
72h	N.A	$\geq 10\mu$ M	$\geq 10\mu$ M	$\geq 50\mu$ M	$\geq 10\mu$ M	$\geq 30\mu$ M

Table 4.4: Summary of data obtained from 24, 48 and 72h treated MIO-M1 cells. A- LD50 values of CHQ and HCQ treated MIO-M1 cells. **B –** Significant differences of CHQ and HCQ treated MIO-M1 cells. [§] indicates value calculated by hand.

Assessment of LDH release in response to CHQ and HCQ gave complex data in that they did not give a standard dose response curve. This can be seen in Figures 4.12 – 4.14 and in Table 4.4. The MTS assay however displayed a clear dose dependent decrease in viability and provided an LD50 and data regarding the dose causing significant changes.

4.3 Discussion

The aim of this chapter was to use two retinal cell lines to assess the toxicity of compounds with known retinotoxicity. These cell lines could then provide preliminary information about the relative toxicity of the drugs of interest, and the information gathered from this could be used to determine the concentration of retinotoxins to be applied to the *ex vivo* retina.

The two retinal cell lines were firstly exposed to a variety of retinotoxins and H₂O₂ as a positive control (section 4.2.1 and 4.2.2). The retinotoxins applied to the cell lines were indomethacin, tamoxifen and chloroquine. It was expected that due to the different nature of the cells, and the compounds, the sensitivity of both cell lines would differ for each of the compounds.

The two retinal cell lines used were ARPE19 cells and MIO-M1 cells. The ARPE19 cell line is a human retinal pigmented epithelial cell line from a primary source of retinal pigmented epithelium. Retinal pigmented cells are highly active cells which are responsible for phagocytosing outer segments of photoreceptors. The cells exhibit a similar physiology to RPE cells, and display similar RPE specific markers such as CRALBP and RPE65 (Dunn et al., 1996).

The MIO-M1 cell line is an immortalized cell line derived from human Müller cells. They are the principle glial cells of the retina, providing structural and metabolic support to neurones and blood vessels. They play an important role in glutamate uptake in order to prevent neurotoxicity from excess glutamate (Haberecht et al., 1997). The MIO-M1 cell line expresses known markers of Müller cells such as EGF-

R (epidermal growth factor receptor), glutamine synthetase, α SMA and CRALBP (Limb et al., 2002).

The cells were firstly exposed to the positive control H_2O_2 . H_2O_2 is an oxidative stressor which has the ability to cause cell death via the apoptotic pathway with low concentrations of H_2O_2 and the necrotic pathway with high concentrations of H_2O_2 (Kim et al., 2003; Li et al., 2010). When exposed to H_2O_2 ARPE19 cells and MIO-M1 cells displayed a dose dependent increase in LDH release / decrease in cell viability.

In ARPE19 cells, the increase in cell death and decrease in cell viability was seen to occur over a small concentration range from 200 μ M and 500 μ M in which cells responded in an all or nothing manner producing variability. This was followed by a significant increase in LDH release from ≥ 1 mM and a significant decrease in cell viability from $\geq 500\mu$ M.

MIO-M1 cells displayed large variability in LDH release which produced no significantly different data. The cell viability data represented the cells response to H_2O_2 better than the LDH release data, showing a dose dependent decrease in cell viability with increasing concentrations of H_2O_2 and a significant decrease in cell viability occurring from ≥ 1 mM.

Even though the LDH data was variable from MIO-M1 cells, the cell viability data and the LD50 data from both MIO-M1 and ARPE19 cell line indicated that the MIO-M1 cells displayed a higher resilience to H_2O_2 than ARPE19 cells. This may indicate that MIO-M1 cells are more effective at processing oxidative stressors better than RPE cells.

Indomethacin was the second drug investigated on the cell lines. It is an anti-inflammatory agent with few reported cases of retinopathy (Graham and Blach, 1988). On the basis of clinical data it would therefore be expected to cause the least toxicity of the drugs investigated.

ARPE19 cells exposed to indomethacin showed no toxicity at lower concentrations with a trend of increased LDH release from $\geq 500\mu$ M. A significant increase in LDH release was not found until 2mM. However, surprisingly the LDH data showed a significant decrease in cell viability from $\geq 50\mu$ M. This concentration is very low, however what can be seen is little dose dependent decrease in viability until a

concentration of 1mM is reached.

MIO-M1 cells displayed a significant increase in LDH release from ≥ 1 mM. This was similar to the MTS data which displayed a significant decrease in cell viability from $\geq 500\mu\text{M}$ treatment. Both cell lines displayed a high LD50 which may reflect the relatively non retinotoxic properties of indomethacin *in vivo*. There is little research investigating the specific method of toxicity which occurs in indomethacin induced retinopathy. It has been speculated that a reactive iminoquinone forms from the oxidation of DMBI (a major metabolite of Indomethacin) (Ju and Uetrecht, 1998) which could bind to GSH and cause GSH depletion. GSH depletion has been shown to cause unregulated oxidative stress and apoptosis in the mouse retina (Roh et al., 2007).

Tamoxifen is used in the treatment of hormone responsive breast cancer (Srikantia et al., 2010). It is known to possess retinotoxic properties and with prolonged use can lead to decreased visual acuity, pigmented retinopathy, macula oedema and macula holes (Watanabe et al., 2010), (Lazzaroni et al., 1998).

ARPE19 cells displayed a dose dependent increase in cell death / decrease in cell viability with increasing concentrations of tamoxifen, and a significant increase in LDH release and a significant decrease in cell viability found from $\geq 500\mu\text{M}$.

MIO-M1 cells also displayed a dose dependent increase in cell death / reduction in cell viability with increasing concentrations of tamoxifen with a significant increase in LDH release occurring from $\geq 200\mu\text{M}$ and a significant decrease in cell viability occurring from $\geq 500\mu\text{M}$.

The data indicated that MIO-M1 cells may be slightly more sensitive to tamoxifen than ARPE19 cells. The LD50 values obtained in which MIO-M1 cells displayed an average LD50 of $193.5\mu\text{M}$ and ARPE19 cells displayed an average LD50 of $312.5\mu\text{M}$. It is commonly thought that RPE cells (and photoreceptors) are the primary target of tamoxifen induced retinopathy (Cho et al., 2012; Engelke et al., 2002), with lysosomal disruption causing a release of hydrolases such as cathepsins which in turn can cause cell death via a multitude of pathways such as apoptosis, necrosis and pyroptosis (Kim et al., 2014). However data obtained here suggests that Müller cells sensitivity to tamoxifen may also influence the retinopathy associated with tamoxifen treatment.

Chloroquine is a lysomotropic agent which was commonly used as an anti-malarial agent, although due to widespread resistance it is now mainly used in the treatment of rheumatoid arthritis (NHS, 2014c).

ARPE19 cells responded to chloroquine in a dose dependent manner, with an increase in LDH release and a decrease in cell viability with increasing concentrations of chloroquine. A significant increase in LDH release was found from $\geq 200\mu\text{M}$, and a significant decrease in cell viability from $\geq 100\mu\text{M}$.

MIO-M1 cells also responded to chloroquine in a dose dependent manner with a significant increase in LDH release and decrease in cell viability from $\geq 50\mu\text{M}$.

This data indicates that MIO-M1 cells are more susceptible to chloroquine toxicity than ARPE19 cells, with chloroquine causing a significantly higher LDH release / lower cell viability at a much lower dose in MIO-M1 cells. LD50 values in MIO-M1 cells displayed an average LD50 of $37.5\mu\text{M}$ and ARPE19 cells displayed an average LD50 of $250\mu\text{M}$

Chloroquine retinopathy is commonly associated with long term use of the drug. Patients may present with visual defects such as central visual loss, night blindness and a loss of colour vision. Clinically, chloroquine retinopathy appears as pigmentary changes, with advanced retinopathy appearing as a bulls eye maculopathy (Pasadhika et al., 2010), (Nogueira and Gama, 2009). The method through which chloroquine is believed to cause retinopathy is due to lysosomal dysfunction. It is believed that the RPE is primarily affected due to its role of phagocytosing shed outer segments of photoreceptors, in turn affecting photoreceptors. However an early study by Rosenthal et al (1978) showed that in the rhesus monkey, ganglion cells are affected first, followed by the photoreceptors and RPE. The current data (Figure 4.4 and 4.8) suggests that Müller cells may be more sensitive to chloroquine toxicity than RPE cells, and this may also contribute to the retinopathy seen with CHQ treatment clinically.

Chloroquine displayed the most retinotoxic properties in both ARPE19 and MIO-M1 cells. The next most retinotoxic drug assessed was tamoxifen and finally indomethacin. This data relates to the clinical prevalence of retinopathy induced by the drugs, in which chloroquine has the highest prevalence of reported retinopathy of the drugs investigated. The actual value of prevalence of chloroquine induced retinopathy in chloroquine treated patients is variable across multiple studies, and

ranges from as high as 24.7% to as low as 0.1% (Browning, 2014). Tamoxifen is the next most reported retinotoxic drug investigated, with an incidence of 0.9% (in a study of 274 patients) (Tang et al., 1997) whereas for indomethacin, only one case of retinopathy has been reported (Graham and Blach, 1988).

Hydroxychloroquine is also an anti-malarial agent that is used in the treatment of rheumatoid arthritis, which superseded the use of chloroquine in the treatment of rheumatoid arthritis and systemic lupus due to its better safety profile (Michaelides et al., 2011). For this reason the difference in toxicity between chloroquine and hydroxychloroquine was investigated on ARPE19 and MIO-M1 cells, to find out if the better safety profile of hydroxychloroquine was reflected in the retinal cell based toxicity assays. A time course was also conducted in order to establish the effect of longer exposure to the drugs.

Both chloroquine and hydroxychloroquine caused a dose dependent decrease in cell viability / increase in LDH release at all-time points in ARPE19 cells, with longer exposure to the drugs causing increased cell death (Figure 4.9, 4.10 and 4.11). Chloroquine caused a significant decrease in cell viability / increase in LDH release at a slightly lower concentration than hydroxychloroquine at all time points, reflecting the better safety profile of hydroxychloroquine. The LD50 values also reflect this data apart from at the 48h time point in which HCQ possessed a lower LD50.

Figures 4.12, 4.13 and 4.14 display the effect of 24, 48 and 72h exposure to CHQ and HCQ on MIO-M1 cells. CHQ and HCQ caused a dose and time dependent decrease in cell viability, however the LDH release data did not show expected patterns of release. Control cells showed release of 10% total LDH at 24h, 20% of total LDH at 48h and 30% at 72h. This indicates that culturing in serum free medium was having a detrimental effect on the MIO-M1 cell line. More surprisingly there was little change in LDH release with treatment of CHQ and HCQ, and interestingly, the LDH results from MIO-M1 cells at later time points displayed a decreasing trend of LDH release with high concentrations of treatment. This may be due to high concentrations of both drugs inducing rapid cell death at early stages, causing early release of LDH which then degraded over time. Whereas concentrations around the

100µM induced slower cell death with a prolonged LDH release, resulting in less LDH degradation and an apparent higher LDH release at the time assessed. This shows that for the MIO-M1 cell line, the LDH assay is not a suitable assessment for investigation of the effects of longer term culture in CHQ or HCQ.

The MTS assay however (cell viability assay) worked in an expected manner, and for this reason the MTS assay was used to interpret the sensitivity of MIO-M1 cells to CHQ and HCQ. This data showed CHQ to be slightly more toxic to the MIO-M1 cell line at all time points than HCQ.

This data reinforces the clinical evidence of HCQ's better safety profile, with CHQ possessing more toxicological properties than that of HCQ in both ARPE19 cells and MIO-M1. The fact that the better safety profile of HCQ is reflected in the cell lines is important, it shows that the cell lines are suitable for the assessment of retinotoxicity and that results which are found clinically may be matched by those within the cell lines.

4.4 Conclusion

Experiments within this chapter investigated the sensitivity of human RPE and Müller cell line's to multiple retinotoxins.

The cell lines showed the predicted responses when assessing the various retinotoxins, with high concentrations of the least retinotoxic drug (Indomethacin) required to cause a significant increase in cell death, and lower concentrations of the known retinotoxins tamoxifen and chloroquine required to cause a significant increase in cell death.

Importantly, both cell lines showed a high degree of sensitivity when determining the toxicity of hydroxychloroquine and chloroquine and the cells displayed a better safety profile for hydroxychloroquine compared to chloroquine.

The Müller cell line was more sensitive to tamoxifen, chloroquine and hydroxychloroquine than the RPE cell line, potentially indicating that RPE cells

display a higher resilience to agents which effect lysosomal activity. A primary function of RPE cells is the degradation of shed photoreceptor outer segments by phagocytosis, and the breakdown of the phagosome through fusion with endosomes and lysosomes (Kevany and Palczewski, 2010). A proposed major mechanism of retinal toxicity is the disruption of lysosomal function which would affect the degradation of photoreceptor outer segments and would therefore cause disruption of the photoreceptor turnover. This research only investigated cell death in response to the retinotoxins, however it may also indicate that Müller cell toxicity also plays a role in retinotoxicity induced by CHQ, HCQ and tamoxifen.

To summarise, this research indicates the usefulness of human retinal cell lines in the establishment of a model to assess retinotoxicity. It has provided information regarding the relative toxicity of the drugs investigated, which in the future could be used alongside the *ex vivo* retina and animal models to provide information about the toxicity of the drugs, and potentially the mechanisms involved with the associated toxicity.

Chapter 5

5.0 Effect of Chloroquine on Human Organotypic Retina Cultures

5.1 Introduction

Organotypic models are a useful tool in the process of drug development. They possess the same cellular and structural properties as the tissue of interest and may provide an accurate insight into the effects of a drug on its target tissue. This makes the development of human organotypic retinal cultures (HORCs) as a model to assess retinotoxicity desirable. HORCs maintain comparable structural and cellular properties to the living retina (as shown in Chapter 3) and would enable a correlation to be made of a drug's potential toxicity in the human retina.

Non-human organotypic retinal cultures have previously been utilised to assess the toxicity of specific compounds. The mouse organotypic retinal culture has also been used for toxicity studies in which the effect of gold and silver nanoparticles were investigated (Soderstjerna et al., 2014). The porcine organotypic retina has also been utilised to investigate the effects of bevacizumab (Kaempf et al., 2008). Rat organotypic retinal cultures have been utilised to investigate the role of adenosine A3 receptor activation in the protection of retinal cells from NMDA excitotoxicity (Galvao et al., 2015), as well as the protective effect of hydrogen against peroxynitrate (Yokota et al., 2015). Human organotypic retinal cultures (HORCS) have been utilised previously for a similar purpose in which Niyadurupola (2011) showed that *THY1* expression (a ganglion cell marker) decreased in response to NMDA excitotoxicity and oxygen / glucose deprivation, representing a decrease in ganglion cell density and health (Osborne et al., 2015a; Niyadurupola et al., 2011). Such data demonstrated the possibilities of using HORCs to investigate degenerative effects on ganglion cells, and opened up the possibilities of investigating degeneration of other retinal cell types in response to stressors including retinotoxins.

Research presented in the previous chapter demonstrated the effect of a variety of known retinotoxins on the RPE cell line ARPE19 and the Müller cell line MIO-M1. Chloroquine was found to be the most potent retinotoxin investigated on both cell

lines; for this reason the effect of chloroquine retinotoxicity on the HORC was investigated.

Research presented in this chapter aims to explore methods to analyse the toxicity of chloroquine in human organotypic retinal cultures (HORCs). The first stage will involve investigating cell death and cell viability in response to chloroquine. The next stage involved investigation of the cells affected by chloroquine, carried out through the use of immunohistochemistry, and the assessment of levels of cell specific mRNA in response to differing concentrations of chloroquine. The mechanism of cell death induced by chloroquine was also investigated.

5.2 Results

5.2.1 The Effect of Hydrogen Peroxide on Cell Death in the HORC

Initial experiments used hydrogen peroxide was used as a positive control to find out if LDH was released from paramacula HORCs as a result of cell death.

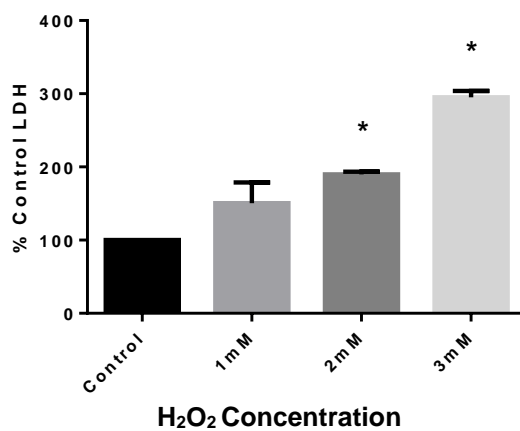


Figure 5.1 - LDH release in response to H₂O₂. Mean + SEM control, 1mM, 2mM, 3mM (n=3). * indicates a significant difference compared to the control (P<0.05) using one way ANOVA with Dunnet's post hoc test.

Paramacula sections showed a dose dependent increase of LDH release with increasing hydrogen peroxide concentrations, a significant increase in LDH release was found at 2mM.

5.2.2 The Effect of Chloroquine on Cell Death / Cell Viability in the HORC

LDH was used then to assess the extent of cell death caused by varying concentrations of CHQ in paramacula HORCS. The MTS assay was also used to assess any changes in cell viability that occur with 24h CHQ treatment.

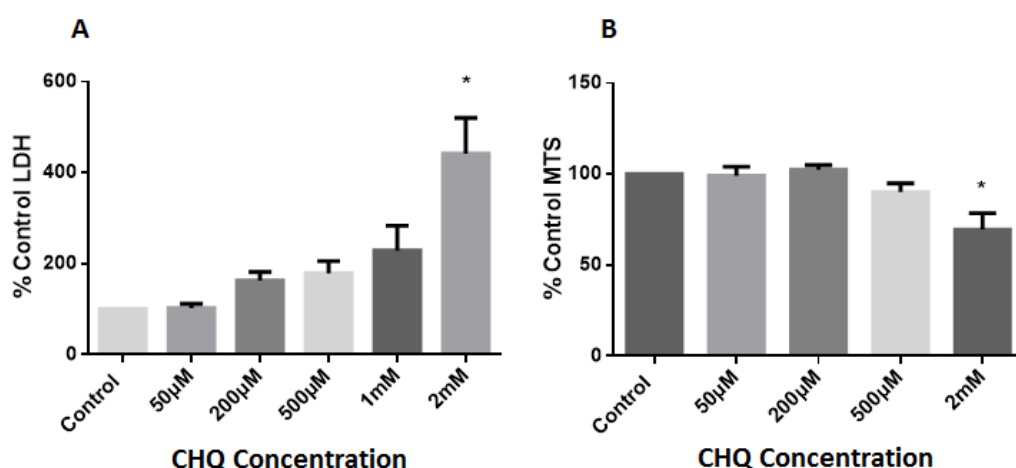


Figure 5.2 - HORC LDH release and cell viability in response to CHQ. **A** - Mean + SEM of cell death (LDH release) in response to 50 μM CHQ (n=31), 200 μM (n=31), 500 μM (n=4), 1 mM (n=4) and 2 mM (n=31). **B** - Mean + SEM of cell viability in response to 50 μM CHQ (n=4), 200 μM (n=4), 500 μM (n=4), and 2 mM (n=4) after 24h exposure. * indicates a significant difference from the control (P<0.05) using one way ANOVA with Dunnett's post-hoc test.

Exposure to CHQ caused LDH release from HORCs. A trend of increased LDH release was found from $\geq 200 \mu\text{M}$ treatment, and a significant increase in LDH release occurred at 2 mM. The MTS assay showed a decreased trend in expression at 500 μM, and a significant decrease in cell viability at 2 mM.

5.2.3 Investigation of Chloroquine Induced Cell Death in the HORC

HORCS were exposed to CHQ for 24h and cell death investigated using colorimetric immunohistochemistry and analysed using ScanScope software in which the result is expressed as percent positive pixels relative to total pixel count (positive being antibody of interest and negative haematoxylin stain). Firstly a marker of cell death (TUNEL) was investigated (Figure 5.3). Note that in these experiments an antibody to FITC was used to allow the colorimetric analysis to be used.

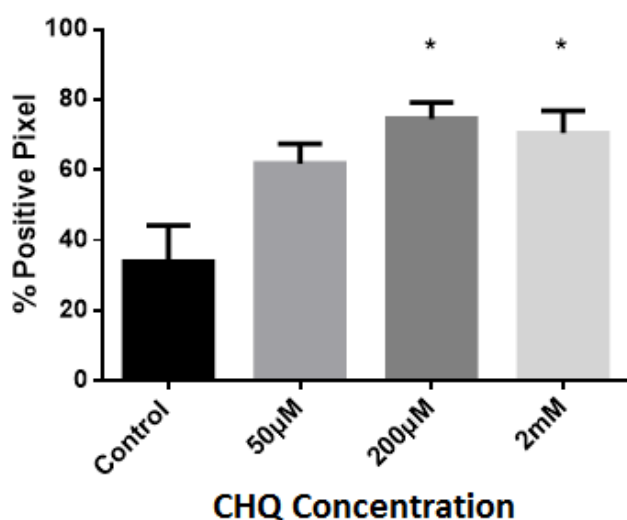


Figure 5.3 - TUNEL % Positive Pixels in Response to CHQ Mean + SEM of cell death (% positive pixel) using the TUNEL assay in 24h CHQ treated HORCS (n=5). * indicates a significant difference to the control ($P < 0.05$) using one way ANOVA with Dunnett's post-hoc test.

Figure 5.3 showed the TUNEL assay to be a sensitive method of cell death analysis in HORCS, displaying a significant increase in TUNEL positive cells from $\geq 200\mu\text{M}$ CHQ. This was a more sensitive assay than LDH or MTS assay, which only showed a significant increase in cell death from 2mM.

Another marker of apoptotic cell death (active caspase 3) was then investigated using the same method. This was analysed as a positive pixel count and the results are shown in Figure 5.4.

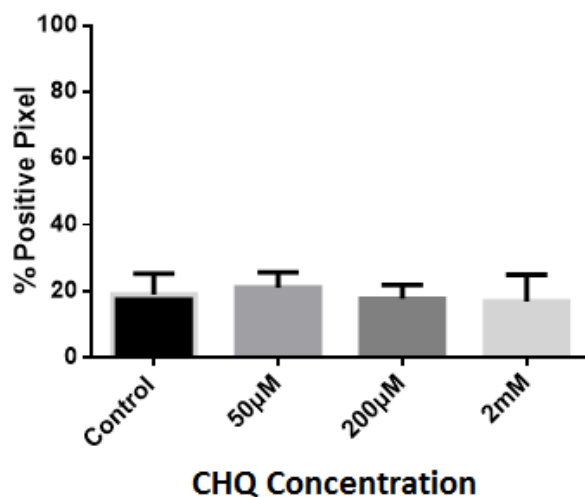


Figure 5.4 - Active Caspase 3 % Positive Pixels in Response to CHQ Mean + SEM of cell death (% positive pixel of Active Caspase 3) in CHQ treated HORCS (n=5). * indicates a significant difference to the control (P<0.05) using one way ANOVA with Dunnett's post-hoc test.

Figure 5.4 indicated that there was no change in the amount of active caspase 3 positive cells with CHQ treatment. Figure 5.2 and 5.3 showed there was a gradual increase in cell death with increased CHQ treatment, indicating that assessment of active caspase 3 may not be a good method to assess CHQ induced cell death.

The positive pixel count method was then utilised to investigate any loss in ganglion cells that may occur (Figure 5.5). Ganglion cells were chosen due to previous research which had shown a decrease in NeuN labelled cells with NMDA excitotoxicity and oxygen glucose deprivation (Osborne et al., 2015a; Niyadurupola et al., 2011). For this experiment, the positive pixel count of the ganglion cell marker NeuN was investigated with varying concentrations of CHQ to determine if any loss of ganglion cells occurred due to CHQ toxicity.

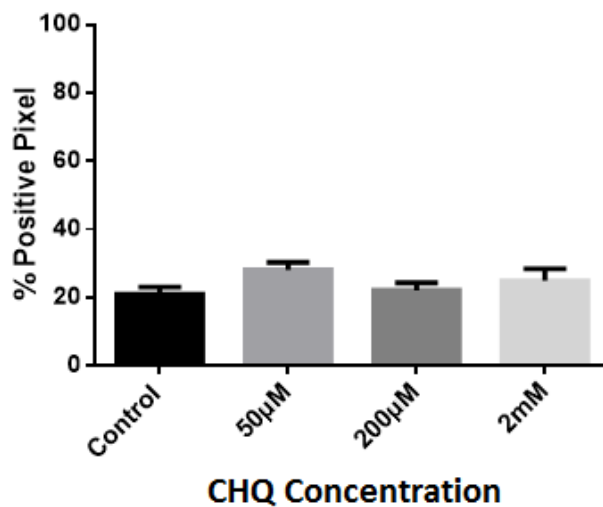


Figure 5.5 - NeuN % Positive Pixels in Response to CHQ Mean + SEM of NeuN (% positive pixel) in CHQ treated HORCS (n=5). * indicates a significant difference to the control (P<0.05) using one way ANOVA with Dunnetts post-hoc test.

The NeuN positive pixel count did not change after 24h of CHQ treatment, either indicating no change in ganglion cell number occurred with CHQ treatment, or that this method of analysis may not be suitable for assessing changes in ganglion cell number.

5.2.4 Effect of Chloroquine on mRNA Expression of Retinal Cell Markers in HORCs

TUNEL analysis provided a sensitive means of assessing cell death in CHQ treated HORCS. However since the analysis was carried out using an automated system, this did not provide information regarding specific cell types affected by chloroquine toxicity. In order to investigate specific cell loss in the retina that may occur due to CHQ toxicity, paramacula samples were exposed to varying concentrations of CHQ and the expression of cell specific mRNA markers investigated. Previous research has shown that *THY1* mRNA expression can be used a sensitive measurement of ganglion cell health / density (Nash and Osborne, 1999; Niyadurupola et al., 2011). *THY1* expression was assessed to determine ganglion cell density, alongside *CHAT* (Amacrine cell), *RLBP* (Müller cell), *PRKCA* (Bipolar cell), *CALBI* (Horizontal cell) and *RCVRN* (Photoreceptor cell).

Figure 5.6 shows the mRNA expression of cell specific markers in response to 24h CHQ treatment.

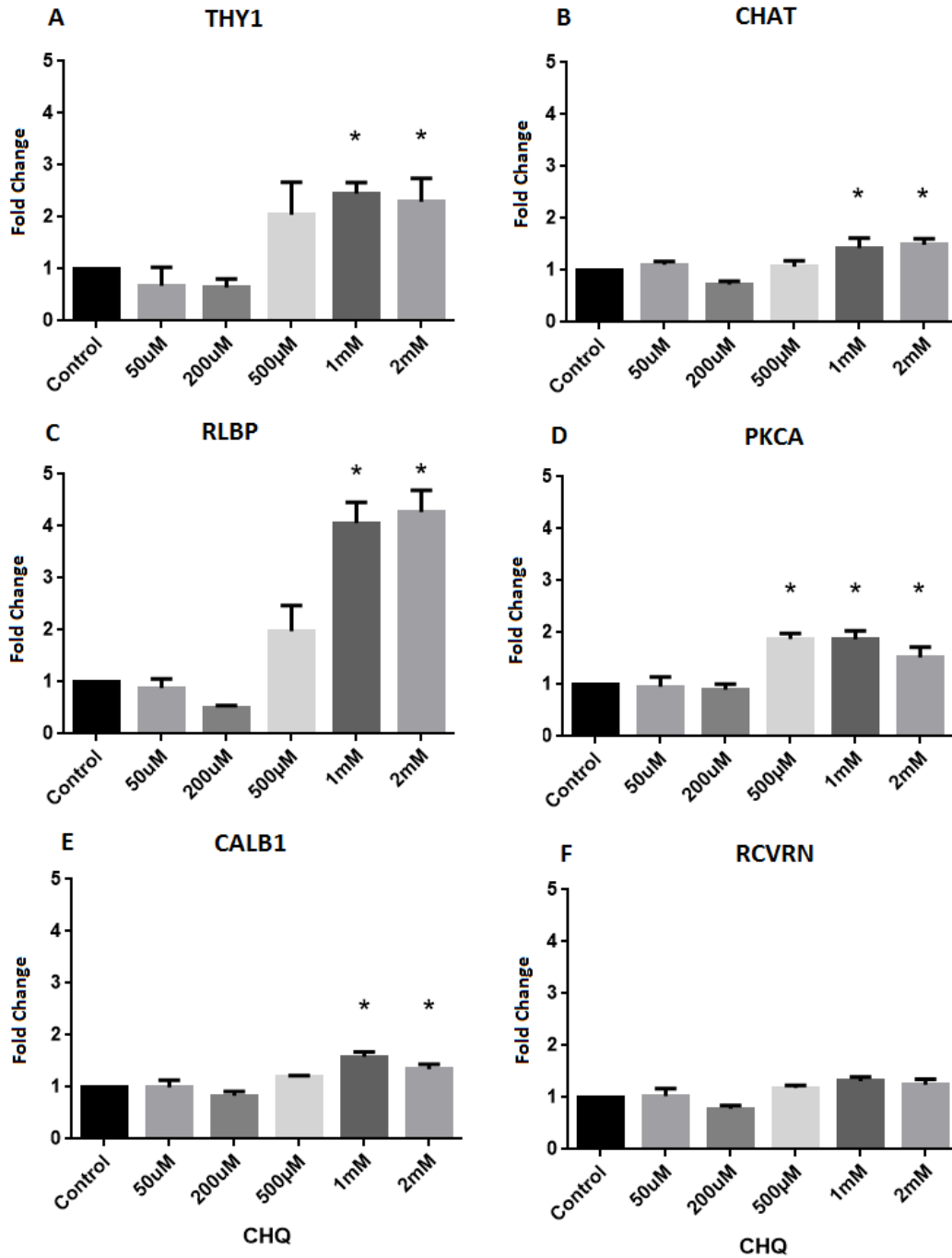


Figure 5.6 - Fold Change in mRNA Expression in Response to CHQ (Delta CT method) (normalised to the housekeeping genes TOP1 and CYC1) in HORCs exposed to CHQ for 24h **A** *THY1*, **B** *ChAT*, **C** *RLBP*, **D** *PKCA*, **E** *CALB1*, **F** *RCVRN* expression. Control (n=8), 50µM (n=4), 200µM (n=8), 500µM (n=4), 1mM (n=4) and 2mM (n=8). * indicates a significant difference to the control (P<0.05) using one way ANOVA with Dunnett's post-hoc test.

THY1 showed a decreased trend in expression after 50 μ M and 200 μ M CHQ treatment for 24h, however the decreased trend was not significant (Figure 5.6 A). This was followed by increased expression at higher concentrations of CHQ, with a significant increase at 1mM and 2mM.

ChAT displayed a similar pattern of expression to *THY1* after exposure to CHQ (Figure 5.6 B), with a trend of decreased expression with 50 μ M and 200 μ M CHQ followed by an increase in expression which became significant at 500 μ M, 1mM and 2mM.

Figure 5.6 C displayed *RLBP* expression in response to CHQ treatment. A trend of decreased expression at 200 μ M can be seen followed by an increase in expression at 500 μ M and a significant increase in expression with 1mM and 2mM CHQ treatment.

PKCA expression did not change in response to low concentrations of CHQ exposure, with no change in expression up to 200 μ M treatment (Figure 5.6 D). However there was a significant increase from \geq 500 μ M.

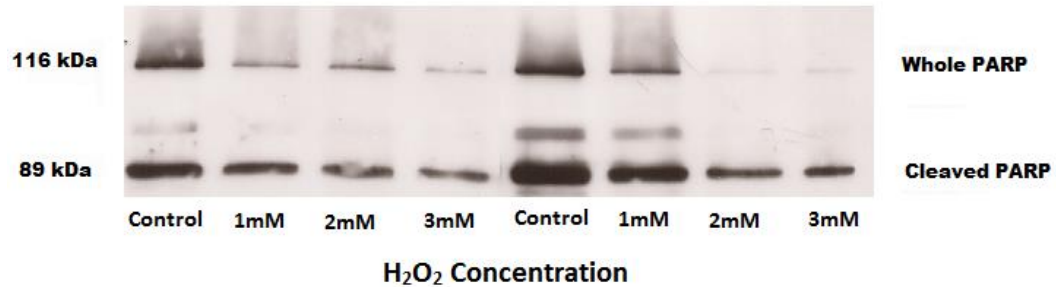
Changes in *CALB1* expression were similar to *THY1*, *ChAT* and *RLBP* with significant increases seen at 1mM and 2mM (Figure 5.6 E). Trends of *CALB1* were also similar to *RCVRN* (Figure 5.6 F), however *RCVRN* expression displayed no significant change with any concentration of CHQ treatment.

5.2.5 Western Blot Analysis of Chloroquine Treated Samples

The previous data provided evidence that cell death that occurred in HORCs with CHQ treatment. Subsequent experiments aimed to further investigate the method through which cell death occurred were carried out on HORCs exposed to CHQ for 24h. It is known that levels of PARP cleavage can be used as a measure of apoptosis (Mullen, 2004), therefore protein extracted from HORCs was analysed by western blotting for PARP cleavage and active caspase 3 to help determine if apoptosis was the cause of cell death in the treated samples.

Levels of PARP cleavage were firstly assessed in hydrogen peroxide treated samples as a positive control (Figure 5.7).

A



B

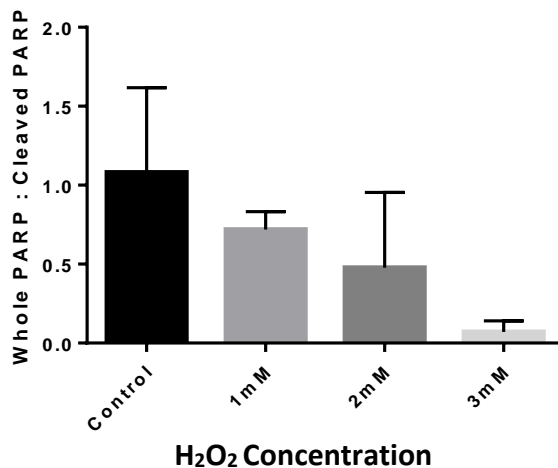


Figure 5.7 - PARP Cleavage in Response to H₂O₂ - **A** Representative western blot for PARP following 24h H₂O₂ treatment of HORCs (n=2) ± SEM. **B** Whole PARP to Cleaved PARP ratio. No significant difference was found with increasing concentrations of CHQ (P>0.05) (one way ANOVA with Dunnett's post-hoc test).

The western blot for PARP (Figure 5.7 A) clearly shows a loss of whole PARP (116kDa) with H₂O₂. This appears to be dose-dependent, with very little whole PARP detected at the higher concentrations of H₂O₂. Cleaved PARP also decreased with H₂O₂, but not as quickly as whole PARP. When analysed using densitometry the ratio of whole PARP to cleaved PARP displayed a dose dependent decrease with increasing concentrations of H₂O₂. It should be noted that this was only n=2,

however the clear trend showed that this may be a useful method to investigate apoptosis.

PARP cleavage was then investigated on CHQ treated samples.

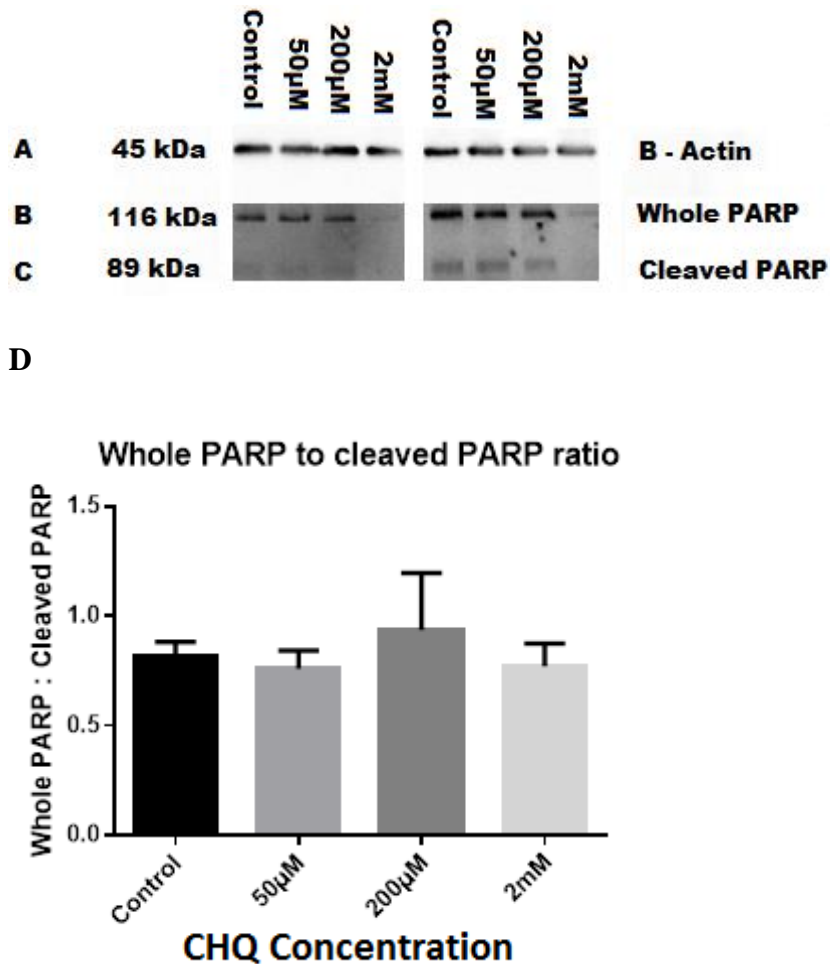


Figure 5.8 - Representative Western blot of PARP following 24h CHQ treatment.

A – β -actin, B – Whole PARP, C – Cleaved PARP

D - Whole PARP : Cleaved PARP ratio after normalisation of each to β actin (n=4). No significant difference was found with increasing concentrations of CHQ ($P>0.05$) (one way ANOVA with Dunnett's post-hoc test).

Figure 5.8 shows the effect of CHQ on PARP in the HORC. What can be seen is very little change in levels of β actin with increasing concentrations of CHQ (Figure 5.8A). Whole PARP also changes very little until 2mM treatment where a decrease can be seen (Figure 5.8 B), this is matched by cleaved PARP (Figure 5.8 C) which

also only shows a decrease with 2mM treatment. Overall this resulted in no change in the ratio of whole PARP to cleaved PARP (Figure 5.8 D).

5.3 Discussion

The aim of this research was to determine whether the HORC could be a suitable model for the assessment of retinotoxicity. This was investigated by assessing the effects of the known retinotoxin CHQ on the *ex vivo* retina.

Levels of cell death were firstly assessed in the positive control treated HORCs (H_2O_2). Figure 5.1 showed that 2mM H_2O_2 was required to cause a significant increase in cell death as measured by the LDH and MTS assays in the HORC. This corresponded well with the cell line data in Chapter 4 in which H_2O_2 caused a significant increase in cell death / decrease in cell viability in ARPE19 cells with 1mM and 500 μM H_2O_2 treatment respectively, and a significant decrease in cell viability was found with 1mM H_2O_2 treatment in the MIO-M1 cell line.

Since the LDH assay proved to be useful in measuring levels of cell death induced by H_2O_2 it was decided that this assay would also be used to assess CHQ induced cell death in HORCs. It was also decided that the MTS assay would be utilised to find out if the assays differed in sensitivity. It was found that CHQ caused a dose dependent increase in cell death in the HORCs (Figure 5.2), with a significant increase in cell death, and a significant decrease in cell viability found at a concentration of 2mM. LDH appeared to provide a more sensitive means of assessing cell death, displaying a gradual increase in cell death from low concentrations of CHQ, whereas the MTS assay did not show a decreased trend of cell viability until 500 μM CHQ.

Previous data from the ARPE19 and MIO-M1 cell lines indicated that CHQ caused a significant increase in cell death at concentrations of $\geq 200\mu\text{M}$ and $\geq 50\mu\text{M}$ respectively. It was therefore expected that the concentrations of CHQ required to induce a significant level of cell death in the HORC would be lower than 2mM. This may indicate that either the LDH and MTS assay are not sensitive enough to assess changes in levels of cell death in the HORC, or that higher concentrations of toxins /

compounds are required to cause a significant increase in cell death in the HORC due to the detoxification of the compound by the retina.

To further investigate CHQ induced toxicity, other methods of assessing cell death were used, specifically TUNEL activation, caspase 3 cleavage and ganglion cell number (levels of NeuN positive cells).

This was accomplished through the use of the Ventana Discovery (Roche, Burgess Hill, UK), a high throughput immunohistochemical platform which allows for the efficient staining of multiple slides with multiple antibodies. The platform was used for colorimetric immunohistochemistry where samples were stained for either active Caspase 3, Anti-FITC (TUNEL) or NeuN. The slides were then scanned and a positive pixel count performed of antibody specific pixels, normalized to the number of haematoxylin pixels using the image analysis software Scanscope. The TUNEL anti-FITC colorimetric method had not been used before in HORCs and was developed for the purpose of assessing CHQ induced toxicity using a high throughput method.

The TUNEL assay is designed to detect cells undergoing apoptosis, more specifically the late stages of apoptosis, in which DNA degradation from endonuclease activation occurs. The DNA degradation produces double stranded DNA fragments of approximately 180 – 200bp in length. The double stranded breaks are recognised by terminal deoxynucleotidyl transferase (TdT), which catalyses the addition of FITC labelled dUTP's to the 3'-OH termini, which can then be visualised through fluorescence microscopy (Kyrylkova et al., 2012). In this method a HRP anti-FITC antibody was used to allow colorimetric assessment of the samples to be used. It should also be noted that TUNEL has also been found to detect cells undergoing necrosis (Kyrylkova et al., 2012), suggesting that DNA fragmentation is not specifically a feature of apoptosis, meaning that care must be taken when interpreting data using this assay (de Torres et al., 1997; Grasl-Kraupp et al., 1995).

Figure 5.3 shows a dose dependent increase in % TUNEL positive pixels with CHQ treatment, with a significant increase from $\geq 200\mu\text{M}$. This assay displayed much higher sensitivity compared to the LDH and MTS assay which only showed a significant increase in LDH with 2mM treatment.

Active caspase 3 was then investigated, as measuring levels of active caspase 3 is a well-established method of analysing apoptotic cells. When cells die they commonly follow two routes of cell death, apoptosis and necrosis. Apoptosis is programmed cell death that is controlled and does not create an inflammatory response, whereas necrosis is uncontrolled cell death which is predominantly due to disruption of the cell membrane or interference with the energy supply of the cell which induces an inflammatory response (Kim et al., 2003; Elmore, 2007).

Apoptosis normally follows one of two main pathways, the extrinsic (death receptor) pathway and the intrinsic (mitochondrial) pathway. However there are other routes such as T-cell mediated cytotoxicity (Elmore, 2007). It is also possible for the extrinsic and intrinsic pathway to influence each other (Igney and Krammer, 2002). The extrinsic pathways initiation of apoptosis includes the activation of transmembrane receptor proteins. More specifically these are part of the tumour necrosis factor (TNF) receptor family which transmit the death signal into an intracellular signal. The T cell mediated cytotoxicity pathway mentioned earlier induces apoptosis via the extrinsic pathway (Brunner et al., 2003).

The intrinsic pathway of apoptosis is activated by a range of intracellular signals which act on internal targets within the cell. There are two types of stimuli which have the ability to activate the intrinsic pathway; these are negative and positive signals. Negative signals are induced by a lack of certain hormones, cytokines and growth factors which normally inhibit the initiation of a death signal. Positive signals are stimulants which induce the apoptosis signal including toxins, temperature change and viral infections. The death signal starts with the loss of the mitochondrial transmembrane potential, the opening of the mitochondrial permeability transition pore and the release of apoptosis inducing proteins (Saelens et al., 2004; Elmore, 2007).

Once either one of these pathways are activated they follow the same termination pathway which starts with the cleavage of Caspase 3. Following a series of intracellular events including; breakdown of cytoskeletal and nuclear proteins, DNA fragmentation and expression of ligands of phagocytes, the death of the cell occurs (Elmore, 2007).

Cleavage of caspase 3 is a common step in apoptosis enables the use of an antibody against active caspase 3 to identify cells which are undergoing apoptosis. In the experiments performed no change in levels of active caspase 3 was detected. This data leaves the root cause of cell death open. The lack of change in active caspase 3, and the significant increase in TUNEL levels with CHQ treatment indicates that either apoptosis is not the cause of cell death and TUNEL is displaying another form of cell death such as necrosis. Or that the tissue is undergoing apoptosis which TUNEL is showing, and the assessment of active caspase 3 is not appropriate for assessing levels of cell death in the human retina. The latter is likely to be the case as others have tried to use caspase 3 cleavage to assess apoptosis in the human retina, but without success (Osborne, personal communication).

Immunohistochemistry was also used to investigate ganglion cell susceptibility. It has been shown that CHQ treatment causes an initial loss of ganglion cells in the retina of rhesus monkeys, with other nuclear layers affected at later time points (Rosenthal et al., 1978). There is also clinical data from CHQ treated patients who are affected by CHQ induced retinopathy which indicates that there is a thinning of the nerve fibre layer in advanced stages of toxicity which may be due to ganglion cell damage / loss (Bonanomi et al., 2006; Korah and Kuriakose, 2008).

The percentage positive pixel method was used to investigate NeuN immunohistochemistry in HORCs after exposure to CHQ to find out if ganglion cell numbers were effected by CHQ treatment. The results (Figure 5.5) displayed no change in NeuN positive pixels with any concentration of CHQ treatment. This may indicate that ganglion cells which express NeuN do not change in number with CHQ treatment, or that ganglion cells are not affected by CHQ.

The next area of interest was to try and determine cell specific loss that occurred in the *ex vivo* retina as a result of CHQ toxicity. This was investigated through changes in expression levels of cell specific markers in response to CHQ induced toxicity. *THY1* mRNA expression has previously been used to assess ganglion cell health / density (Nash and Osborne, 1999; Niyadurupola et al., 2011), however no other cell specific markers have been used for this purpose in the *ex vivo* retina. For this reason expression levels of *THY1* (Ganglion cells), *CHAT* (Amacrine cells), *RLBP* (Müller

cells), *PRKCA* (Bipolar cells), *CALBI* (Horizontal cells) and *RCVRN* (Photoreceptor cells) were assessed to investigate cell health / density of the respective cells.

A common theme throughout these results is the decreased trend in expression with 200 μ M treatment, followed by an increased trend / significant increase in expression with 500 μ M, 1mM and 2mM CHQ treatment. This decreased trend in expression at 200 μ M could be indicative of cellular loss as a result of CHQ toxicity, however this is not matched by results from higher concentrations of CHQ treatment (1 and 2mM), which consistently led to increased expression of the cell specific markers. This increased trend / significantly higher expression of cell specific markers with high concentrations of CHQ was not expected as previous work with *THY1* as a marker of RGC survival showed a decreased expression correlating with RGC loss. It was possible that the increase in expression could be explained by alterations in expression of the housekeeping genes, however after reviewing the data, no changes in housekeeping gene expression was found, which indicates that CHQ was responsible for the upregulation of expression of multiple cell specific genes.

The reason for the increase in expression of the cell specific markers is not clear, however it has shown that the method of looking at decreased expression of cell specific markers in response to CHQ toxicity is unsuitable for the analysis of cell death associated with CHQ induced cell death.

It should be noted that even though the previous chapter showed that increased time exposed to CHQ induced higher levels of cell death in MIO-M1 and ARPE19 cells, the 24h time point was decided upon for HORC investigation. This time point was chosen because of previous research conducted into the expression of mRNA cell specific markers within the human retina over time. This research displayed a 50% decrease in the expression of the ganglion cell marker *THY1* after 24h in culture, followed by a further 25% decrease after 48h and reaching basal levels after 72h (Niyadurupola et al., 2011). If a decrease in markers are to be used as an assessment of a specific cell types vulnerability to CHQ, there must be as little change in the initial levels of that marker itself.

The next aim was to provide further information regarding the cause of cell death within the HORC. Protein from CHQ treated HORCs was extracted and analysed for PARP cleavage.

To help confirm whether CHQ toxicity causes apoptosis, PARP cleavage was investigated. Poly (ADP-ribose) polymerase (PARP) is a DNA repair enzyme which binds to DNA strand breaks and catalyses the formation of poly (ADP-ribose) polymers using NAD^+ as a substrate. PARP then detaches from the DNA, and the poly (ADP-ribose) polymers are degraded by poly (ADP-ribose) glycohydrolase (PARG) allowing DNA repair complexes to repair the DNA (Herceg and Wang, 2001). When a cell undergoes apoptosis, caspases cleave PARP from a single 116kD unit into two fragments (89kD and 24kD), to prevent DNA repair from occurring (Mullen, 2004). All caspases have the ability to cleave PARP, however caspase 3 and caspase 7 are the most efficient at this process (Ghayur et al., 1997).

PARP cleavage may be quantified and used to measure of apoptosis (Mullen, 2004). Due to the nature of cleavage by caspases, the amount of cleaved PARP can be used as an indication of apoptosis within the tissue / cells investigated. This method of investigation was of interest as it would provide more information regarding the mechanism of cell death caused by CHQ. Previous data indicated that CHQ treatment caused no rise in active caspase 3, however this does not rule out apoptosis. Many other caspases are involved with apoptotic cell death, and since all caspases have the ability to cleave PARP, PARP cleavage should indicate if apoptosis occurs as a result of CHQ toxicity.

In order to investigate if PARP cleavage is a suitable method to assess cell death in HORCs, a positive control was firstly investigated. PARP cleavage is known to be caused by caspases, therefore any inducer of apoptosis should act as a positive control. For this reason H_2O_2 was firstly investigated as it has been shown to induce apoptosis at low concentrations in ARPE19 cells (Kim et al., 2003).

Figure 5.7 showed a decrease in whole PARP, cleaved PARP also decreased and when the whole PARP : cleaved PARP ratio was measured there was a decreased trend with increasing concentrations of H_2O_2 . Although this decrease was not significant, due to the positive nature of the trend it was decided that PARP cleavage would be assessed in response to CHQ treatment.

Figure 5.8 shows the effect of CHQ treatment on PARP cleavage. Figure 5.7 D displays the ratio of whole PARP : cleaved PARP normalised to β actin in response to differing concentrations of CHQ. Although a decrease could be seen in both whole

PARP and cleaved PARP, there was no significant difference in this ratio with CHQ treatment, indicating that apoptosis may not be the route of cell death caused by CHQ treatment.

CHQ is a known inhibitor of autophagy, which is primarily linked with roles in pro-survival; it has however also been linked with roles in cell death. It is known to aid with numerous roles such as adaptation to starvation, immunity and recycling of organelles. For the process to be termed autophagy, the targeted cell constituents must be delivered into lysosomes for degradation (Boya et al., 2013). There are currently three well described types of autophagy described below:

Chaperone mediated autophagy is a form of autophagy in which a subset of soluble cytosolic proteins are recognised and transported into the lysosome for degradation. Chaperone mediated autophagy requires the protein to be degraded to contain a pentapeptide motif related to the amino acid sequence KFERQ. This motif is recognised by cytosolic chaperones which bring the protein to the surface of the lysosome where it docks with LAMP-2A. Once docked the protein unfolds and translocates into the lysosome (Kaushik et al., 2011).

Microautophagy is a non-specific form of autophagy (induced via nitrogen starvation) in which cytoplasmic substances / organelles are engulfed by the lysosome and broken down into their components (Li et al., 2012).

Macroautophagy involves a double membrane wrapping the targeted cytoplasmic region to form an autophagosome. The autophagosome then fuses with an endosome forming the amphisome. The amphisome then fuses with the lysosome forming the autolysosome which degrades the contained substances (Holt et al., 2011).

The effect of inhibiting autophagy on ARPE19 cells (using CHQ) has been investigated by Yoon et al (2010). The results indicated that the main cause of cell death may be due to lysosomal dysfunction, where an increased accumulation of endocytosed proteins and lipids have cytotoxic consequences. Yoon et al (2010) also found that an increase in LC3-II occurred due to the inhibition of autophagosome and lysosome binding. Autophagic cell death however was not likely to be the cause of cell death found with CHQ treatment, since inhibition of autophagy using 3-MA failed to reduce levels of CHQ induced cell death, whereas co treatment with bafilomycin A1 (a lysosomal acidifier) attenuated cell death, indicating lysosomal dysfunction may be involved with the cell death found. Interestingly this study also

revealed that caspase dependent cell death was not the root cause of cell death, as the broad range caspase inhibitor z-VAD-FMK did not reduce CHQ induced cell death and no activation of caspase 3 was found. This could match research in this chapter which displayed a lack of caspase 3 activation with CHQ treatment, however contradictory to this TUNEL labelling did increase which could also indicate apoptosis may be involved.

5.4 Conclusion

This chapter aimed to investigate the best methods available to analyse cell death in the *ex vivo* human retina in order to assess the effects of the retinotoxin CHQ.

Cell death was firstly assessed using the LDH and MTS assay, which revealed a significant increase in cell death and cell viability with 2mM CHQ treatment. The LDH assay showed an increased trend of LDH release at lower concentrations of CHQ treatment, indicating that the LDH assay is more sensitive at assessing levels of CHQ induced cell death.

When immunohistochemical methods of analysing cell death were investigated, TUNEL positive cells displayed a significant increase from $\geq 200\mu\text{M}$ CHQ treatment. Active caspase 3 was also investigated, however no change in active caspase 3 staining was found with any concentration of CHQ treatment. Finally, ganglion cell loss was investigated (levels of NeuN), however no change in NeuN was found with any concentration of CHQ treatment. This data showed that the most sensitive method utilised to assess cell death in response to CHQ was the TUNEL assay.

To explore specific cell sensitivities to CHQ, quantitative PCR was utilised to investigate expression of cell specific markers in response to CHQ treatment. This produced consistent increases in expression of all cell specific markers with 1 and 2mM treatment, showing that measuring decreased expression of cell markers is unsuitable for the assessment of cell health / density in response to CHQ induced toxicity.

Further analysis was carried out to determine whether the route of cell death caused by CHQ toxicity could be investigated in HORCs. PARP cleavage was investigated as a measure of apoptosis, however no change in the ratio of whole PARP to cleaved PARP was found.

Overall the research presented in this chapter has shown that cell death can be observed in the *ex vivo* retina through the use of medium assays such as LDH and MTS, with the most sensitive means of assessing cell death being TUNEL analysis.

Chapter 6

6.0 Cyclin Dependent Kinase Expression in the Adult Human Retina

6.1 Introduction

Research presented in previous chapters has shown the effectiveness of both the extraction template (the five paramacula explants and the macula explant) and the planar sectioning technique in the process of identifying cell type and density through the investigation of mRNA expression. Whole explant analysis provided information about cell density within certain regions of the retina (paramacula and macula). Whereas analysis of planar sections showed the expression profile of cell specific mRNA was as would be expected in relation to positioning across the retinal layers. Using the latter technique the ganglion cell layer expressed peak levels of *THY1* and other ganglion cell specific markers. The inner nuclear layer expressed peak levels of *PKCA* and other inner nuclear layer markers, and the outer nuclear layer expressed peak levels of *RCVN* compared to the rest of the retina. This shows that this technique could be used to assess the expression profile of specific genes of interest, including genes related to retinotoxic drugs.

Cyclin Dependent Kinases (CDKs) are part of a family of heterodimeric serine / threonine protein kinases which are primarily involved in the cellular processes and signals which time the cell cycle (Malumbres and Barbacid, 2005). CDK's are named so because of their dependence on cyclin subunits for activation. These cyclins are synthesized and degraded throughout the cell cycle in order regulate the activity of the CDK's (Malumbres and Barbacid, 2005). There are 21 genes which encode for CDK's and a further 5 genes which encode CDK-like proteins (Figure 6.1) (Malumbres et al., 2009).

Recent research has begun to show that the role of CDK's are not strictly bound to the cell cycle. They also play roles within the regulation of RNA polymerase II (CDK7, 8 and 9) (Parry et al., 2010; Bregman et al., 2000) and, in the case of post mitotic neurons, cell migration and synaptogenesis (D.W. Rickman, 2005). Some CDK's have also been shown to have important roles within photoreceptor activity, for example, CDK5 is involved in the recovery phase of phototransduction in frog and other vertebrate photoreceptors (Hayashi et al., 2000).

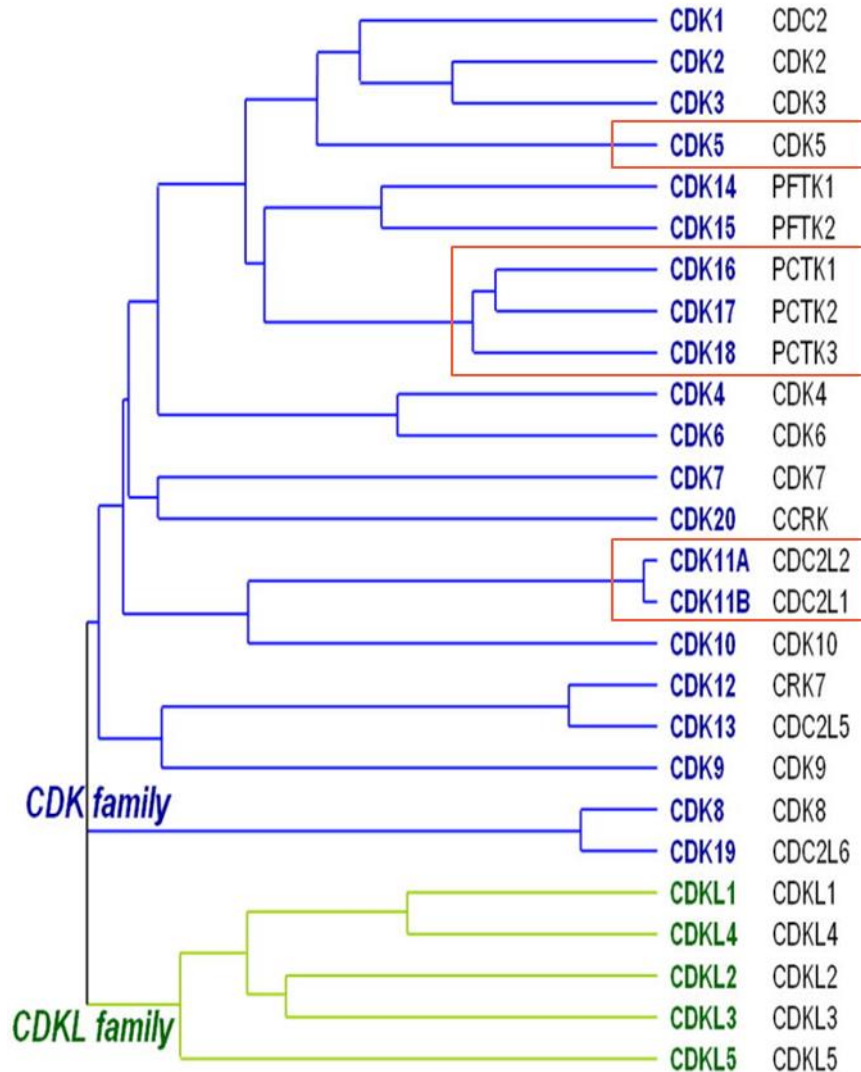


Figure 6.1 - CDK family tree. CDKL = CDK like, for explanations of the genes highlighted in the red box, refer to the text (Malumbres et al., 2009)

CDK inhibitors have been of interest recently due to their potential to be used as cancer therapeutics. This has stemmed from research which has found that CDK's can be over expressed in many tumors (Nemunaitis et al., 2013). One such example of a successful CDK inhibitor is dinaciclib, a small molecule CDK inhibitor which has progressed through to human phase 1 clinical trials for patients with advanced malignancies (Nemunaitis et al., 2013) and has been used for early phase 2 trials for non-small cell lung cancer (Stephenson et al., 2014). Broad spectrum pan CDK inhibitors would be expected to have similar side effects as chemotherapy agents,

with other rapidly dividing cells being affected such as those within the gut and bone marrow (Illanes et al., 2006). Interestingly it has been noted that the use of pan-CDK inhibitors can cause toxic side effects and cell death within non-rapidly dividing cells, and non-dividing cells.

AG-012986 is a pan-CDK inhibitor which was found to cause photoreceptor toxicity in the mouse retina (Illanes et al., 2006). Since inhibition of CDK's would normally prevail in toxicity related to dividing cells this was of interest, especially since photoreceptors are post-mitotic having an "arrested" cell cycle. This further demonstrates CDK's potential involvement in non cell cycle roles.

The research presented in this chapter investigates the expression profile of CDK isoforms in the retina. CDK mRNA expression was investigated in whole explants of the human retina to reveal firstly whether the CDK isoform was expressed and secondly whether any differences in regional expression throughout the retina (macula vs paramacula) were present. Following this, the mRNA expression profile of selected CDK isoforms was investigated throughout retina using the planar sectioning technique. CDK mRNA was analysed alongside three cell specific markers: *THY1* to identify the ganglion cell layer, *PKCA* to identify the inner nuclear layer and *RCVRN* to identify the outer nuclear layer.

The aims of this chapter are firstly to select CDK's which might be potential mediators of retinotoxicity caused by the CDK inhibitor and to determine the expression profile of these genes in the human retina. Secondly, the effects of the pan CDK-inhibitor AG-012986 on the two retinal cell lines ARPE19 and MIO-M1 cells will be investigated. This research aims to aid in the future development of CDK inhibitors, providing information relating to which CDK's may be the cause behind the toxicity of photoreceptors.

6.2 Results

6.2.1 CDK Selection

Due to large vast family of CDK's and CDK-like proteins, the research was directed to a set of CDK's agreed with AstraZeneca. In order to make a decision on which CDK's to investigate, AstraZeneca provided data regarding the affinities of two pan-CDK inhibitors with known neurotoxicity and one pan-CDK inhibitor and a selective CDK9 inhibitor which has no reported neurotoxicity. This data is shown in Figure 6.2.

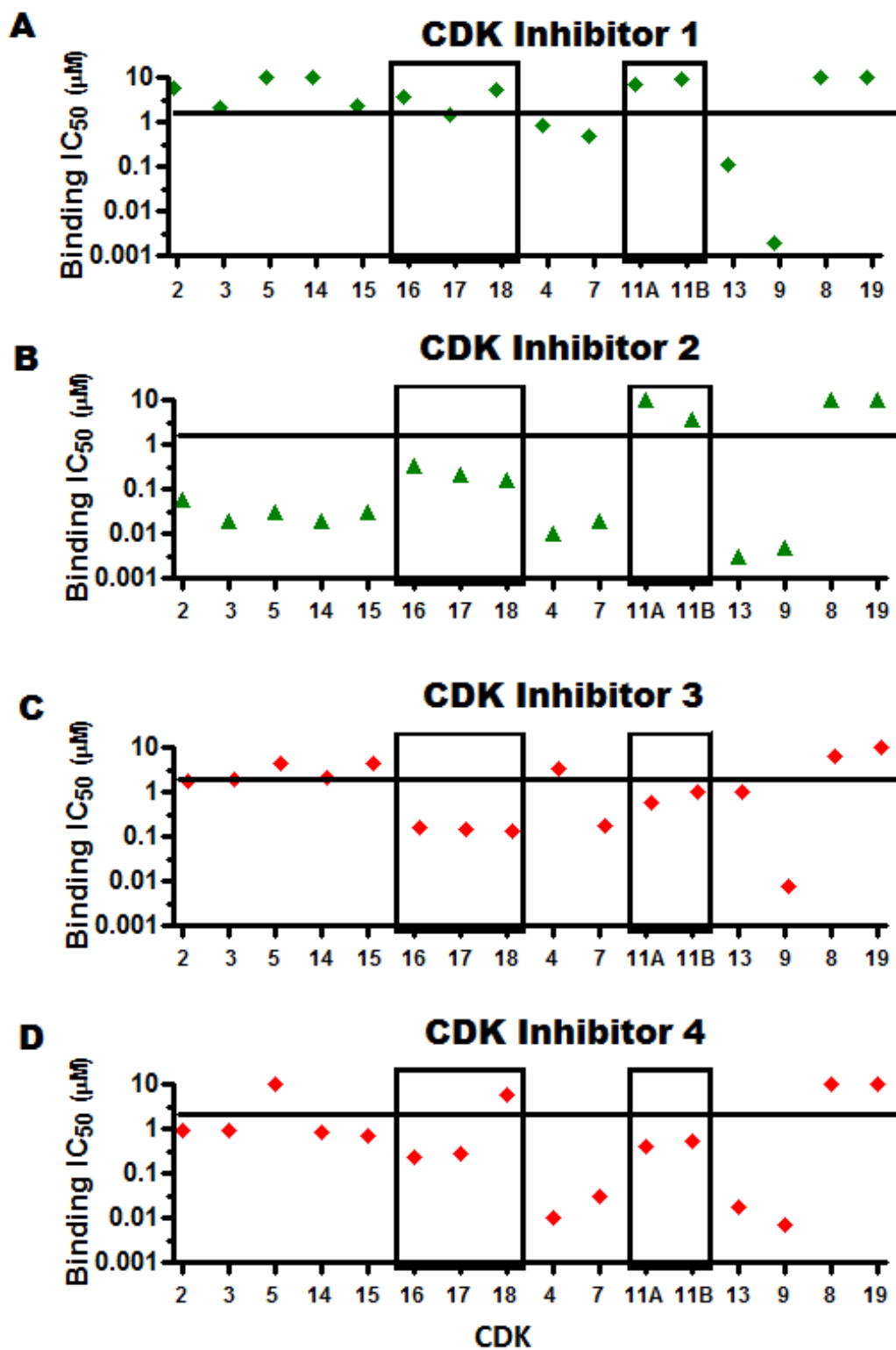


Figure 6.2 - Affinities of four CDK inhibitors towards different CDK isoforms. A and B (green dots) represent two CDK inhibitors with no recorded neurotoxic side effects. C and D (red dots) represent two CDK inhibitors with recorded neurotoxicity. Source: AstraZeneca.

The CDK's agreed upon were CDK16, 17 and 18, and CDK11A and B. This was decided because both CDK inhibitors which cause retinotoxicity possessed higher affinity for CDK 16, 17 and 18 along with CDK11A and B, and it was believed that the combined effect of inhibiting these CDK's may be the reason behind the retinotoxicity found. It was also agreed that CDK 5 would be investigated due to previous data suggesting the role CDK5 possesses in the retina.

6.2.2 Whole Explant CDK analysis

Whole explant analysis of CDK expression throughout the five paramacula explants and the macula explant was performed to investigate if CDK expression was present, and if any variation in regional expression occurred (Figure 6.3)

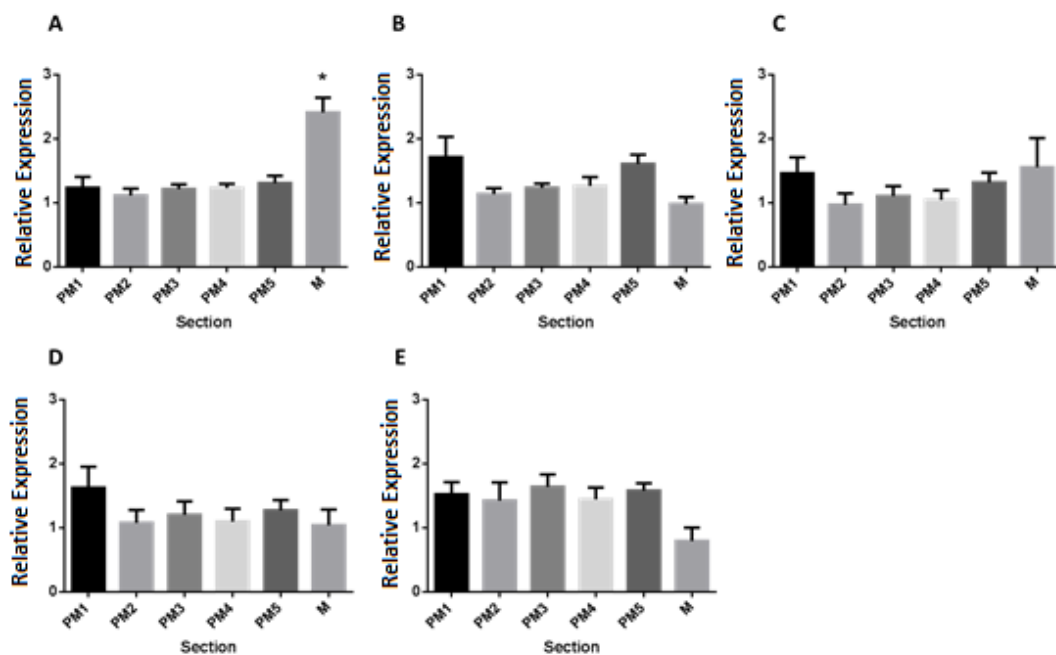


Figure 6.3 - Expression of CDK's throughout whole retinal explants. Relative expression of CDK 5 (A), 11 (B), 16 (C), 17 (D) and 18 (E) mRNA within paramacula and macula explants (n=5) \pm SEM, * indicates significance (one way ANOVA with Tukeys multiple comparison test) (P<0.05).

CDK5 expression levels were consistent throughout the 5 paramacula explants, however the macula had significantly higher expression compared to paramacula explants (Figure 6.3 A). CDK11 expression levels were similar throughout the paramacula and macula explants (Figure 6.3 B).

CDK16 and 17 expression levels were consistent throughout the paramacula and the macula explants. CDK18 displayed a reduced trend of expression in the macula compared to the paramacula explants, but no significant difference was seen (Figure 6.3 C, D and E).

This data indicates that each of the CDKs investigated are expressed within the human retina, and there is evidence to suggest that some of the CDKs may be more highly expressed in certain cell types, with CDK5 possessing significantly higher expression in the macula and CDK18 displaying a reduced trend of expression in the macula compared to the paramacula. Planar sectioning may be utilised to confirm any expression patterns that may occur throughout the nuclear layers of the retina.

6.2.2 mRNA Profiling of the Macula and Paramacula Explants

Planar sectioning allows assessment of mRNA expression in individual retinal layers. Expression of CDK5, 11, 16, 17 and 18 was assessed alongside cell specific markers to determine the expression profile.

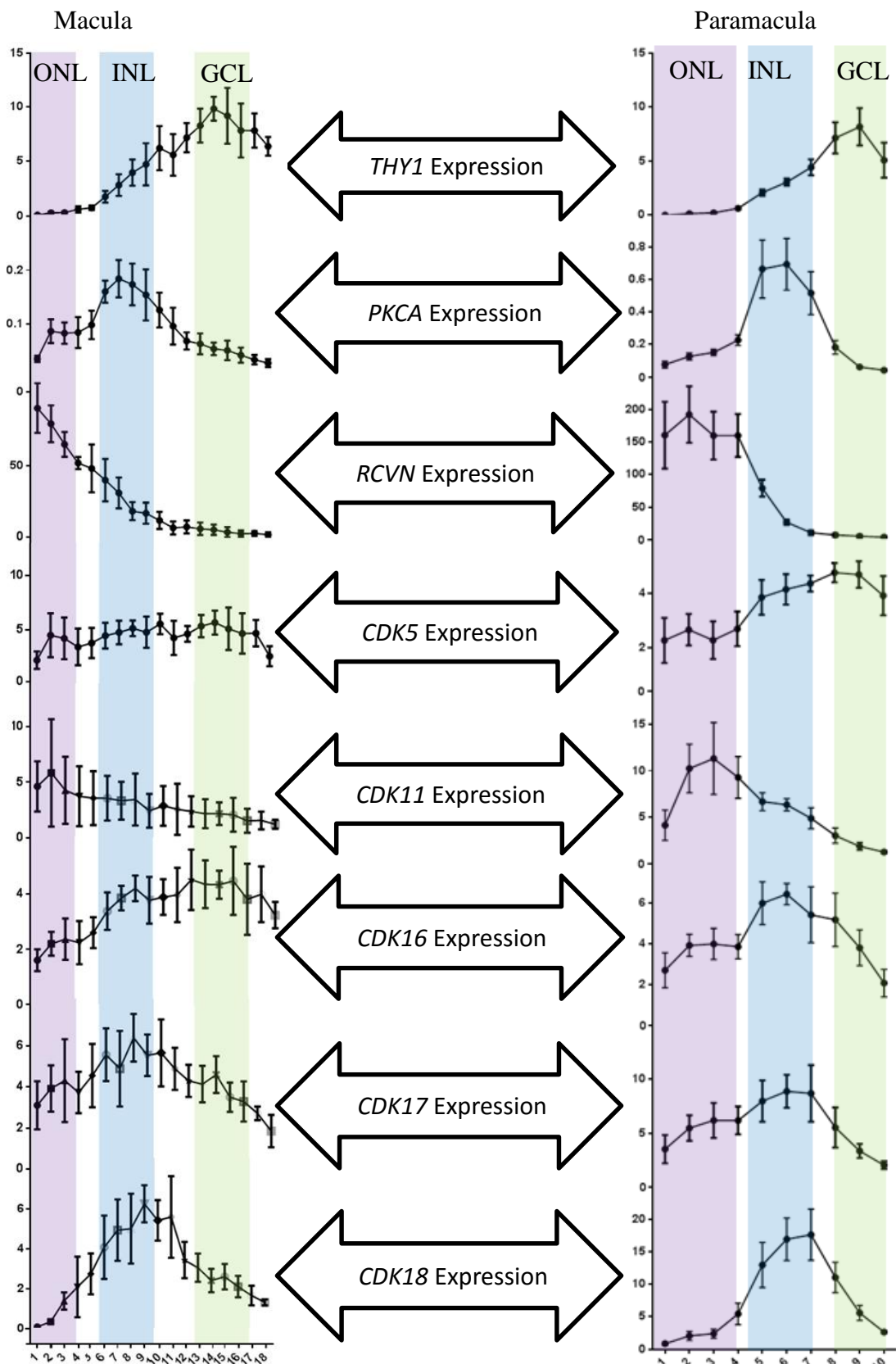


Figure 6.4 - Expression of *THY1*, *PKCA*, *RCVRN*, *CDK5*, *CDK11*, *CDK16*, *CDK17* and *CDK18* mRNA throughout planar sectioned macula and paramacula samples. Mean \pm SEM (n=4). The outer nuclear layer is represented by the purple bar, the inner nuclear layer by the blue bar and the ganglion cell layer by the green bar.

Figure 6.4 shows the mRNA profile of the cell specific markers and CDKs throughout the macula and paramacula explants. The cell specific markers *THY1*, *PKCA* and *RCVN* were located in their normal positions and helped identify the ganglion cell layer, the inner nuclear layer and the outer nuclear layer respectively.

CDK5 expression was evenly distributed throughout the macula whereas in the paramacula, peak expression was found in the ganglion cell layer.

CDK11 showed peak expression in the outer nuclear layer of both macula and paramacula samples, although this peak was more defined in the paramacula.

CDK16 expression was low in the outer nuclear layer of both the macula and paramacula, before gradually increasing throughout the inner nuclear layer. Expression then remained high in the ganglion cell layer of the macula, whereas a decrease in expression was found in the ganglion cell layer of the paramacula.

CDK17 displayed a similar expression pattern in both the macula and the paramacula, with low expression levels in the outer nuclear layer and the ganglion cell layer and peak expression in the inner nuclear layer.

CDK18 expression was also very similar in both macula and paramacula samples, with a defined peak in the inner nuclear layer, no expression in the outer nuclear layer and little expression in the ganglion cell layer.

6.2.3 Effect of AG-012986 on ARPE19 and MIO-M1 Cells

It is of interest to investigate the effect of AG-012986 on the retinal cell lines due to the toxicity found *in vivo* in mice by Illanes et al (2006). The photoreceptor degeneration found with AG-012986 may be caused as a side effect of RPE or Müller cell malfunction, therefore it is of interest to investigate the effect of the pan CDK inhibitor on the two cell lines ARPE19 and MIO-M1.

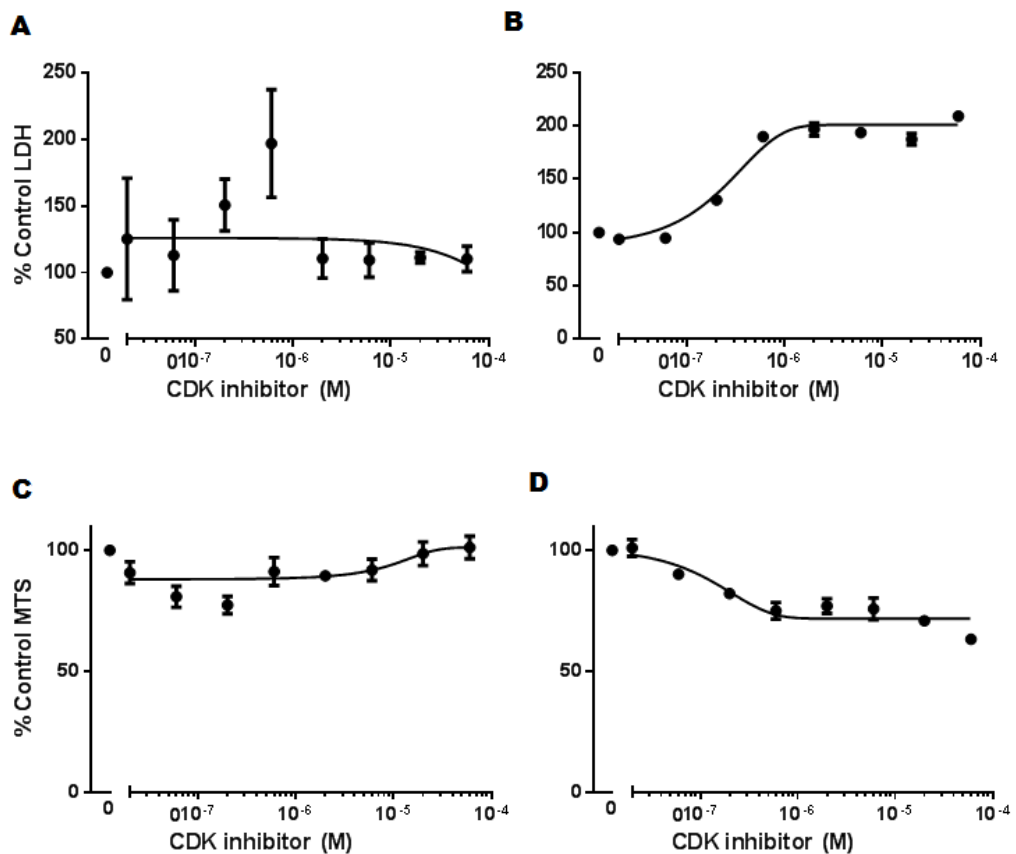


Figure 6.5 - LDH release and Cell Viability of ARPE19 and MIO-M1 Cells in Response to AG-012986. A and B, LDH release in ARPE19 and MIO-M1 cells (respectively) in response to the pan CDK inhibitor AG-012986. C and D cell viability of ARPE19 and MIO-M1 cells (respectively) in response to differing concentrations of AG-012986. * indicates a significant difference from the control (one way ANOVA with Dunnett's post hoc test) ($P < 0.05$)

The pan-CDK inhibitor AG-012986 was found to possess toxic effects on the MIO-M1 cell line, but not the ARPE19 cell line. This was displayed by the significant

increase in cell death found from 200nM treatment on MIO-M1 cells in both LDH and MTS assays. ARPE19 cells displayed a significant decrease in MTS with 60nM and 200nM treatment, however this is more than likely an anomaly as no other significant decrease in MTS followed and was not matched by an increase in LDH.

6.3 Discussion

Recent evidence has brought to light the role of CDKs outside of the cell cycle. The importance of this has been demonstrated by the development of drugs aimed at CDK inhibition which cause toxicity in post mitotic cells. An example of this is the pan CDK inhibitor AG-012986 which caused specific photoreceptor toxicity when applied to mice *in vivo* (Illanes et al., 2006).

In order to investigate the distribution of CDKs within the human retina, mRNA expression levels were measured in whole paramacula and macula explants, providing an insight into firstly whether the CDKs were expressed, and secondly the expression pattern throughout the topographical regions of the retina. The CDK expression profile were then investigated throughout planar sectioned macula and paramacula explants. This provided a location of CDK expression within the nuclear layers of the retina, and details of the density of expression, all of which aid in the identification of the cell type expressing CDKs.

Due to the large number of CDKs, it was decided that the research conducted would be focussed onto specific CDKs which were predicted to be the cause of the retinotoxicity found with AG-012986 (Illanes et al., 2006). In order to decide on the CDKs to investigate, AstraZeneca provided CDK affinity data from four CDK inhibitors. Two of these CDK inhibitors were known to cause retinotoxicity, and two had no reported retinotoxicity. After review, the two CDK families that the retinotoxic CDK inhibitors possessed higher affinities for than the non-toxic inhibitors were the CDC2L family (CDK11A and 11B) which had higher affinities in the two neurotoxic CDK inhibitors, and the PCTK family (CDK16, 17 and 18) which also possessed high affinities in both neurotoxic CDK inhibitors (highlighted in Figure 6.2). It was also decided that CDK5 would be investigated, as previous data had suggested that CDK5 may possess a role in the RGC apoptosis in the rat retina (Chen et al., 2011a).

Each of the CDK's investigated are discussed in turn, and any differences found interpreted.

Whole explant CDK mRNA analysis (Figure 6.3) revealed that *CDK5* had significantly higher expression within the macula explant compared to all 5 paramacula explants ($P < 0.05$). Referring back to chapter 3 it can be seen that the cell specific marker genes of ganglion cells (*THY1*, *AHNAK2* and *RBFOX3*) all show significantly higher expression in macula samples compared to paramacula. This could indicate that *CDK5* is expressed in ganglion cells. mRNA profiling revealed that in macula samples, expression was evenly distributed and showed no indication of peak expression within the ganglion cell layer (Figure 6.4). Interestingly however, within paramacula samples there was highest expression in the ganglion cell layer (Figure 6.4). This indicates that expression is not restricted to the ganglion cells, but that in the paramacula region, there is higher *CDK5* expression in the GCL than in other layers of the retina.

CDK5 has been found to play an important role within the CNS. It is expressed universally, however it has high activity within the CNS due to the distribution of its activators (P35 and P39). P35 and P39 are non-cyclins, with P35 being the main activator of *CDK5*. P39 possesses a 57% homology with P35 and can therefore also activate *CDK5* (Dhariwala and Rajadhyaksha, 2008). *CDK5* is known to play a role in neural development, aiding in neuronal migration and differentiation, axonal elongation and synaptogenesis. However it also plays a role in post mitotic neurones. This is because post mitotic neurones express P35 activity (Paglini and Caceres, 2001; Chen et al., 2011a). *CDK5* has also been linked with multiple neurological disorders such as Alzheimer's Disease, Parkinson's Disease, Amyotrophic Lateral Sclerosis (ALS) and Huntington's Disease (Dhariwala and Rajadhyaksha, 2008).

Interestingly *CDK5* has also been shown to play a role in rat RGC death within a model of glaucoma where it was found that *CDK5* was upregulated significantly at day 21, which was matched by TUNEL positive cells. P35 expression was also elevated significantly on day 14 and day 21 of the glaucoma model, suggesting that the increase in P35 caused the increase in *CDK5* expression. Intriguingly roscovine (a *CDK5* inhibitor) significantly reduced levels of P35 and the number of apoptotic RGC's, emphasising the importance of *CDK5* in neuronal cell survival (Chen et al.,

2011a). This is interesting in that roscovine (CDK5 inhibitor) possessed pro-survival properties for ganglion cells in a glaucoma model, whereas the pan-CDK inhibitor AG-012986 caused photoreceptor toxicity in healthy mice, potentially indicating that CDK5 inhibition may not be involved with the cell death found with AG-012986. Planar sectioning data showed that *CDK5* was not expressed highly in the outer retina compared to the rest of the retina.

CDK11 expression throughout whole paramacula explants was relatively consistent although the macula displayed a trend of slightly lower expression compared to paramacula explants. The cell specific markers that show a similar pattern of lower expression in macula vs paramacula are: the Müller cell marker; *RLBP*, the bipolar cell marker *PKCA* and the photoreceptor marker *RCVRN* (Chapter 3). Planar sectioning revealed higher expression of *CDK11* in the photoreceptor layer of both macula and paramacula samples, although the difference was more noticeable in the paramacula. This indicates that *CDK11* is more highly expressed in photoreceptors and that expression of *CDK11* could be higher within rod photoreceptors, which become more densely populated as distance from the fovea increases.

CDK11 has two isoforms p58 and p110, neither of which has been studied within the retina. The CDK^{p110} isoform is known to be expressed throughout the cell cycle and is involved in transcriptional regulation and RNA processing, whereas the CDK^{p58} variant is specifically expressed at the G2/M phase (Rakkaa et al., 2014). Deletion of the CDK 11 gene in mice caused embryonic death at E3.5 and when further investigated, blastocysts showed proliferative defects and mitotic arrest (Hu et al., 2007). As photoreceptors are terminally differentiated CDK11's high presence within the photoreceptors is not likely to be due to its role within the cell cycle. Interestingly CDK11^{p58} has also been investigated for its role in apoptosis in PC12 cells (rat neuronal cell line), in which a knockdown of CDK11 repressed neuronal apoptosis, and overexpression promoted neuronal apoptosis (Liu et al., 2013). This would imply that CDK11 found within photoreceptors might be involved in the regulation of apoptosis, however if effects were similar to that of the knockdown of CDK11 in the PC12 cell line, inhibiting CDK11 would repress apoptosis, not induce it. The literature combined with our data may indicate that photoreceptors possess higher levels of CDK11 to aid with transcription / pre-mRNA splicing of photoreceptor specific mRNA's.

CDK16 expression showed no distinct pattern of expression between paramacula and macula explants. Interestingly mRNA profiling of macula sections revealed increasing expression within the inner nuclear layer before reaching peak expression in the ganglion cell layer, whereas in paramacula sections there was peak expression within the inner nuclear layer. This could indicate that *CDK16* is expressed within a cell type which resides within both the inner nuclear layer and the ganglion cell layer, this may imply expression in amacrine cells. Interestingly, in howler monkeys (*Alouatta caraya*) displaced amacrine cell density reached its peak at 0.5mm from the fovea (Muniz et al., 2014). The macula sections in these experiments measures 4mm in diameter and therefore would encompass this region of high displaced amacrine cells. This could explain the difference found between the macula and paramacula planar sections; with a high density of displaced amacrine cells in the macula, expression of *CDK16* would display high levels in the inner nuclear layer and the ganglion cell layer, whereas the paramacula sections would show peak expression only in the inner nuclear layer. This, however, does not tie in with previous data regarding amacrine cells. When the mRNA profile of *CHAT* marker was assessed in Chapter 3, peak expression in macula sections was found in the inner nuclear layer, whereas peak expression in paramacula sections was found in the ganglion cell layer. This data could therefore indicate that *CDK16* is expressed in amacrine cells which do not express *CHAT*.

CDK16, also known as PCTAIR1 (PCTK1) is expressed in testes, skeletal muscle and terminally differentiated neurons (Shimizu et al., 2014). In the testes it is known to play a role in spermatogenesis (Mikolcevic et al., 2012) and the cell cycle. It is also thought to have interactions with p35 / CDK5. Cheng displayed *CDK16*'s ability to bind to p35 and that the two co-immunoprecipitated together and were found to be concentrated at neuromuscular junctions. The *CDK5/p25* complex was also found to phosphorylate *CDK16*, this was re-enforced by *CDK5* null mice which showed a significant reduction in *CDK16* activity (Cheng et al., 2002) (Graeser et al., 2002). Interestingly *CDK16* is important for melanoma cell proliferation, and it has been found in melanoma cell lines that high levels of *CDK16* cause degradation of p27 (a tumor suppressor), whereas knockdown of *CDK16* caused elevated p27 levels and in turn apoptosis (Yanagi et al., 2014). Whether inhibition of *CDK16* could cause a similar effect and potentially apoptosis of photoreceptor cells such as that found with AG-012986 would need more research.

CDK17 expression was evenly distributed throughout the whole sections (macula and paramacula). mRNA profiling of macula and paramacula samples showed low expression in the outer nuclear layer, with peak expression in the inner nuclear layer and very low expression in the ganglion cell layer. The higher expression within the inner nuclear layer is suggestive of expression in: horizontal cells, amacrine cells, bipolar cells or Müller cells. mRNA which showed similar distribution in planar sections and whole macula / paramacula explant expression were *CHAT* and *CALB1*. This data could indicate that the amacrine and / or horizontal cells possess high levels of *CDK17*, however, the cell specific mRNA for these cells (Chapter 3) shows a more defined peak, restricted to one nuclear layer, whereas the *CDK17* peak is gradual.

CDK17, also known as PCTAIR2 (PCTK2), is a poorly characterised protein which is expressed within terminally differentiated neurones, only appearing within the brain at development stages P-7 to P-15 upon neurones exiting the cell division cycle (Hirose et al., 1997). Hirose et al (1997) implied that due to the location of immunocytochemical analysis of PCTAIR2, it could be involved with cytoskeletal proteins of post mitotic neurones (Hirose et al., 1997). This would indicate that *CDK17* may play a role in the cytoskeleton of amacrine and horizontal cells, however its potential link with the toxicity found with AG-012986 is still unclear.

CDK18 mRNA showed even distribution throughout all 5 paramacula explants and lower expression in the macula explant. This is similar to the distribution of the inner nuclear layer markers *PKCA* (bipolar cells), *RLBP* and *GLUL* (Müller cells), and also the photoreceptor marker *RCVRN*. mRNA profiling of macula and paramacula explants showed no expression in the outer nuclear layer, high expression in the inner nuclear layer and very low expression within the ganglion cell layer. The peak of *CDK18* expression within planar sectioned macula samples was seen at section 9, which matched *RLBP* expression (Figure 6.4). Planar sectioned paramacula samples also show *CDK18* possesses a very similar expression profile as *RLBP* (Figure 6.4). Expression is most likely localised in Müller cells rather than bipolar cells because the peak of *CDK18* expression lies closer to the ganglion cell layer than the peak of *PKCA* expression, as did the peak of *RLBP* expression (Chapter 3).

CDK18, also known as PCTAIR3 (PCTK3) is another poorly described member of the CDK family. The activators of *CDK18* are thought to be cyclin A2 (proposed to

aid in the transition from S to M phase) and phosphorylation by PKA (Matsuda et al., 2014). Interestingly it is also believed that CDK18 plays a role in the progression of Alzheimer's disease since it is found in high concentrations in pathological tissue, and is proposed to modulate Tau phosphorylation (Herskovits and Davies, 2006). Since CDK18's peak expression matches that of Müller cells it is possible that inhibition of CDK18 by AG-012986 could have downstream effects in the support that Müller cells provide to the retina and in turn cause photoreceptor toxicity.

Since AG-012986 is known to cause photoreceptor toxicity *in vivo* in mice, it is of interest to know if this may also occur in humans. When CHQ and the other retinotoxins were firstly investigated (chapter 4), the two cell lines ARPE19 and MIO-M1 cells were exposed to the retinotoxins and provided valuable information regarding the potency of the drugs. To utilise the cell lines further and provide information about the potency of the pan-CDK inhibitor, AG-012986 was applied to the two cell lines ARPE19 and MIO-M1 at various concentrations. The cell lines revealed an interesting feature about the toxicity of AG-012986, that the RPE cell line was not affected by AG-012986 whereas the Müller cell line was. This is interesting because photoreceptors rely on the RPE cells for maintenance and turnover of outer segments, therefore any damage to the RPE is likely to result in damage to the photoreceptors which could have explained the photoreceptor toxicity found with AG-012986.

Müller cells are also known to play a crucial role in the support of photoreceptors as well as other neuronal cells of the retina. They provide anti-oxidative support to photoreceptors by the release of glutathione as well as providing photoreceptor protection by secreting neurotrophic factors, growth factors and cytokines (Reichenbach and Bringmann, 2013). The importance of the supportive role that Müller cells play for photoreceptors is emphasised by a study conducted by Shen et al (2012) in which Müller cell ablation caused photoreceptor apoptosis (Shen et al., 2012).

The data obtained from the ARPE19 and MIO-M1 cell lines suggests that the Müller cells are more sensitive to AG-012986 and therefore may also play a role with the photoreceptor toxicity found with AG-012986 treatment.

6.4 Conclusion

The research presented in this chapter investigated CDK expression throughout the human retina. This could help identify the CDK which is inhibited by the CDK inhibitor AG-012986 that causes specific photoreceptor toxicity.

One of the CDK's investigated (CDK11) displayed higher expression in the photoreceptor layer. This occurred in both paramacula and macula samples, however the peak was more defined in paramacula samples. Whole explant analysis showed that CDK11 possessed lower expression in macula samples compared to paramacula samples, which was similar to the whole explant analysis of RCVRN. This indicates that CDK11 may be preferentially expressed within rod photoreceptors which are present at a much higher density within the peripheral retina, and at a lower density within the foveal region.

Interestingly the pan-CDK inhibitor displayed a higher toxicity to the MIO-M1 cell line than the ARPE19 cell line, indicating that Müller cells may be more sensitive to the inhibitor than RPE cells. This may coincide with the planar sectioning data which showed CDK18 expression was high in Müller cells, and could indicate the cause of the photoreceptor toxicity may be downstream of damage to Müller cells through inhibition of CDK18 in Müller cells.

Chapter 7

7.0 General Discussion

7.1 Thesis summary

The aim of this study was to develop the *ex vivo* human retina as a model to assess retinotoxicity. The need to develop this model comes from the high levels of ocular toxicity associated with drug development; data from Pfizer reported that 7% of therapeutic candidate attrition was due to ocular toxicity, of which 99% was due to retinal toxicity (Huang et al., 2015).

Current models available for the assessment of retinotoxicity are *in vitro* models and *in vivo* models. The *in vitro* human models available for use are two human retinal cell lines, the MIO-M1 cell line (Müller cells) and the ARPE19 cell line (RPE cells). The cell lines are useful for early research stages such as drug discovery and preclinical development and provide a relatively easy way to perform investigative toxicology. However the toxicity of a potential drug cannot be based entirely on cell work and *in vivo* models are still required as a safety evaluation step in the preclinical development stage (Huang et al., 2015).

Human organotypic models are desirable within drug development research as they provide a multicellular system which can be representative of the target tissue. They also possess advantages over *in vivo* work as they can be directly related to the species of interest and involve no animal studies. The disadvantage of these models is that human tissue is not always readily available, and they do not represent a multi organ system which may produce toxic metabolites. For this reason this human organotypic models are an ideal intermediate, bridging *in vitro* and *in vivo* studies to provide information regarding toxicity. This model has the potential to save the pharmaceutical industry vast amounts of money from investing further into a drug which may, or may not possess retinotoxic properties in humans.

To investigate if the human *ex vivo* retina is a suitable model to assess retinotoxicity, multiple stages of research were conducted. Firstly, profiling of cell markers in the human retina, and the similarity between the living donor retina and the post mortem

retina was investigated. The profiling of cell markers showed which markers were suitable for the identification of specific cell types in the human retina.

Immunohistochemically, it was shown that a suitable marker for the outer nuclear layer was recoverin as this stained photoreceptors within the outer retina. Suitable inner nuclear layer markers were calbindin and PKC α . Calbindin appeared to immunostain horizontal and amacrine cells within the inner nuclear layer, as well as cone photoreceptors outer segments, whereas PKC α solely identified rod ON bipolar cells, making PKC α a more suitable inner nuclear layer marker. Suitable ganglion cell layer markers were THY1, NeuN, β Tubulin III and AHNAK2. Further profiling of the retina was accomplished through the investigation of mRNA. It was shown that whole sample mRNA analysis could identify the density of specific cell populations, and that mRNA profiling of planar sections showed the cell markers were specific for the cell type associated (shown with planar sectioning).

This stage was important as it provided the basis for further research. The methods conducted to profile the human retina are able to be adapted for use as toxicological investigators. Immunohistochemical markers of specific cells could in future be co-localised with cell death markers such as TUNEL to identify cell populations affected by retinotoxins. And whole sample mRNA could be used to identify changes in whole section cell populations. The assessment of changes in mRNA has been used before, and it was shown that decreases in *THY1* expression occurred with NMDA excitotoxicity and preceded a decrease in NeuN immunohistochemistry (Niyadurupola et al., 2011), however this method has never been used to assess changes in other cell specific markers. This technique requires expression equivalence across the five paramacula samples in order for any changes compared to control samples to be assessed. For this reason expression equivalence throughout the five paramacula sections of cell specific markers was investigated. It was found that the photoreceptor specific marker *RCVRN* possessed expression equivalence throughout the five paramacula sections alongside the inner nuclear layer marker for horizontal cells (*CALB1*), bipolar cells (*PKCA*) and amacrine cells (*CHAT*). The ganglion cell markers *THY1*, *RBFOX3* and *AHNAK2* also showed expression equivalence through the five paramacula sections, allowing for investigation into the effect of retinotoxins on expression.

The next stage was to utilise the human retinal cell lines MIO-M1 and ARPE19 cells for the investigation of retinotoxicity with a variety of retinotoxins. The two cell lines were exposed to varying concentrations of hydrogen peroxide, indomethacin, tamoxifen and chloroquine. Both cell lines responded in a dose dependent manner to the retinotoxins and showed the usefulness of the LDH and MTS assay in the investigation of toxicity. Interestingly the cell lines displayed the highest sensitivity towards chloroquine which is also the most well documented of the retinotoxins. To further investigate the sensitivity of the cell lines and the cell death / viability assays, hydroxychloroquine and chloroquine were applied to ARPE19 and MIO-M1 cells and the responses measured over a 72h period. Data obtained from this displayed chloroquine's more toxicological properties to the cell lines than hydroxychloroquine, reflecting three main points. Firstly, hydroxychloroquines better safety profile, secondly the sensitivity of the LDH and MTS assay in their ability to distinguish between the two drugs, and finally the usefulness of the cell lines in the investigation of retinotoxins.

The effectiveness of HORCs in the assessment of retinotoxicity towards a known retinotoxin was then investigated. Out of the retinotoxins applied to the cell lines chloroquine proved to be the most potent. It is also a well-documented retinotoxin and therefore degenerative effects would be expected if applied to the *ex vivo* retina. For this reason chloroquine induced toxicity on the HORC was investigated. Medium based cell death assays (LDH and MTS) displayed a significant increase in cell death at 2mM concentrations. The immunohistochemical assay for TUNEL proved more sensitive, showing a significant increase in cell death at 200 μ M CHQ. The method with which this was analysed involved adapting the TUNEL assay for use with the Ventana Discovery (Roche, Burgess Hill, UK), an automated immunohistochemical platform. The TUNEL assay is normally analysed using fluorescence microscopy, with fluorescein-12-dUTP incorporated at fragmented 3'-OH ends through the use of rTdT. To convert this to the colormetric system used by the Ventana Discovery, HRP anti-FITC was applied to the samples post TUNEL assay completion. The advantages of using the colormetric system is that the analysis method of the slides is automated and has the potential to be used for rapid analysis in toxicological investigations used throughout drug development.

After chloroquine had been shown to induce cell death, another method for analysing retinal cell health / density was also investigated. Previous data from Niyadurupola et al (2011) showed that NMDA excitotoxicity caused changes in *THY1* expression levels which was related to changes in retinal ganglion cell population (Niyadurupola et al., 2011). However investigations into other cell specific markers has never been conducted. The mRNA markers investigated were *THY1*, *CHAT*, *RLBP*, *PKCA*, *CALBI* and *RCVRN*. These markers were chosen for two reasons, firstly because they represent a marker of each one of the major cell groups of the retina, and secondly because they displayed expression equivalence across the five paramacula sections, allowing for changes in expression compared to a control to be assessed. The data obtained from this displayed that an increase in expression was common throughout the higher concentrations of chloroquine treatment, contrary to what was expected. The reason as to the increase in expression is unclear, however it has displayed that this method of analysis is not suitable for the assessment of chloroquine toxicity.

The final area of research conducted in this project was into the expression of genes relating to a novel retinotoxin. Recently CDK inhibitors have come to light as potential cancer therapeutics, however when investigated in mice the pan CDK inhibitor AG-012986 displayed specific retinal toxicity localised to photoreceptors (Illanes et al., 2006). CDKs are normally associated with the cell cycle, and the intended target of this drug was rapidly dividing cells, therefore the reason as to why the drug is toxic to cells with an “arrested cell cycle” was of interest. With the help of AstraZeneca, the affinities of two CDK inhibitors that caused neurotoxicity, and two Pan CDK inhibitors which did not cause neurotoxicity towards CDKs were investigated. From this data it was decided that the CDKs to investigate further were CDK 5, 11, 16, 17 and 18.

Investigation into mRNA expression from whole explants and planar sectioning of explants had been extremely valuable in confirming the position of peak expression of cell specific marker genes, therefore this method was adapted to show the position of peak expression of the CDK's of interest. The data obtained from investigating CDK expression across the retina showed that CDK's displayed differential expression across the retinal layers. One of the CDK's investigated (*CDK11*) displayed higher expression in the photoreceptor layer of both paramacula and

macula samples, and the whole explant data showed lower expression in macula samples compared to paramacula samples. This was similar to the expression pattern of *RCVRN*, and as the higher expression was more pronounced in the paramacula regions, expression in rod photoreceptors is inferred. Further to this, if *CDK11* is inhibited by AG-012986, this may play a role in the photoreceptor toxicity found in mice treated with AG-012986. *CDK18* also displayed a defined peak of expression in the inner nuclear layer of both macula and paramacula samples, and a trend of lower expression in the whole macula explant compared to the paramacula explants. *RLBP* displayed a similar expression profile, indicating that *CDK18* expression may be localised to Müller cells.

The toxicity of AG-012986 was then investigated on the ARPE19 and MIO-M1 cell line. Interestingly the MIO-M1 cell line displayed a high level of sensitivity to AG-012986 whereas the ARPE19 cell line showed no pattern of increased cell death with increasing concentrations of AG-012986. This is interesting because *CDK18* expression was high in Müller cells, therefore if AG-012986 can cause a detrimental effect on Müller cells through the inhibition of CDK18, a secondary effect of this may be photoreceptor toxicity such as that found in mice.

7.2 Future work

Research conducted throughout this thesis has the potential to be continued and opens a lot future work. Some of this work was planned and ready to be conducted, however due to unforeseen circumstances and the reformation of the transplantation service, the supply of donated human retinas was halted and the planned work was unable to be completed.

One area of interest is the further development of whole section mRNA analysis in response to retinotoxicity. As described, this method of analysis was used to assess the effect of NMDA excitotoxicity on ganglion cell health / density (Niyadurupola et al., 2011). However when this method was utilised to assess the effect of CHQ on multiple cell specific markers, there was an increase in expression with high concentrations of CHQ treatment. The reason as to this increase in expression was

unclear, and it is of interest to perform further investigations, perhaps on other retinotoxins to investigate if this effect is similar.

It would also be of interest to further investigate the mechanism of CHQ induced retinotoxicity. During this study PARP cleavage was assessed to measure levels of apoptosis, however there are many other mechanisms which would be interesting to investigate such as levels of autophagy. Levels of autophagy can be assessed via the relationship between two forms of microtubule associated protein 1 light chain 3 (LC3-I and LC3-II). LC3-I is found diffusely throughout the cytoplasm (Rosenfeldt et al., 2012), however during autophagy LC3-I conjugates to phosphatidylethanolamine (a phospholipid found within membranes) forming LC3-II which is tightly bound to the membrane of the autophagosome. Upon the final stages of autophagy LC3-II is converted back to LC3-I via protease cleavage. The alteration in production of LC3-II throughout different stages of autophagy allows us to measurement of LC3-II to confirm that either; autophagy has been induced or that a build-up of autophagosomes has occurred (Holt et al., 2011), (Mizushima and Yoshimori, 2007).

One major project which was planned, was a detailed investigation into the effect of two CDK inhibitors on HORCs. During this project, a selective array was planned in which whole sample and planar sectioned pan CDK inhibitor treated HORCS were going to be investigated for the effect on mRNA expression of multiple cell specific markers, CDK's and cell death / stress markers. Unfortunately before this work was conducted the supply of donated tissue was halted.

Another interesting project that has potential to be further developed is the analysis system of the colorimetric immunohistochemically stained slides using the Ventana Discovery platform. The analysis system (Image scope software) can be adapted to analyse certain areas, leaving the potential for the investigation of cell death levels (using the TUNEL assay) within specific nuclear layers. The TUNEL assay was shown to be the most sensitive means of assessing cell death within HORCS. This could be particularly useful if for example the CDK inhibitor was applied to the HORC, and a degenerative effect was found in the photoreceptor layer but not the other layers. This could then be quantified and expressed as percentage positive pixel within the specific nuclear layer.

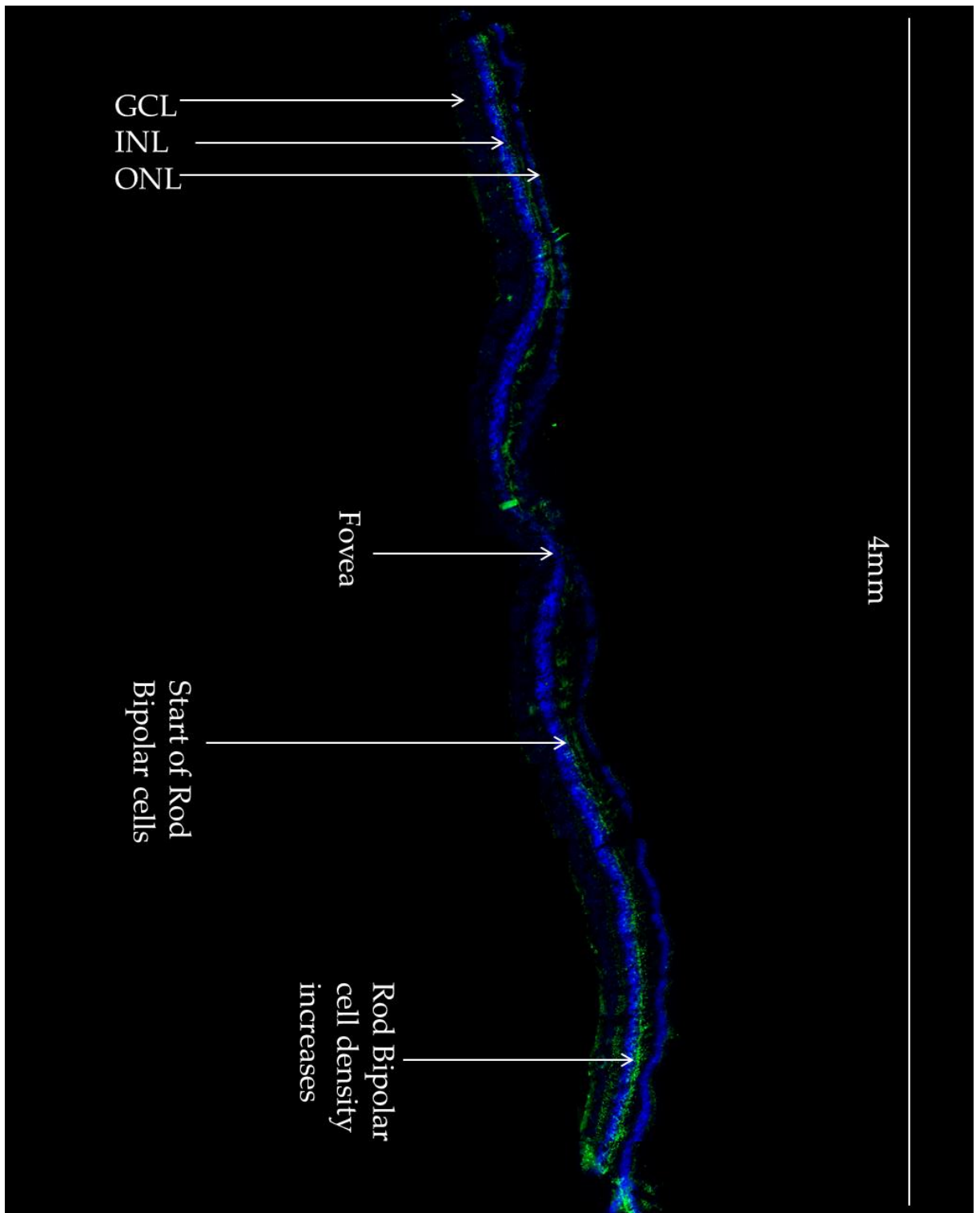
7.3 Concluding remarks

The work conducted within this thesis has displayed the suitability of the *ex vivo* human retina as a model to assess retinotoxicity. I have also shown the most effective methods of assessing and analysing the retinotoxicity. The most effective methodology appeared to come from TUNEL immunohistochemical staining, and the analysis through which this was completed.

This research also showed that the model can be utilised for other research such as the investigation into genes associated with a retinotoxin. This was demonstrated with the investigation into the expression of multiple CDK's throughout the human retina, and the association of CDK's with specific cell types. The planar sectioning technique proved to be extremely useful within this research and opens up many possibilities of investigating other genes associated with retinotoxins.

Overall this research has shown the effectivity of the HORC in the assessment of retinotoxicity, and the most suitable methods in which to determine cell death. It has the potential to be used as a bridge between *in vitro* and *in vivo* research, and potentially between animal and human studies to provide new information regarding the retinotoxicity of current drugs, and novel drugs under development.

Supplementary Data



Supplementary data Figure 1 - Supplementary data (SPD) Figure 1 showing a whole macula section at 4mm across immunostained with PKC. This figure represents the starting point of the Rod ON bipolar cells and shows the density of the cells increasing as they progress further away from the fovea.

Abbreviations

AHNAK2	AHNAK nucleoprotein 2
AMD	Age related macular degeneration
ARPE19	Retinal pigmented epithelium cell line
BCA	Bicinchoninic acid assay
BRB	Blood retinal barrier
BSA	Bovine serum albumin
CALB1	Calbindin
ChAT	Choline acetyl transferase
CHQ	Chloroquine
CRALBP	Cellular retinaldehyde binding protein
CT	Cycle threshold
CYC1	Cytochrome c-1
DLE	Discoid lupus erythmatosus
DMBI	Desmethyldeschlorobenzoylindomethacin
DMEM	Dulbeccos modified eagles medium
DMI	Desmethylindomethacin
DNA	Deoxyribonucleic acid
DPBS	Dulbeccos phosphate buffered saline
EOG	Electrooculogram
ERG	Electroretinogram
FBS	Feotal bovine serum
G-6-PD	Glucose-6-phoshate dehydrogenase
GCL	Ganglion cell layer
GFAP	Glial fibrillary acidic protein
GLUL	Glutamate-Ammonia Ligase
GS	Glutamine synthetase
GSH	Glutathione
GSH-PX	Glutathione peroxidase
GSSG	Glutathione disulphide
HCQ	Hydroxychloroquine
HORC	Human organotypic retinal culture
HPLC	High performance liquid chromatoraphy
HSP70	Heat shock protein 70
IFT	Intraflagellar transport
INL	Inner nuclear layer
LAMP	Lysosome associated membrane protein
LC3	Microtubule associated protein light chain 3
LDH	Lactose dehydrodenase
MIO-M1	Muller cell line
M-PER	Mammalian protein extraction reagent
mRNA	Messenger ribonucleic acid
MTS	3-(4,5-dimethylthiazol-2-yl)-5-(3-carboxymethoxyphenyl)-2-(4sulfophenyl)-2H-tetra-zolium
NAC	N-acetyleyteine

NeuN	Neuronal nuclei
NSAID	Non steroidal anti inflammatory drug
OCT	Ocular coherence tomography
OCT	Optimal cutting temperature
OGD	Oxygen glucose deprivation
ONL	Outer nuclear layer
PARP	Poly (ADP-ribose) polymerase
PBS	Phosphate buffered solution
PCR	Polymerase chain reaction
PKCa	Protein kinase C alpha
PM	Post mortem
PVDF	Polyvinylidene fluoride
RA	Rheumatoid arthritis
RBFOX3	Neuronal nuclei (NeuN)
RCVN	Recoverin
RGC	Retinal ganglion cell
RLBP	Retinaldehyde binding protein
RNA	Ribonucleic acid
ROS	Reactive oxygen species
RPE	Retinal pigmented epithelium
SDS	Sodium dodecyl sulphate
SERM	Selective estrogen receptor modulator
SLE	Systemic lupus erythematosus
TOP1	Topoisomerase I
TRX-RED	Thioredoxin
TUNEL	Terminal deoxynucleotidyl transferase-mediated biotindeoxyuridine triphosphate nick end-labelling
U.S.A	United States of America
UK	United Kingdom

References

- AHNELT, P. & KOLB, H. 1994. Horizontal cells and cone photoreceptors in human retina: a Golgi-electron microscopic study of spectral connectivity. *The Journal of comparative neurology*, 343, 406-27.
- BALTAZAR, G. C., GUHA, S., LU, W., LIM, J., BOESZE-BATTAGLIA, K., LATIES, A. M., TYAGI, P., KOMPELLA, U. B. & MITCHELL, C. H. 2012. Acidic nanoparticles are trafficked to lysosomes and restore an acidic lysosomal pH and degradative function to compromised ARPE-19 cells. *PLoS One*, 7, e49635.
- BECHGAARD, H., BRODIE, R. R., CHASSEAUD, L. F., HOUMOLLER, P., HUNTER, J. O., SIKLOS, P. & TAYLOR, T. 1982. Bioavailability of indomethacin from two multiple-units controlled-release formulations. *Eur J Clin Pharmacol*, 21, 511-5.
- BERNSTEIN, H., ZVAIFLER, N., RUBIN, M. & MANSOUR, A. M. 1963. The Ocular Deposition of Chloroquine. *Invest Ophthalmol*, 2, 384-92.
- BLOMQUIST, P. H. 2011. Ocular complications of systemic medications. *Am J Med Sci*, 342, 62-9.
- BONANOMI, M. T., DANTAS, N. C. & MEDEIROS, F. A. 2006. Retinal nerve fibre layer thickness measurements in patients using chloroquine. *Clin Experiment Ophthalmol*, 34, 130-6.
- BONNER, J. A., SLOAN, J. A., ROWLAND, K. M., JR., KLEE, G. G., KUGLER, J. W., MAILLIARD, J. A., WIESENFELD, M., KROOK, J. E., MAKSYMUK, A. W., SHAW, E. G., MARKS, R. S. & PEREZ, E. A. 2000. Significance of neuron-specific enolase levels before and during therapy for small cell lung cancer. *Clin Cancer Res*, 6, 597-601.
- BOYA, P., REGGIORI, F. & CODOGNO, P. 2013. Emerging regulation and functions of autophagy. *Nat Cell Biol*, 15, 713-20.
- BREGMAN, D. B., PESTELL, R. G. & KIDD, V. J. 2000. Cell cycle regulation and RNA polymerase II. *Front Biosci*, 5, D244-57.
- BRINGMANN, A., PANNICKE, T., GROSCHE, J., FRANCKE, M., WIEDEMANN, P., SKATCHKOV, S. N., OSBORNE, N. N. & REICHENBACH, A. 2006. Muller cells in the healthy and diseased retina. *Prog Retin Eye Res*, 25, 397-424.
- BROWNING, D. J. 2014. *Hydroxychloroquine and Chloroquine Retinopathy*, Springer-Verlag New York.
- BRUNNER, T., WASEM, C., TORGLER, R., CIMA, I., JAKOB, S. & CORAZZA, N. 2003. Fas (CD95/Apo-1) ligand regulation in T cell homeostasis, cell-mediated cytotoxicity and immune pathology. *Semin Immunol*, 15, 167-76.

- CAMPBELL, M. & HUMPHRIES, P. 2012. The blood-retina barrier: tight junctions and barrier modulation. *Adv Exp Med Biol*, 763, 70-84.
- CDC 2014. Medicines for the Prevention of Malaria While Traveling Hydroxychloroquine (Plaquenil™).
- CHAUHAN, B. C., STEVENS, K. T., LEVESQUE, J. M., NUSCHKE, A. C., SHARPE, G. P., O'LEARY, N., ARCHIBALD, M. L. & WANG, X. 2012. Longitudinal in vivo imaging of retinal ganglion cells and retinal thickness changes following optic nerve injury in mice. *PLoS One*, 7, e40352.
- CHEN, J., MIAO, Y., WANG, X. H. & WANG, Z. 2011a. Elevation of p-NR2A(S1232) by Cdk5/p35 contributes to retinal ganglion cell apoptosis in a rat experimental glaucoma model. *Neurobiol Dis*, 43, 455-64.
- CHEN, P. M., GOMBART, Z. J. & CHEN, J. W. 2011b. Chloroquine treatment of ARPE-19 cells leads to lysosome dilation and intracellular lipid accumulation: possible implications of lysosomal dysfunction in macular degeneration. *Cell Biosci*, 1, 10.
- CHENG, K., LI, Z., FU, W. Y., WANG, J. H., FU, A. K. & IP, N. Y. 2002. Pctaire1 interacts with p35 and is a novel substrate for Cdk5/p35. *J Biol Chem*, 277, 31988-93.
- CHIQUET, C., DKHISSI-BENYAHYA, O. & COOPER, H. M. 2005. Calcium-binding protein distribution in the retina of strepsirhine and haplorhine primates. *Brain Res Bull*, 68, 185-94.
- CHO, K. S., YOON, Y. H., CHOI, J. A., LEE, S. J. & KOH, J. Y. 2012. Induction of autophagy and cell death by tamoxifen in cultured retinal pigment epithelial and photoreceptor cells. *Invest Ophthalmol Vis Sci*, 53, 5344-53.
- COSTA, J. G., VIDAL, K. S. M., VIDAL, L. L. M. & YAMADA, E. S. 2007. Histopathologic Analyses of Human Retina and Rat Retinas Intoxicated by Chloroquine.
- CURCIO, C. A. & ALLEN, K. A. 1990. Topography of ganglion cells in human retina. *J Comp Neurol*, 300, 5-25.
- D.W. RICKMAN, P. S., B. JESSEN, M.R. NIESMAN 2005. The Pan Cyclin-Dependent Kinase Inhibitor, AG-012986, Perturbs Postnatal Retinal Development and Disrupts Photoreceptor Maintenance in the Differentiated Retina. *Invest Ophthalmol Vis Sci E-Abstract* 2972.
- DE TORRES, C., MUNELL, F., FERRER, I., REVENTOS, J. & MACAYA, A. 1997. Identification of necrotic cell death by the TUNEL assay in the hypoxic-ischemic neonatal rat brain. *Neurosci Lett*, 230, 1-4.
- DHARIWALA, F. A. & RAJADHYAKSHA, M. S. 2008. An unusual member of the Cdk family: Cdk5. *Cell Mol Neurobiol*, 28, 351-69.

- DIZHOOR, A. M., RAY, S., KUMAR, S., NIEMI, G., SPENCER, M., BROLLEY, D., WALSH, K. A., PHILIPPOV, P. P., HURLEY, J. B. & STRYER, L. 1991. Recoverin: a calcium sensitive activator of retinal rod guanylate cyclase. *Science*, 251, 915-8.
- DUBBELMAN, M., VAN DER HEIJDE, G. L. & WEEBER, H. A. 2001. The thickness of the aging human lens obtained from corrected Scheimpflug images. *Optom Vis Sci*, 78, 411-6.
- DUNN, K. C., AOTAKI-KEEN, A. E., PUTKEY, F. R. & HJELMELAND, L. M. 1996. ARPE-19, a human retinal pigment epithelial cell line with differentiated properties. *Exp Eye Res*, 62, 155-69.
- ELMORE, S. 2007. Apoptosis: a review of programmed cell death. *Toxicol Pathol*, 35, 495-516.
- ENGELKE, M., TYKHONOVA, S., ZORN-KRUPPA, M. & DIEHL, H. 2002. Tamoxifen induces changes in the lipid composition of the retinal pigment epithelium cell line D407. *Pharmacol Toxicol*, 91, 13-21.
- ETIENNE, M. C., MILANO, G., FISCHER, J. L., FRENAY, M., FRANCOIS, E., FORMENTO, J. L., GIOANNI, J. & NAMER, M. 1989. Tamoxifen metabolism: pharmacokinetic and in vitro study. *Br J Cancer*, 60, 30-5.
- FAN, P. W. & BOLTON, J. L. 2001. Bioactivation of tamoxifen to metabolite E quinone methide: reaction with glutathione and DNA. *Drug Metab Dispos*, 29, 891-6.
- FORRESTER, J. V. 2007. *The eye : basic sciences in practice*, Edinburgh ; New York, Saunders.
- GALVAO, J., ELVAS, F., MARTINS, T., CORDEIRO, M. F., AMBROSIO, A. F. & SANTIAGO, A. R. 2015. Adenosine A3 receptor activation is neuroprotective against retinal neurodegeneration. *Exp Eye Res*, 140, 65-74.
- GAYNES, B. I., TORCZYNSKI, E., VARRO, Z., GROSTERN, R. & PERLMAN, J. 2008. Retinal toxicity of chloroquine hydrochloride administered by intraperitoneal injection. *J Appl Toxicol*, 28, 895-900.
- GHAYUR, T., BANERJEE, S., HUGUNIN, M., BUTLER, D., HERZOG, L., CARTER, A., QUINTAL, L., SEKUT, L., TALANIAN, R., PASKIND, M., WONG, W., KAMEN, R., TRACEY, D. & ALLEN, H. 1997. Caspase-1 processes IFN-gamma-inducing factor and regulates LPS-induced IFN-gamma production. *Nature*, 386, 619-23.
- GIORGIO, M., TRINEI, M., MIGLIACCIO, E. & PELICCI, P. G. 2007. Hydrogen peroxide: a metabolic by-product or a common mediator of ageing signals? *Nat Rev Mol Cell Biol*, 8, 722-8.
- GRAESER, R., GANNON, J., POON, R. Y., DUBOIS, T., AITKEN, A. & HUNT, T. 2002. Regulation of the CDK-related protein kinase PCTAIRE-1 and its

- possible role in neurite outgrowth in Neuro-2A cells. *J Cell Sci*, 115, 3479-90.
- GRAHAM, C. M. & BLACH, R. K. 1988. Indomethacin retinopathy: case report and review. *Br J Ophthalmol*, 72, 434-8.
- GRASL-KRAUPP, B., RUTTKAY-NEDECKY, B., KOUDELKA, H., BUKOWSKA, K., BURSCH, W. & SCHULTE-HERMANN, R. 1995. In situ detection of fragmented DNA (TUNEL assay) fails to discriminate among apoptosis, necrosis, and autolytic cell death: a cautionary note. *Hepatology*, 21, 1465-8.
- GUNHAN, E., VAN DER LIST, D. & CHALUPA, L. M. 2003. Ectopic photoreceptors and cone bipolar cells in the developing and mature retina. *J Neurosci*, 23, 1383-9.
- H. P. RANG, M. M. D. 2012. *Pharmacology*, Elsevier.
- HABERECHT, M. F., MITCHELL, C. K., LO, G. J. & REDBURN, D. A. 1997. N-methyl-D-aspartate-mediated glutamate toxicity in the developing rabbit retina. *J Neurosci Res*, 47, 416-26.
- HANUS, J., ZHANG, H., WANG, Z., LIU, Q., ZHOU, Q. & WANG, S. 2013. Induction of necrotic cell death by oxidative stress in retinal pigment epithelial cells. *Cell Death Dis*, 4, e965.
- HAVERKAMP, S., HAESELEER, F. & HENDRICKSON, A. 2003. A comparison of immunocytochemical markers to identify bipolar cell types in human and monkey retina. *Vis Neurosci*, 20, 589-600.
- HAYASHI, F., MATSUURA, I., KACHI, S., MAEDA, T., YAMAMOTO, M., FUJII, Y., LIU, H., YAMAZAKI, M., USUKURA, J. & YAMAZAKI, A. 2000. Phosphorylation by cyclin-dependent protein kinase 5 of the regulatory subunit of retinal cGMP phosphodiesterase. II. Its role in the turnoff of phosphodiesterase in vivo. *J Biol Chem*, 275, 32958-65.
- HERCEG, Z. & WANG, Z. Q. 2001. Functions of poly(ADP-ribose) polymerase (PARP) in DNA repair, genomic integrity and cell death. *Mutat Res*, 477, 97-110.
- HERSKOVITS, A. Z. & DAVIES, P. 2006. The regulation of tau phosphorylation by PCTAIRE 3: implications for the pathogenesis of Alzheimer's disease. *Neurobiol Dis*, 23, 398-408.
- HIROSE, T., TAMARU, T., OKUMURA, N., NAGAI, K. & OKADA, M. 1997. PCTAIRE 2, a Cdc2-related serine/threonine kinase, is predominantly expressed in terminally differentiated neurons. *Eur J Biochem*, 249, 481-8.
- HOGAN, M. J., ALVARADO, J. A. & WEDDELL, J. E. 1971. *Histology of the human eye; an atlas and textbook*, Philadelphia, Saunders.

- HOLLBORN, M., ULBRICHT, E., RILLICH, K., DUKIC-STEFANOVIC, S., WURM, A., WAGNER, L., REICHENBACH, A., WIEDEMANN, P., LIMB, G. A., BRINGMANN, A. & KOHEN, L. 2011. The human Muller cell line MIO-M1 expresses opsins. *Mol Vis*, 17, 2738-50.
- HOLT, S. V., WYSPIANSKA, B., RANDALL, K. J., JAMES, D., FOSTER, J. R. & WILKINSON, R. W. 2011. The development of an immunohistochemical method to detect the autophagy-associated protein LC3-II in human tumor xenografts. *Toxicol Pathol*, 39, 516-23.
- HU, D., VALENTINE, M., KIDD, V. J. & LAHTI, J. M. 2007. CDK11(p58) is required for the maintenance of sister chromatid cohesion. *J Cell Sci*, 120, 2424-34.
- HUANG, W., COLLETTE, W., 3RD, TWAMLEY, M., AGUIRRE, S. A. & SACAAN, A. 2015. Application of electroretinography (ERG) in early drug development for assessing retinal toxicity in rats. *Toxicol Appl Pharmacol*, 289, 525-33.
- HUTCHINS, J. B. & HOLLYFIELD, J. G. 1987. Cholinergic neurons in the human retina. *Exp Eye Res*, 44, 363-75.
- IGNEY, F. H. & KRAMMER, P. H. 2002. Death and anti-death: tumour resistance to apoptosis. *Nat Rev Cancer*, 2, 277-88.
- ILLANES, O., ANDERSON, S., NIESMAN, M., ZWICK, L. & JESSEN, B. A. 2006. Retinal and peripheral nerve toxicity induced by the administration of a pan-cyclin dependent kinase (cdk) inhibitor in mice. *Toxicol Pathol*, 34, 243-8.
- INDUSTRY, T. A. O. T. B. P. 2016. Available: <http://www.abpi.org.uk/industry-info/new-medicines/Pages/default.aspx>.
- JIANG, Z. & SHEN, W. 2010. Role of neurotransmitter receptors in mediating light-evoked responses in retinal interplexiform cells. *Journal of neurophysiology*, 103, 924-33.
- JOHNSON, C. A. 1976. Effects of luminance and stimulus distance on accommodation and visual resolution. *J Opt Soc Am*, 66, 138-42.
- JOHNSON, T. V. & MARTIN, K. R. 2008. Development and characterization of an adult retinal explant organotypic tissue culture system as an in vitro intraocular stem cell transplantation model. *Invest Ophthalmol Vis Sci*, 49, 3503-12.
- JU, C. & UETRECHT, J. P. 1998. Oxidation of a metabolite of indomethacin (Desmethyldeschlorobenzoylindomethacin) to reactive intermediates by activated neutrophils, hypochlorous acid, and the myeloperoxidase system. *Drug Metab Dispos*, 26, 676-80.

- KAEMPF, S., JOHNEN, S., SALZ, A. K., WEINBERGER, A., WALTER, P. & THUMANN, G. 2008. Effects of bevacizumab (Avastin) on retinal cells in organotypic culture. *Invest Ophthalmol Vis Sci*, 49, 3164-71.
- KAUSHIK, S., BANDYOPADHYAY, U., SRIDHAR, S., KIFFIN, R., MARTINEZ-VICENTE, M., KON, M., ORENSTEIN, S. J., WONG, E. & CUERVO, A. M. 2011. Chaperone-mediated autophagy at a glance. *J Cell Sci*, 124, 495-9.
- KAYAMA, M., NAKAZAWA, T., THANOS, A., MORIZANE, Y., MURAKAMI, Y., THEODOROPOULOU, S., ABE, T., VAVVAS, D. & MILLER, J. W. 2011. Heat shock protein 70 (HSP70) is critical for the photoreceptor stress response after retinal detachment via modulating anti-apoptotic Akt kinase. *Am J Pathol*, 178, 1080-91.
- KEVANY, B. M. & PALCZEWSKI, K. 2010. Phagocytosis of retinal rod and cone photoreceptors. *Physiology (Bethesda)*, 25, 8-15.
- KIM, L. A., AMARNANI, D., GNANAGURU, G., TSENG, W. A., VAVVAS, D. G. & D'AMORE, P. A. 2014. Tamoxifen toxicity in cultured retinal pigment epithelial cells is mediated by concurrent regulated cell death mechanisms. *Invest Ophthalmol Vis Sci*, 55, 4747-58.
- KIM, M. H., CHUNG, J., YANG, J. W., CHUNG, S. M., KWAG, N. H. & YOO, J. S. 2003. Hydrogen peroxide-induced cell death in a human retinal pigment epithelial cell line, ARPE-19. *Korean J Ophthalmol*, 17, 19-28.
- KIRINO, T., BRIGHTMAN, M. W., OERTEL, W. H., SCHMECHEL, D. E. & MARANGOS, P. J. 1983. Neuron-specific enolase as an index of neuronal regeneration and reinnervation. *J Neurosci*, 3, 915-23.
- KOKHAN, O., WRAIGHT, C. A. & TAJKHORSHID, E. 2010. The binding interface of cytochrome c and cytochrome c(1) in the bc(1) complex: rationalizing the role of key residues. *Biophys J*, 99, 2647-56.
- KOLB, H., FERNANDEZ, E., SCHOUTEN, J., AHNELT, P., LINBERG, K. A. & FISHER, S. K. 1994. Are there three types of horizontal cell in the human retina? *The Journal of comparative neurology*, 343, 370-86.
- KOLB, H., LINBERG, K. A. & FISHER, S. K. 1992. Neurons of the human retina: a Golgi study. *The Journal of comparative neurology*, 318, 147-87.
- KOLB, H., ZHANG, L. & DEKORVER, L. 1993. Differential staining of neurons in the human retina with antibodies to protein kinase C isozymes. *Vis Neurosci*, 10, 341-51.
- KORAH, S. & KURIAKOSE, T. 2008. Optical coherence tomography in a patient with chloroquine-induced maculopathy. *Indian J Ophthalmol*, 56, 511-3.
- KYRYLKOVA, K., KYRYACHENKO, S., LEID, M. & KIOUSSI, C. 2012. Detection of apoptosis by TUNEL assay. *Methods Mol Biol*, 887, 41-7.

- LAMEIRAO, S. V., HAMASSAKI, D. E., RODRIGUES, A. R., SM, D. E. L., FINLAY, B. L. & SILVEIRA, L. C. 2009. Rod bipolar cells in the retina of the capuchin monkey (*Cebus apella*): characterization and distribution. *Vis Neurosci*, 26, 389-96.
- LAZZARONI, F., SCOROLLI, L., PIZZOLO, C. F., SAVINI, G., DE NIGRIS, A., GIOIA, F. & MEDURI, R. A. 1998. Tamoxifen retinopathy: does it really exist? *Graefes Arch Clin Exp Ophthalmol*, 236, 669-73.
- LEBLANC, B., JEZEQUEL, S., DAVIES, T., HANTON, G. & TARADACH, C. 1998. Binding of drugs to eye melanin is not predictive of ocular toxicity. *Regul Toxicol Pharmacol*, 28, 124-32.
- LI, G. Y., FAN, B. & ZHENG, Y. C. 2010. Calcium overload is a critical step in programmed necrosis of ARPE-19 cells induced by high-concentration H₂O₂. *Biomed Environ Sci*, 23, 371-7.
- LI, W. W., LI, J. & BAO, J. K. 2012. Microautophagy: lesser-known self-eating. *Cell Mol Life Sci*, 69, 1125-36.
- LIMB, G. A., SALT, T. E., MUNRO, P. M., MOSS, S. E. & KHAW, P. T. 2002. In vitro characterization of a spontaneously immortalized human Muller cell line (MIO-M1). *Invest Ophthalmol Vis Sci*, 43, 864-9.
- LIU, X., CHENG, C., SHAO, B., WU, X., JI, Y., LU, X. & SHEN, A. 2013. LPS-stimulating astrocyte-conditioned medium causes neuronal apoptosis via increasing CDK11(p58) expression in PC12 cells through downregulating AKT pathway. *Cell Mol Neurobiol*, 33, 779-87.
- LODISH, H. F. 2000. *Molecular cell biology*, New York, W.H. Freeman.
- LYE, M. H., JAKOBS, T. C., MASLAND, R. H. & KOIZUMI, A. 2007. Organotypic culture of adult rabbit retina. *J Vis Exp*, 190.
- MALUMBRES, M. & BARBACID, M. 2005. Mammalian cyclin-dependent kinases. *Trends Biochem Sci*, 30, 630-41.
- MALUMBRES, M., HARLOW, E., HUNT, T., HUNTER, T., LAHTI, J. M., MANNING, G., MORGAN, D. O., TSAI, L. H. & WOLGEMUTH, D. J. 2009. Cyclin-dependent kinases: a family portrait. *Nat Cell Biol*, 11, 1275-6.
- MARG, A., HAASE, H., NEUMANN, T., KOUNO, M. & MORANO, I. 2010. AHNAK1 and AHNAK2 are costameric proteins: AHNAK1 affects transverse skeletal muscle fiber stiffness. *Biochem Biophys Res Commun*, 401, 143-8.
- MARKS, J. S. 1982. Chloroquine retinopathy: is there a safe daily dose? *Ann Rheum Dis*, 41, 52-8.
- MARMOR, M. F., CARR, R. E., EASTERBROOK, M., FARJO, A. A., MIELER, W. F. & AMERICAN ACADEMY OF, O. 2002. Recommendations on

- screening for chloroquine and hydroxychloroquine retinopathy: a report by the American Academy of Ophthalmology. *Ophthalmology*, 109, 1377-82.
- MARTOLA, E. L. & BAUM, J. L. 1968. Central and peripheral corneal thickness. A clinical study. *Arch Ophthalmol*, 79, 28-30.
- MATSUDA, S., KOMINATO, K., KOIDE-YOSHIDA, S., MIYAMOTO, K., ISSHIKI, K., TSUJI, A. & YUASA, K. 2014. PCTAIRE kinase 3/cyclin-dependent kinase 18 is activated through association with cyclin A and/or phosphorylation by protein kinase A. *J Biol Chem*, 289, 18387-400.
- MICHAELIDES, M., STOVER, N. B., FRANCIS, P. J. & WELEBER, R. G. 2011. Retinal toxicity associated with hydroxychloroquine and chloroquine: risk factors, screening, and progression despite cessation of therapy. *Arch Ophthalmol*, 129, 30-9.
- MIKOLCEVIC, P., SIGL, R., RAUCH, V., HESS, M. W., PFALLER, K., BARISIC, M., PELLINIEMI, L. J., BOESL, M. & GELEY, S. 2012. Cyclin-dependent kinase 16/PCTAIRE kinase 1 is activated by cyclin Y and is essential for spermatogenesis. *Mol Cell Biol*, 32, 868-79.
- MIZUSHIMA, N. & YOSHIMORI, T. 2007. How to interpret LC3 immunoblotting. *Autophagy*, 3, 542-5.
- MOJUMDER, D. K., WENSEL, T. G. & FRISHMAN, L. J. 2008. Subcellular compartmentalization of two calcium binding proteins, calretinin and calbindin-28 kDa, in ganglion and amacrine cells of the rat retina. *Mol Vis*, 14, 1600-13.
- MOLNAR, M. L., STEFANSSON, K., MARTON, L. S., TRIPATHI, R. S. & MOLNAR, G. K. 1984. Immunohistochemistry of retinoblastomas in humans. *Am J Ophthalmol*, 97, 301-7.
- MORENO, M. C., SANDE, P., MARCOS, H. A., DE ZAVALIA, N., KELLER SARMIENTO, M. I. & ROSENSTEIN, R. E. 2005. Effect of glaucoma on the retinal glutamate/glutamine cycle activity. *FASEB J*, 19, 1161-2.
- MULLEN, P. 2004. PARP cleavage as a means of assessing apoptosis. *Methods Mol Med*, 88, 171-81.
- MULLEN, R. J., BUCK, C. R. & SMITH, A. M. 1992. NeuN, a neuronal specific nuclear protein in vertebrates. *Development*, 116, 201-11.
- MUNIZ, J. A., DE ATHAIDE, L. M., GOMES, B. D., FINLAY, B. L. & SILVEIRA, L. C. 2014. Ganglion cell and displaced amacrine cell density distribution in the retina of the howler monkey (*Alouatta caraya*). *PLoS One*, 9, e115291.
- NADAL-NICOLAS, F. M., JIMENEZ-LOPEZ, M., SOBRADO-CALVO, P., NIETO-LOPEZ, L., CANOVAS-MARTINEZ, I., SALINAS-NAVARRO, M., VIDAL-SANZ, M. & AGUDO, M. 2009. Brn3a as a marker of retinal

- ganglion cells: qualitative and quantitative time course studies in naive and optic nerve-injured retinas. *Invest Ophthalmol Vis Sci*, 50, 3860-8.
- NASH, M. S. & OSBORNE, N. N. 1999. Assessment of Thy-1 mRNA levels as an index of retinal ganglion cell damage. *Invest Ophthalmol Vis Sci*, 40, 1293-8.
- NELSON, R. & CONNAUGHTON, V. 1995. Bipolar Cell Pathways in the Vertebrate Retina. In: KOLB, H., FERNANDEZ, E. & NELSON, R. (eds.) *Webvision: The Organization of the Retina and Visual System*. Salt Lake City (UT).
- NEMUNAITIS, J. J., SMALL, K. A., KIRSCHMEIER, P., ZHANG, D., ZHU, Y., JOU, Y. M., STATKEVICH, P., YAO, S. L. & BANNERJI, R. 2013. A first-in-human, phase 1, dose-escalation study of dinaciclib, a novel cyclin-dependent kinase inhibitor, administered weekly in subjects with advanced malignancies. *J Transl Med*, 11, 259.
- NHS 2014a. Hydroxychloroquine.
- NHS 2014b. Indomethacin.
- NHS 2014c. Medicines A-Z - Chloroquine.
- NHS 2014d. Tamoxifen Citrate, Macmillan.
- NIYADURUPOLA, N., SIDAWAY, P., OSBORNE, A., BROADWAY, D. C. & SANDERSON, J. 2011. The development of human organotypic retinal cultures (HORCs) to study retinal neurodegeneration. *Br J Ophthalmol*, 95, 720-6.
- NOGUEIRA, H. M. & GAMA, R. D. 2009. Images in clinical medicine. Bull's-eye maculopathy. *N Engl J Med*, 360, 2224.
- OH, H., KIM, H., AHN, M., JEONG, C., JEONG, J., MOON, C. & SHIN, T. 2011. Immunohistochemical localization of cyclic AMP-responsive element binding protein (CREB)-binding protein in the pig retina during postnatal development. *Anat Cell Biol*, 44, 143-50.
- OPHTHALMOLOGISTS, T. R. C. O. 2009. Hydroxychloroquine and Ocular Toxicity Recommendations on Screening.
- OSBORNE, A., ALDARWESH, A., RHODES, J. D., BROADWAY, D. C., EVERITT, C. & SANDERSON, J. 2015a. Hydrostatic pressure does not cause detectable changes in survival of human retinal ganglion cells. *PLoS One*, 10, e0115591.
- OSBORNE, A., HOPES, M., WRIGHT, P., BROADWAY, D. C. & SANDERSON, J. 2015b. Human Organotypic Retinal Cultures (HORCs) as a Chronic Experimental Model for investigation of Retinal Ganglion Cell Degeneration. *Exp Eye Res*.

- PAGLINI, G. & CACERES, A. 2001. The role of the Cdk5--p35 kinase in neuronal development. *Eur J Biochem*, 268, 1528-33.
- PARRY, D., GUZI, T., SHANAHAN, F., DAVIS, N., PRABHAVALKAR, D., WISWELL, D., SEGHEZZI, W., PARUCH, K., DWYER, M. P., DOLL, R., NOMEIR, A., WINDSOR, W., FISCHMANN, T., WANG, Y., OFT, M., CHEN, T., KIRSCHMEIER, P. & LEES, E. M. 2010. Dinaciclib (SCH 727965), a novel and potent cyclin-dependent kinase inhibitor. *Mol Cancer Ther*, 9, 2344-53.
- PARTIDA, G. J., STRADLEIGH, T. W., OGATA, G., GODZDANKER, I. & ISHIDA, A. T. 2012. Thy1 associates with the cation channel subunit HCN4 in adult rat retina. *Invest Ophthalmol Vis Sci*, 53, 1696-703.
- PASADHIKA, S., FISHMAN, G. A., CHOI, D. & SHAHIDI, M. 2010. Selective thinning of the perifoveal inner retina as an early sign of hydroxychloroquine retinal toxicity. *Eye (Lond)*, 24, 756-62; quiz 763.
- PENHA, F. M., RODRIGUES, E. B., MAIA, M., DIB, E., FIOD COSTA, E., FURLANI, B. A., NUNES MORAES FILHO, M., DREYFUSS, J. L., BOTTOS, J. & FARAH, M. E. 2010. Retinal and ocular toxicity in ocular application of drugs and chemicals--part I: animal models and toxicity assays. *Ophthalmic Res*, 44, 82-104.
- PEPONIS, V., KYTTARIS, V. C., CHALKIADAKIS, S. E., BONOVAS, S. & SITARAS, N. M. 2010. Ocular side effects of anti-rheumatic medications: what a rheumatologist should know. *Lupus*, 19, 675-82.
- POTTS, A. M. 1964. The Reaction of Uveal Pigment in Vitro with Polycyclic Compounds. *Invest Ophthalmol*, 3, 405-16.
- QIAGEN. 2016. *Comparative Ct Method Quantification* [Online]. Qiagen. Available: <http://sabiosciences.com/manuals/IntrotoqPCR.pdf> [Accessed 03/02/16 2016].
- RAKKAA, T., ESCUDE, C., GIET, R., MAGNAGHI-JAULIN, L. & JAULIN, C. 2014. CDK11(p58) kinase activity is required to protect sister chromatid cohesion at centromeres in mitosis. *Chromosome Res*, 22, 267-76.
- RAMAMURTHY, V. & CAYOUILLE, M. 2009. Development and disease of the photoreceptor cilium. *Clinical genetics*, 76, 137-45.
- REICHENBACH, A. & BRINGMANN, A. 2013. New functions of Muller cells. *Glia*, 61, 651-78.
- REMINGTON, L. A. 2012. *Clinical anatomy and physiology of the visual system*, St. Louis, Mo., Elsevier/Butterworth Heinemann.
- RIEPE, R. E. & NORENBURG, M. D. 1977. Muller cell localisation of glutamine synthetase in rat retina. *Nature*, 268, 654-5.

- ROH, Y. J., MOON, C., KIM, S. Y., PARK, M. H., BAE, Y. C., CHUN, M. H. & MOON, J. I. 2007. Glutathione depletion induces differential apoptosis in cells of mouse retina, in vivo. *Neurosci Lett*, 417, 266-70.
- ROSENFELDT, M. T., NIXON, C., LIU, E., MAH, L. Y. & RYAN, K. M. 2012. Analysis of macroautophagy by immunohistochemistry. *Autophagy*, 8, 963-9.
- ROSENTHAL, A. R., KOLB, H., BERGSMA, D., HUXSOLL, D. & HOPKINS, J. L. 1978. Chloroquine retinopathy in the rhesus monkey. *Invest Ophthalmol Vis Sci*, 17, 1158-75.
- RUNKLE, E. A. & ANTONETTI, D. A. 2011. The blood-retinal barrier: structure and functional significance. *Methods Mol Biol*, 686, 133-48.
- RUSSELL, S. R., SHEPHERD, J. D. & HAGEMAN, G. S. 1991. Distribution of glycoconjugates in the human retinal internal limiting membrane. *Investigative ophthalmology & visual science*, 32, 1986-95.
- SAELENS, X., FESTJENS, N., VANDE WALLE, L., VAN GURP, M., VAN LOO, G. & VANDENABEELE, P. 2004. Toxic proteins released from mitochondria in cell death. *Oncogene*, 23, 2861-74.
- SASAKI, M., OZAWA, Y., KURIHARA, T., KUBOTA, S., YUKI, K., NODA, K., KOBAYASHI, S., ISHIDA, S. & TSUBOTA, K. 2010. Neurodegenerative influence of oxidative stress in the retina of a murine model of diabetes. *Diabetologia*, 53, 971-9.
- SHACKA, J. J., KLOCKE, B. J., SHIBATA, M., UCHIYAMA, Y., DATTA, G., SCHMIDT, R. E. & ROTH, K. A. 2006. Bafilomycin A1 inhibits chloroquine-induced death of cerebellar granule neurons. *Mol Pharmacol*, 69, 1125-36.
- SHARMA, R. K., ORR, W. E., SCHMITT, A. D. & JOHNSON, D. A. 2005. A functional profile of gene expression in ARPE-19 cells. *BMC ophthalmology*, 5, 25.
- SHEN, W., FRUTTIGER, M., ZHU, L., CHUNG, S. H., BARNETT, N. L., KIRK, J. K., LEE, S., COOREY, N. J., KILLINGSWORTH, M., SHERMAN, L. S. & GILLIES, M. C. 2012. Conditional Muller cell ablation causes independent neuronal and vascular pathologies in a novel transgenic model. *J Neurosci*, 32, 15715-27.
- SHIMIZU, K., UEMATSU, A., IMAI, Y. & SAWASAKI, T. 2014. Pctaire1/Cdk16 promotes skeletal myogenesis by inducing myoblast migration and fusion. *FEBS Lett*, 588, 3030-7.
- SHIN, S. C., CHOI, J. S. & LI, X. 2006. Enhanced bioavailability of tamoxifen after oral administration of tamoxifen with quercetin in rats. *Int J Pharm*, 313, 144-9.
- SODERSTJERNA, E., BAUER, P., CEDERVALL, T., ABDSHILL, H., JOHANSSON, F. & JOHANSSON, U. E. 2014. Silver and gold

nanoparticles exposure to in vitro cultured retina--studies on nanoparticle internalization, apoptosis, oxidative stress, glial- and microglial activity. *PLoS One*, 9, e105359.

- SRIKANTIA, N., MUKESH, S. & KRISHNASWAMY, M. 2010. Crystalline maculopathy: a rare complication of tamoxifen therapy. *J Cancer Res Ther*, 6, 313-5.
- STEPHENSON, J. J., NEMUNAITIS, J., JOY, A. A., MARTIN, J. C., JOU, Y. M., ZHANG, D., STATKEVICH, P., YAO, S. L., ZHU, Y., ZHOU, H., SMALL, K., BANNERJI, R. & EDELMAN, M. J. 2014. Randomized phase 2 study of the cyclin-dependent kinase inhibitor dinaciclib (MK-7965) versus erlotinib in patients with non-small cell lung cancer. *Lung Cancer*, 83, 219-23.
- STRAUSS, O. 2005. The retinal pigment epithelium in visual function. *Physiol Rev*, 85, 845-81.
- SUNDELIN, S. P. & TERMAN, A. 2002. Different effects of chloroquine and hydroxychloroquine on lysosomal function in cultured retinal pigment epithelial cells. *APMIS*, 110, 481-9.
- TANG, R., SHIELDS, J., SCHIFFMAN, J., LI, H., LOCHER, D., HAMPTON, J., PRAGER, T. & PARDO, G. 1997. Retinal changes associated with tamoxifen treatment for breast cancer. *Eye*, 11, 295-297.
- TANIDA, I., UENO, T. & KOMINAMI, E. 2008. LC3 and Autophagy. *Methods Mol Biol*, 445, 77-88.
- TETT, S. E., CUTLER, D. J., DAY, R. O. & BROWN, K. F. 1989. Bioavailability of hydroxychloroquine tablets in healthy volunteers. *Br J Clin Pharmacol*, 27, 771-9.
- TIMBRELL, J. A. 1995. *Introduction to Toxicology*, Taylor & Francis.
- TOLER, S. M. 2004. Oxidative stress plays an important role in the pathogenesis of drug-induced retinopathy. *Exp Biol Med (Maywood)*, 229, 607-15.
- TZEKOV, R. 2005. Ocular toxicity due to chloroquine and hydroxychloroquine: electrophysiological and visual function correlates. *Doc Ophthalmol*, 110, 111-20.
- URBAK, L. & VORUM, H. 2010. Heat shock proteins in the human eye. *Int J Proteomics*, 2010, 479571.
- VAN BUSKIRK, E. M. 1989. The anatomy of the limbus. *Eye (Lond)*, 3 (Pt 2), 101-8.
- VERBEECK, R. K., JUNGINGER, H. E., MIDHA, K. K., SHAH, V. P. & BARENDIS, D. M. 2005. Biowaiver monographs for immediate release solid oral dosage forms based on biopharmaceutics classification system (BCS) literature data: chloroquine phosphate, chloroquine sulfate, and chloroquine hydrochloride. *J Pharm Sci*, 94, 1389-95.

- W. M. HASCHEK, C. G. R., M. A. WALLIG 2013. *Handbook of Toxicologic Pathology Third Edition*.
- WATANABE, S. E., BEREZOVSKY, A., MOTONO, M., SACAI, P. Y., PEREIRA, J. M., SALLUM, J. M., GEBRIM, L. H. & SALOMAO, S. R. 2010. Retinal function in patients treated with tamoxifen. *Doc Ophthalmol*, 120, 137-43.
- WHO 2014. WHO Model Prescribing Information: Drugs Used in Parasitic Diseases - Second Edition.
- WOOLLEY, A. 2003. *A Guide to Practical Toxicology, Evaluation, Prediction and Risk*, Taylor & Francis.
- YANAGI, T., REED, J. C. & MATSUZAWA, S. 2014. PCTAIRE1 regulates p27 stability, apoptosis and tumor growth in malignant melanoma. *Oncoscience*, 1, 624-33.
- YOKOTA, T., KAMIMURA, N., IGARASHI, T., TAKAHASHI, H., OHTA, S. & OHARAZAWA, H. 2015. Protective effect of molecular hydrogen against oxidative stress caused by peroxynitrite derived from nitric oxide in rat retina. *Clin Experiment Ophthalmol*, 43, 568-77.
- YOON, Y. H., CHO, K. S., HWANG, J. J., LEE, S. J., CHOI, J. A. & KOH, J. Y. 2010. Induction of lysosomal dilatation, arrested autophagy, and cell death by chloroquine in cultured ARPE-19 cells. *Invest Ophthalmol Vis Sci*, 51, 6030-7.
- ZHANG, F., FAN, P. W., LIU, X., SHEN, L., VAN BREEMAN, R. B. & BOLTON, J. L. 2000. Synthesis and reactivity of a potential carcinogenic metabolite of tamoxifen: 3,4-dihydroxytamoxifen-o-quinone. *Chem Res Toxicol*, 13, 53-62.
- ZULUAGA-IDARRAGA, L., YEPES-JIMENEZ, N., LOPEZ-CORDOBA, C. & BLAIR-TRUJILLO, S. 2014. Validation of a method for the simultaneous quantification of chloroquine, desethylchloroquine and primaquine in plasma by HPLC-DAD. *J Pharm Biomed Anal*, 95, 200-6.